Serviceability Behavior of Reinforced Concrete Discontinuity Regions

by

Jessica L. Kettelkamp

Thesis

Submitted in Partial Fulfillment

of the Requirements for the Degree of

Master of Science

in Engineering

Northern Arizona University

May 2016

Approved:

Robin G. Tuchscherer, Ph.D., P.E., S.E., Chair ______________________

Joshua Hewes, Ph.D, P.E. ______________________

Andrew Scanlon, Ph.D, S.E. ______________________

ABSTRACT

SERVICEABILITY BEHAVIOR OF REINFORCED CONCRETE DISCONTINUITY REGIONS

JESSICA L. KETTELKAMP, M.S.E.

This purpose of this project is to investigate the serviceability behavior of discontinuity regions using the strut and tie modeling method. To accomplish this objective, the following aims are targeted:(1) to investigate the serviceability behavior of concrete in terms of maximum crack width and tie strain estimated in representative STM;(2) to investigate the serviceability behavior of concrete in terms of total crack area and strain energy estimated in representative STM and;(3) to recommend a procedure for distinguishing a 'good' strut and tie model from a 'bad' model. A secondary goal of this project is to refine existing methods for processing digital images in the collection of crack width, crack area and displacement data. This effort is accomplished by testing twelve concrete deep beams with a 10×20 in. cross-section. Experimental variables include web reinforcement ratio and spacing, shear span-to-depth ratio, and configuration of the primary tension reinforcement. An extensive amount of data are collected to establish serviceability behavior including, maximum crack width, area of cracked surface, and displacement of targets placed on a 3-inch grid on beam surfaces. Findings indicate a strong correlation between crack area and strain energy in a representative strut-and-tie model for beams with an *a/d* of one. For beams with an *a/d* of two, the correlation is offered more strongly by modeling assumptions and alternate load paths. It is recommended to limit the estimated strain within the ties of a strut-and-tie model to achieve acceptable serviceability performance and predictable crack widths. This study represents an improved design approach for estimating the serviceability performance of reinforced discontinuity regions.

Acknowledgements

Firstly, I would like to say the last two and a half years working on this project has been the hardest, and most rewarding experience I have been a part of at Northern Arizona University. I could not have done this without the support of family, friends, faculty, and funding.

To all the participants who helped with the fabrication phase of this project, thank you. Your assistance, elbow grease, input, and good company were greatly appreciated. I physically, could not have completely this project without you guys.

Thank you to the sponsors of this project: Portland Cement Association, American Concrete Institute and the Faculty Grant Proposals. Without their generous support, this project would not have been financially possible.

Thank you to Dr. Hewes and Dr. Scanlon for your participation in my committee. The knowledge and insight you two brought to the project was needed and is greatly appreciated

To Sabrina Ballard, you are an absolute lifesaver. Your contribution to this project cannot be understated. The assistance and knowledge you provided in the fabrication and testing phase played a large role in the success of this project. Also, your assistance in all things camera related cannot be appreciated enough. Thank you.

I would like to also thank Dr. Robin Tuchscherer who put his faith in me to carry out his vision for this project. Without his initial suggestion of working with him for my masters, I would not have ever considered graduate school and for that I cannot thank him enough. Also your patience and support throughout this project has far exceeded any expectations I had. I truly appreciate you. Thanks for setting the bar high.

Last but most certainly not least, I would like to thank my family. I would not be the person I am today without their love, support, and encouragement. You guys always push me to do my absolute best in anything I set out to accomplish and I can’t thank you enough for that. I love you.

Table of Contents

CHAPTER 1 INTRODUCTION **1**

1.1 Motivation 1

1.2 Introduction 1

1.3 Project Objective 2

1.4 Project Scope 3

1.5 Thesis Organization 4

CHAPTER 2 BACKGROUND **5**

2.1 Overview 5

2.2 Discontinuity Regions 5

2.3 Design of D-Regions 7

2.3.1 Overview 7

2.3.2 Strut and Tie Model (STM) 8

2.3.3 Nonlinear Analysis 14

2.3.4 Strength Design Using an STM 15

2.3.5 Serviceability Design using an STM 21

2.4 Crack Width Database 26

2.4.1 Overview 26

2.4.2 Kong et al., 1970 (Kong, Robins, and Cole 1970) 27

2.4.3 Smith and Vantsiotis, 1982 28

2.4.4 Birrcher et al., 2009 29

2.4.5 Deschenes, 2009 30

2.4.6 Summary 31

2.5 Crack Width Prediction Models 32

2.5.1 Overview 32

2.5.2 Walraven, 1981 32

2.5.3 Mihaylov et. al., 2014 33

2.6 Crack Collection 37
2.7 Need for current research 38
CHAPTER 3 EXPERIMENTAL PROGRAM 40
3.1 Overview 40
3.2 Testing Program 40
3.2.1 Overview 40
3.2.2 Specimen Details 42
3.3 Strut and Tie Model 46
3.3.1 Overview 46
3.3.2 Geometric Assumptions 46
3.4 Fabrication 49
3.4.1 Overview 49
3.4.2 Longitudinal Reinforcement for Flexure 50
3.4.3 Web Reinforcement 51
3.4.4 Concrete Mixture 51
3.4.5 Formwork 51
3.4.6 Reinforcement Cages 52
3.4.7 Concrete Placement 53
3.5 Experimental Test Setup 55
3.5.1 Overview 55
3.5.2 Steel Reinforcement Strain Gauges 56
3.5.3 Concrete Strain Gauge 58
3.5.4 Hydraulic Cylinders 59
3.5.5 Load Cells 60
3.5.6 String Potentiometer 60
3.5.7 Data Acquisition (DAQ) 61
3.5.8 Photogrammetry 62

3.6 Test Procedure 68

3.7 Crack Measurements.. 68

3.7.1 Overview.. 68

3.7.2 Maximum Crack Width, w_{cr} 69

3.7.3 Crack Area, A_{cr}.. 70

3.8 All Specimen Details 71

CHAPTER 4 RESULTS **71**

4.1 Overview 71

4.2 Specimen Legend.. 71

4.3 Load versus Displacement 72

4.4 Photogrammetry Data 74

4.5 Strain Data 76

4.6 Max Crack Width.. 78

4.7 Crack Area 82

CHAPTER 5 DISCUSSION OF RESULTS **84**

5.1 Overview 84

5.2 Max Crack Width vs Strain Energy.. 84

5.2.1 Shear Reinforcement.. 85

5.2.2 Shear Stirrup Spacing 87

5.2.3 Tie Model and Shear Span-to-Depth Ratio.. 88

5.3 Crack Area vs Strain Energy.. 90

5.3.1 Web Reinforcement 90

5.3.2 Shear Stirrup Spacing 92

5.3.3 Tie Model.. 94

5.3.4 Shear Span-to-Depth Ratio 94

5.4 Design Procedure.. 96

5.4.1 Predicting Maximum Crack Width, w_{cr}.. 96

5.4.2 Predicting Area of Cracked Surface, A_{cr} 97
5.4.3 Distinguishing a "Good" from a "Bad" model 98
5.5 Implications and Limitations of results 101
5.6 Suggestions for Future Work 102
CHAPTER 6 CONCLUSION 104
6.1 Summary 104
6.2 Conclusions and Recommendations 104
6.2.1 Project Goal 104
6.2.2 Maximum crack width, w_{cr}, versus estimated strain in tie, ε_t 105
6.2.3 Area of crack surface, A_{cr}, versus estimated stain energy in STM, U_{total} 105
6.2.4 Distinguishing a "good" STM from a "bad" STM 106
6.2.5 Design Recommendations 106
REFERENCES 107
LIST OF APPENDICES 112
APPENDIX A: CRACK WIDTH DATABASE 113
APPENDIX B: SPECIMEN SHOP DRAWINGS 118
APPENDIX C: STM DIMENSIONS 124
APPENDIX D: CONCRETE CONTROL CYLINDERS 126
APPENDIX E: STRAIN GAUGE LOCATIONS 127
APPENDIX F: STRAIN ENERGY CALCULATIONS 130
APPENDIX G: CRACK PATTERNS 134

List of Tables

Table 2-1: Guide to Reasonable Crack Widths for Reinforced Concrete Under Service Loads (ACI 224 2008) ... 22
Table 2-2: Beams in Crack Width Database ... 31
Table 3-1: Testing Program ... 42
Table 3-2: Model G Nodal Widths ... 47
Table 3-3: Model B Nodal Widths ... 48
Table 3-4: Strut and Tie Proportioning ... 49
Table 3-5: Mix Design (Cemex, 2015) ... 51
Table 3-6: Concrete Cylinder Data ... 54
Table 3-7: Steel Strain Gauge Specifications ... 56
Table 3-8: Concrete Strain Gauge Specifications ... 58
Table 3-9: Hydraulic Cylinder Specifications ... 60
Table 3-10: Camera and lens specifications ... 62
Table 3-11: Camera Settings for Photogrammetry ... 63
Table 3-12: Summary of Specimen Details ... 70
Table 4-1: Specimen Legend ... 72
Table 5-1: Strain Energy Normalized by Load ... 99

List of Figures

Figure 2-1: Beam theory based on the assumption that planar sections remain planar. 5
Figure 2-2: Typical concrete beam showing B- and D-regions 6
Figure 2-3: Example STM for a point-loaded beam. 8
Figure 2-4: Strut and Tie Model shows truss elements and applied internal forces 9
Figure 2-5: STM containing bottle-shaped and prismatic struts.. 10
Figure 2-6: Dispersion of Compressive Stress (Guyon 1953) 11
Figure 2-7: Bottle shaped strut adapted from (ACI 318 2014)... 11
Figure 2-8: Classification of Nodes (ACI 318-14) 12
Figure 2-9: Stresses on Hydrostatic and Non-Hydrostatic Nodes (Thompson 2002) 13
Figure 2-10: Strut and Tie Design Flowchart 16
Figure 2-11: CCT Node 18
Figure 2-12: CCC Node 19
Figure 2-13: Curved Bar CTT Node 20
Figure 2-14: Identical structures with force paths represented by a (a) “Good” and (b) “Bad” STM (Schlaich et al, 1987). 24
Figure 2-15: Procedure for Designing Suitable Stress Fields (Muttoni et al., 1997).................... 26
Figure 2-16: Cross-sectional dimensions and number of beams in the database 27
Figure 2-17: Predicted versus experimental crack widths predicted per Mihaylov et al., 2014... 36
Figure 2-18: a) Crack comparator card; b) Calipers and; c) Microscope 37
Figure 3-1: Testing Program Notation 41
Figure 3-2: Specimens BG-1-0-0 & BG-2-0-0 43
Figure 3-3: Specimen BG-1-0.3-2 & BG-2-0.3-2... 43
Figure 3-4: Specimens BG-1-0.3-6 & BG-2-0.3-6 44
Figure 3-5: Specimens BB-1-0-0 & BB-2-0-0.. 44
Figure 3-6: Specimens BB-1-0.3-2 & BB-2-0.3-2... 45
Figure 3-7: Specimens BB-1-0.3-6 & BB-2-0.3-6... 45
Figure 3-9: Strut and Tie Label Notation for a.) Model B and b.) Model G Beams 46
Figure 3-10: Model G Node Locations 47
Figure 3-11: Model B Nodal Geometry 48
Figure 3-12: Formwork Platforms for Twelve Concrete Beam (wall bracing not shown for clarity). 52
Figure 3-13: a) Rebar Cage for BB-2-0.3-6 and b) Assembled Cages in Formwork 53
Figure 3-14: Concrete Beams and Cylinders after 28 days of Curing.. 54
Figure 3-15: Beam Test Setup 55
Figure 3-16: Strain Gauge Locations for BG-1-0.3-6.. 56
Figure 3-17: Rebar Strain Gauges... 57
Figure 3-18: Example of Concrete Strain Gauges on Beam 58
Figure 3-19: Hydraulic Cylinders 59
Figure 3-20: String Potentiometers.. 60
Figure 3-21: Data Acquisition 61
Figure 3-22: Set up of Camera for Photogrammetry 63
Figure 3-23: Resulting Photogrammetric Model using Photomodeler 64

Figure 3-24: Photogrammetry Setup Flowchart 66
Figure 3-25: Results of Measured Crack Widths Using Three Different Methods 69
Figure 3-26: Crack Area Measurement 70
Figure 4-1: Series 1 Load vs. Displacement Data 73
Figure 4-2: Series 2 Load vs. Displacement Data 73
Figure 4-3: Photomodeler vs. String Potentiometer Centerline Deflection on BB-2-0.3-6 74
Figure 4-4: Target and Concrete Strain Gauge Location Used for Comparison on BB-2-0.3-6 .. 75
Figure 4-5: Photomodeler vs. Concrete Strain Gauge Data for locations shown in Figure 4-4 ... 76
Figure 4-6: BG-2-0.3-6 Steel and Concrete Gauge Locations 77
Figure 4-7: Concrete Strain Data for Gauges Shown in Figure 4-6 77
Figure 4-8: Steel Strain Data for Gauges Shown in Figure 4-6. 78
Figure 4-9: Maximum Crack Widths for Series 1 Specimens 79
Figure 4-10: Maximum Crack Widths for Series 2 Specimens 79
Figure 4-11: Max Diagonal Crack Width vs. Strain Energy for ρ = 0.0%, s = 0 80
Figure 4-12: Max Diagonal Crack Width vs. Total Strain Energy for ρ = 0.3%, s = d/2 81
Figure 4-13: Max Diagonal Crack Width vs. Total Strain Energy for ρ = 0.3%, s = d/6 81
Figure 4-14: Normalized Crack Area vs. Strain Energy for ρ = 0.0%, s = 0 82
Figure 4-15: Normalized Crack Area vs. Total Strain Energy for ρ = 0.3%, s = d/2 83
Figure 4-16: Normalized Crack Area vs. Total Strain Energy for ρ = 0.3%, s = d/6 83
Figure 5-1: Influence of Web Reinforcement on Max Crack (a/d = 1) 85
Figure 5-2: Influence of Web Reinforcement on Max Crack (a/d = 2) 86
Figure 5-3: Influence of Web Reinforcement Spacing on Max Crack (a/d = 1) 87
Figure 5-4: Influence of Web Reinforcement Spacing on Max Crack (a/d =2) 88
Figure 5-5: Influence of Tie Design on Max Crack (ρ = 0.0%) 89
Figure 5-6: Influence of Web Reinforcement on Crack Area (a/d =1) 91
Figure 5-7: Influence of Web Reinforcement on Crack Area (a/d = 2) 92
Figure 5-8: Influence of Web Reinforcement Spacing on Crack Area (a/d = 1, ρ = 0.3%) 93
Figure 5-9: Influence of Web Reinforcement Spacing on Crack Area (a/d = 2, ρ = 0.3%) 93
Figure 5-10: Influence of Tie Model on Crack Area (ρ = 0.0%) 94
Figure 5-11: Influence on Shear Span-to-Depth Ratio on Crack Area (Model G) 95
Figure 5-12: Influence of Shear Span-to-Depth Ratio on Crack Area (Model B) 95
Figure 5-13: Relationship of Tie Strain and Maximum Crack Width (ρ = 0.3%) 97
Figure 5-14: Relationship between Strain Energy and Crack Area 98
Figure 5-15: U_{tie}/U_{total} versus Maximum Crack Width up to 70% of ultimate capacity 99
Figure 5-16: Design Tool for Estimating Crack Widths (ρ = 0.3%) 100
Figure 5-17: Design Tool for Predicting Crack Area 101

List of Equations

Equation 2-1 16
Equation 2-2 16
Equation 2-3 17
Equation 2-4 17
Equation 2-5 18
Equation 2-6 19
Equation 2-7 20
Equation 2-8 23
Equation 2-9 23
Equation 2-10 24
Equation 2-11 32
Equation 2-12 33
Equation 2-13 33
Equation 2-14 34
Equation 2-15 34
Equation 2-16 35
Equation 2-17 35
Equation 2-18 35
Equation 2-19 35
Equation 3-1 50
Equation 5-1 100

Dedication

I dedicate this thesis to my sisters, Charisse and Melissa, because we run this world.

Notation

A = Cross-sectional area of strut or tie

a = Shear span; depth of equivalent rectangular stress block; height of the back face of the CCC Node, in.

a/d = Shear span-to-depth ratio measured center of span to center of support

A_{cr} = Total area of cracked concrete (Equation 2-10)

A_n = Effective area of concrete strut or node face

A_s = Area of longitudinal reinforcing bar on flexural tension side, in^2

A_s' = Area of compression reinforcement, in^2

A_{si} = is the total area of disturbed reinforcement at spacing

A_{ts} = Area of non-prestressed tie reinforcement

A_v = Area of shear reinforcement perpendicular to the flexural tension reinforcement, in^2

b_s = The width of the strut transverse to the plane of the STM

b_w = Web width, in.

d = Distance from extreme compression fiber to centroid of longitudinal tension reinforcement

d_b = Diameter of longitudinal reinforcing steel bars

E = Modulus of elasticity in strut or tie

E_s = Specified modulus of steel reinforcing bars

F = Force in strut or tie

f_c' = Specified concrete compressive strength, psi

f_{ce} = allowable nodal stress as specified by ACI 318-14

f_s = Stress in tension reinforcement, psi

f_s' = Stress in compression reinforcement, psi

f_y = the specified yield strength of tie reinforcement

F_n = Nominal capacity of strut, tie or node

F_{strut} = *Force in Strut*

F_{tie} = *Force in Tie*

F_u = *Factored force resisted by strut, tie or node*

h = *Total depth of section*

L = *Length of member*

l_0 = *Length of heavily cracked zone at bottom of critical diagonal crack (Equation 2-18)*

l_b = *Length of bearing plate, in.*

l_{b1e} = *Effective width of bearing plate parallel to longitudinal axis of member*

l_c = *Length of crack (Equation 2-10)*

l_k = *Length of bottom reinforcement's elongation contributing to crack width (Equation 2-17)*

N = *Number of specimens, or measurements*

r_b = *Radius of bend in a curved bar node*

s = *Spacing of web reinforcement*

s_h = *Horizontal spacing of web reinforcement*

s_i = *The spacing in the i-th direction of reinforcement crossing a strut at angle to the axis of strut*

s_{max} = *Maximum spacing of radial cracks (Equation 2-16)*

s_v = *Vertical spacing of web reinforcement*

T_{max} = *Maximum tensile force in bottom reinforcement*

U_{tie} = *Estimated strain in tie in an STM*

U_{total} = *Estimated internal strain energy in a representative STM*

v = *Factor related to efficiency or effectiveness of concrete compressive strength in the presence of varying degrees of tension*

V = *The total shear resistance of deep beams (Equation 2-12)*

V_{ci} = *Shear force resisted by aggregate interlock (Equation 2-13)*

V_{CLZ} = *Shear force resisted by the critical loading zone*

V_d = *Shear force resisted by dowel action*

V_n = *Shear Carried in the testing region*

V_s = *Shear force resisted by stirrups*

W = *External work (Equation 2-9)*

w_{avg} = *Average crack width (Equation 2-10)*

w_{cr} = *Maximum crack width*

w_t = *Height of backface of node equal to the minimum of two times the distance between centroid of tie and exterior surface, or* $\frac{F_{nt}}{f_{ce}b_s}$

w_s = *Strut-to-node interface width*

α = *Angle of line extending from inner edge of support plate to far edge of tributary area of loading plate responsible for shear force (V).*

α_1 = *Angle of critical diagonal crack*

α_i = *The strut angle*

Δ_c = *Ultimate shear displacement (Equation 2-15)*

ε = *Mean strain in member (Equation 2-8)*

ε_t = *Strain along bottom longitudinal reinforcement (Equation 2-19)*

ρ = *Ratio of transverse reinforcement perpendicular to the axis of the strut*

ρ_h = *Ratio of horizontal transverse reinforcement to effective area*

ρ_v = *Ratio of vertical transverse reinforcement to effective area*

ρ_l = *ratio of bottom longitudinal reinforcement*

θ = *Angle of strut measure form the horizontal axis; Angle of diagonal cracks in uniform stress field*

σ_{trans} = *Stress transverse to the strut*

CHAPTER 1

Introduction

1.1 MOTIVATION

Currently, the concrete industry contributes roughly 5% to the global CO_2 emissions through (Crow 2008). To put into perspective, that is greater than the total carbon footprint of Japan in 2014, who produced the fifth largest amount of CO_2 emissions in the world (Global Carbon Project 2015). This environmental impact is in part, due to the frequent repair and replacement of existing concrete structures. Our ability to predict maintenance and replacement costs for infrastructure is directly connected to our understanding of its durability and remaining service life. This project seeks to improve the sustainability of the constructed environment by improving upon our understanding of its durability and serviceability.

1.2 INTRODUCTION

A discontinuity region is a region whose behavior is dominated by shear deformations. In these regions, the theory to describe the mechanical behavior is complex. Methods available to designers include nonlinear analysis and strut and tie modeling. Due to the relative complexity of nonlinear analysis and the computational experience required, strut and tie modeling is by far the more common method.

Strut-and-tie modeling is a plasticity-based approach used for determining a lower bound estimate of a structure's ultimate strength. In other words, it is not intended for determining service limit states. Given this fact, there is a need for a design procedure which can be used to determine the crack behavior expected under service-level loading. The study presented in this paper seeks to correlate maximum crack width and area of cracked surface to the internal strain energy estimated from a representative strut and tie model. Though estimating total strain energy is an elastic approach, if the strut and tie model closely matches elastic distribution of forces, then estimated strain energy will correlate with the ultimate plastic model.

The serviceability design for reinforced concrete structures is an important consideration. Practicing engineers demand a better understanding of the service rather than strength behavior. The inadequate and inconsistent treatment of discontinuity regions has been a main reason for poor performance and even structural failures (Schlaich et al. 1987).

1.3 PROJECT OBJECTIVE

The purpose of this project is to investigate the serviceability behavior of discontinuity regions using the strut and tie modeling method. To accomplish this objective, the following aims are targeted:

1. To investigate the serviceability behavior of concrete in terms of maximum measured crack width and tie strain estimated in representative STM;
2. To investigate the serviceability behavior of concrete in terms of total measured crack area and strain energy estimated in representative STM;
3. To recommend a procedure for distinguishing a ‘good’ strut and tie model from a ‘bad’ model.

A secondary goal of this project is to refine existing methods for processing digital images in the collection of crack width, crack area and displacement data.

1.4 PROJECT SCOPE

First, past literature is reviewed and a database containing 88 deep beams compiled. This database contains the crack width data available for reinforced concrete discontinuity regions. Available methods for designing discontinuity regions are examined along with serviceability practices.

To accomplish the objectives of this study, twelve specimens with 10 in. x 20 in. cross-sections were fabricated and experimentally tested to failure. Specimen details regarding size, material, and design practice were chosen to observe the effect of the following variables:

1) Web Reinforcement (ρ = 0% and 0.3%)
2) Spacing of web reinforcement (d/2 and d/6)
3) Tie Model (Model G and B)
4) Shear span-to-depth ratio (a/d = 1 and 2)

Experimental data collected as part of this study includes load, displacement, concrete and steel reinforcing strain, maximum crack width, and total area of cracked concrete. New crack measurement techniques were investigated and a method selected. This method allowed the collection of maximum crack width and total crack area using digital images collected during testing.

Finally, the variables within the testing program are isolated and their effects presented in terms of total strain energy in a representative truss model. Given these results, a design tool is proposed for practicing engineers to use for both design and assessment of the serviceability performance of discontinuity regions.

1.5 THESIS ORGANIZATION

All work conducted over this two and a half year study is reviewed within the following six chapters: Background (Chapter 2), Experimental Program (Chapter 3), Results (Chapter 4), Discussion of Results (Chapter 5) and Conclusion (Chapter 6). A brief outline of each chapter is provided below.

All background information pertinent to the objectives of this study is presented in Chapter 2. To start, discontinuity regions in reinforced concrete are defined. Methods of designing such regions are presented and current serviceability provisions and predictions are listed. Also, a database compiling all available crack width information is presented. Finally, new methods of crack width collection are reviewed.

The design, fabrication, and test procedure of the twelve specimens used in this study are outlined in Chapter 3. Specimen details are determined in terms of the projects objectives. Discussion of material properties and assumed strut and tie models are provided. Fabrication of the concrete specimens is discussed including formwork construction, assembly of steel reinforcement cages, and placement of concrete. The instrumentation used during testing is described and justified. Lastly, the testing procedure for each specimen is detailed and crack collection methods outlined.

Results collected during the tests of all specimens are presented in Chapter 4 and discussed with respect to the project's objectives in Chapter 5. The implications of the results are explained. Limitations of this study and recommendations for future work are listed.

Lastly, experimental work completed during the course of this study are briefly summarized in Chapter 6. Conclusions regarding the serviceability behavior of reinforced discontinuity regions are presented.

CHAPTER 2

Background

2.1 OVERVIEW

This chapter presents the theoretical basis and experimental precedent for this research study. Discontinuity regions are defined Section 2.2. Available design methods for the strength and serviceability of discontinuity regions are discussed in Section 2.3. A database of crack widths collected from past studies is presented in Section 2.4. Section 2.5 summarizes existing crack width prediction models. Finally, limitations of existing methods and need for current research is given in Section 2.6.

2.2 DISCONTINUITY REGIONS

Design of slender reinforced concrete members to resist shear and flexural forces is based on the assumption that strains vary linearly at a section. Referred to as the "Bernoulli hypothesis" or "beam theory", planar sections are assumed to remain planar. Flexural deformations dominate the behavior such that the member bends with a constant curvature, see Figure 2-1.

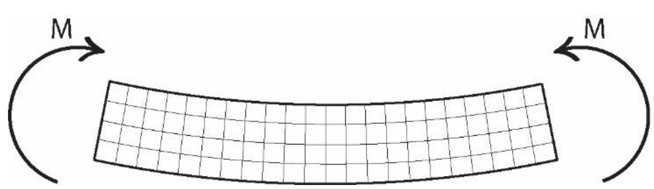

Figure 2-1: Beam theory based on the assumption that planar sections remain planar.

Beam theory is used to explain a slender beam's mechanical behavior. The regions of a structure where beam theory is valid are commonly referred to as a "B-regions". When analyzing

B-regions, internal stresses at a cross-section are equilibrated with external forces. As such, the behavior of these regions is often referred to as a “sectional behavior”.

Regions containing load or geometric discontinuities must be treated differently than B-regions because the assumptions used to derive Bernoulli’s beam theory are no longer valid. The behavior of discontinuity or “D-regions” are heavily influenced by shear deformations. Thus, the structural behavior of D-regions is heavily influenced by nonlinear shear strains. D-regions are often defined as those which have relatively small shear span-to-depth ratios (*a/d)*, or with a *a/d* ratio less than or equal to approximately two. Figure 2-2 presents an asymmetrically loaded beam showing both B- and D-regions.

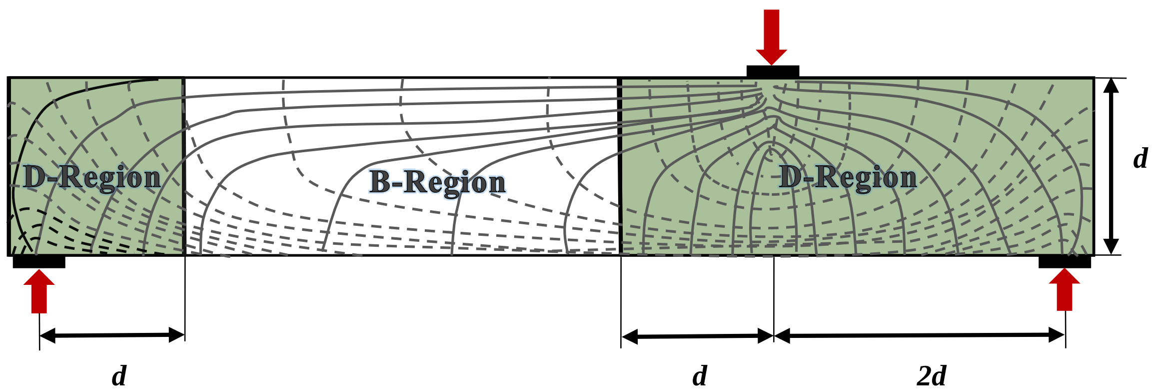

Figure 2-2: Typical concrete beam showing B- and D-regions

In the figure above, the nonlinear distribution of strain in D-regions is caused by load discontinuities. St. Venant’s Principle suggests the confining effect of a concentrated load or geometric discontinuity diminishes near one member depth from the discontinuity. Thus, D-regions are assumed to extend one member depth from the load or discontinuity. In practice, engineers typically encounter D-regions when designing transfer girders, pile-supported foundations, shear walls, corbels, and connections.

2.3 DESIGN OF D-REGIONS

2.3.1 Overview

In D-regions, a general theory of behavior is difficult if not impossible to derive due to the nonlinearity of strain and inelasticity of concrete. Engineer's ability to accurately predict capacity is either empirical or requires substantial computational effort. Current design for D-Regions is generally limited to two types of methods: 1) strut and tie modeling; or 2) a nonlinear analysis (ACI 318-14). Strut and tie modeling is based on a lower bound theory of plasticity. Thus, a member's ultimate capacity is, at a minimum, equal to that predicted by the method. As a result, while conservative, strut and tie modeling is a poor predictor of ultimate capacity. Nonlinear analysis is accomplished through a finite element analysis. Subsequently, accurate estimations of capacity generally require substantial computational effort.

A strut and tie model is a lower bound estimate of ultimate strength and cannot be used to predict a member's serviceability behavior. A nonlinear inelastic finite element analysis could be used to predict serviceability behavior but requires substantial expertise. As a result, service limit states for reinforced concrete D-regions are satisfied through rules of thumb, past experience, prescriptive code requirements, or combination. There is a need for a theoretically-based serviceability design approach that is accessible to practicing engineers.

The strut and tie modeling methodology is further discussed in Section 2.3.2. The nonlinear analysis approach is further discussed in Section 2.3.3. Finally, current design provisions related to the strength and serviceability of D-regions are given in Section 2.3.4 and 2.3.5, respectively.

2.3.2 Strut and Tie Model (STM)

2.3.2.1 Introduction

Strut and tie modeling is the most common approach available to engineers for the design of reinforced concrete D-regions. This method assigns resultants to stress fields in a D-region and idealizes these resultants as compressive and tensile elements in a simplified truss. Concrete struts represent the resultants of compressive stress fields and reinforcing steel ties represent the resultants of the tensile stress fields. Struts and ties intersect at regions called nodes. An example STM is shown in Figure 2-3.

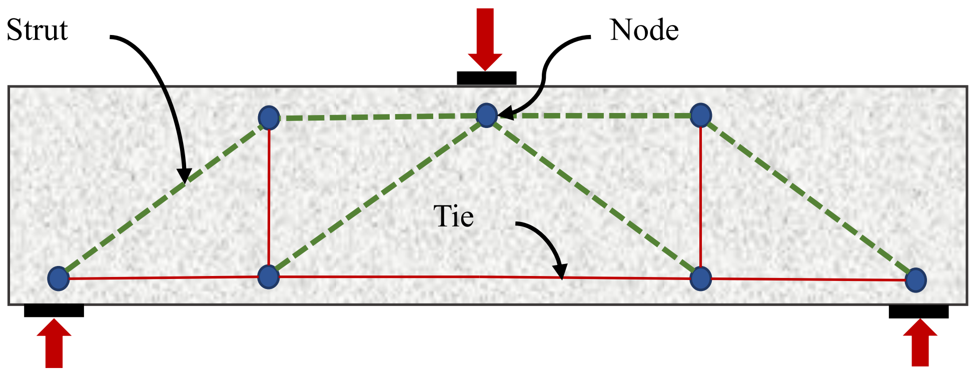

Figure 2-3: Example STM for a point-loaded beam.

Figure 2-3 illustrates an example of a STM as a determinate truss prior to proportioning the elements to withstand applied forces. An example of an STM with proportioned elements and resulting internal forces is shown in Figure 2-4.

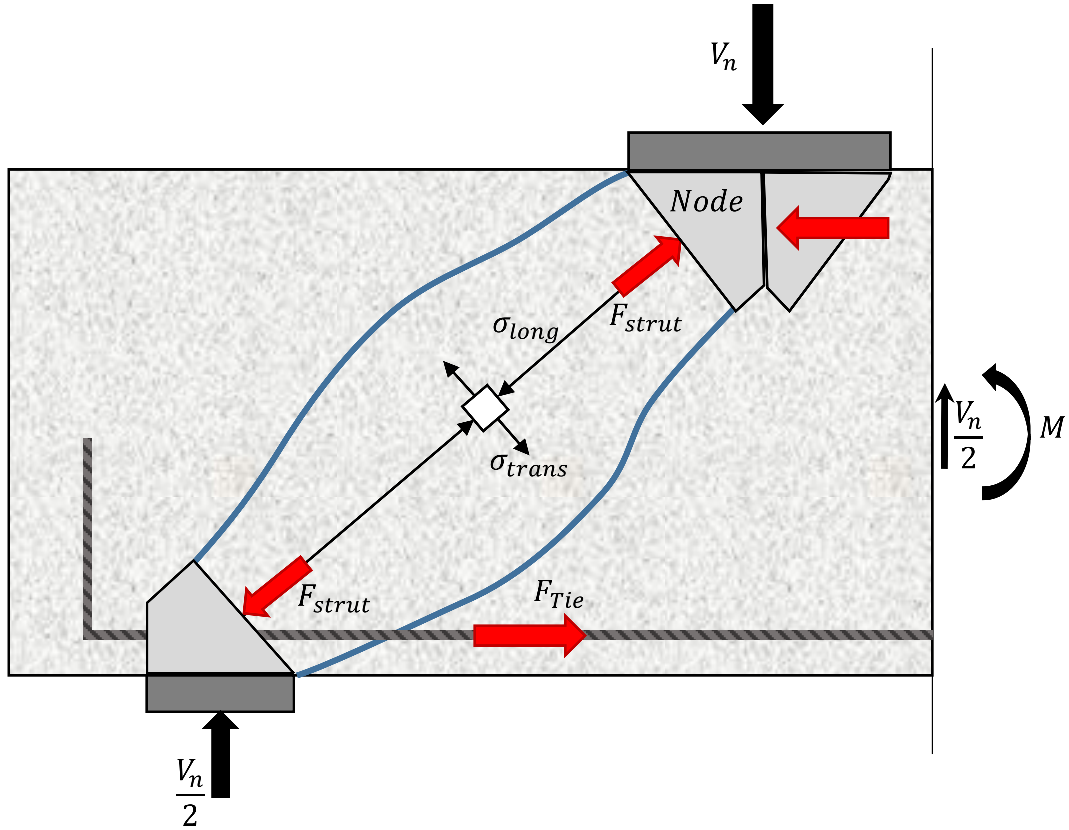

Figure 2-4: Strut and Tie Model shows truss elements and applied internal forces

The capacity of a STM is always less than the structure's actual capacity provided the truss is in equilibrium and safe, meaning the model has sufficient deformation capacity to redistribute forces into the assumed truss elements and stresses applied to the elements do not exceed their "yield" capacity (Figure 2-4). Failure of a STM typically include the crushing of struts, crushing of concrete at the face of a node, yielding of the ties, or anchorage failure of the ties.

From a designer's perspective, the advantage of a STM is very complex stress regions can be idealized into a simple truss model. As a result, a STM can provide an engineer with an intuitive visualization of load path, and critical stress locations. Another advantage of strut and tie modeling is more than one model can be provided to carry the load. As long as the model satisfies the principals of a lower bound solution, the selected model will "safely" carry the load.

2.3.2.2 Strut

Struts are the compressive members of an STM. In a beam, the geometry of the strut depends largely on the path of the load. Consider two types of strut shapes, prismatic and bottle-shaped, as shown in Figure 2-5.

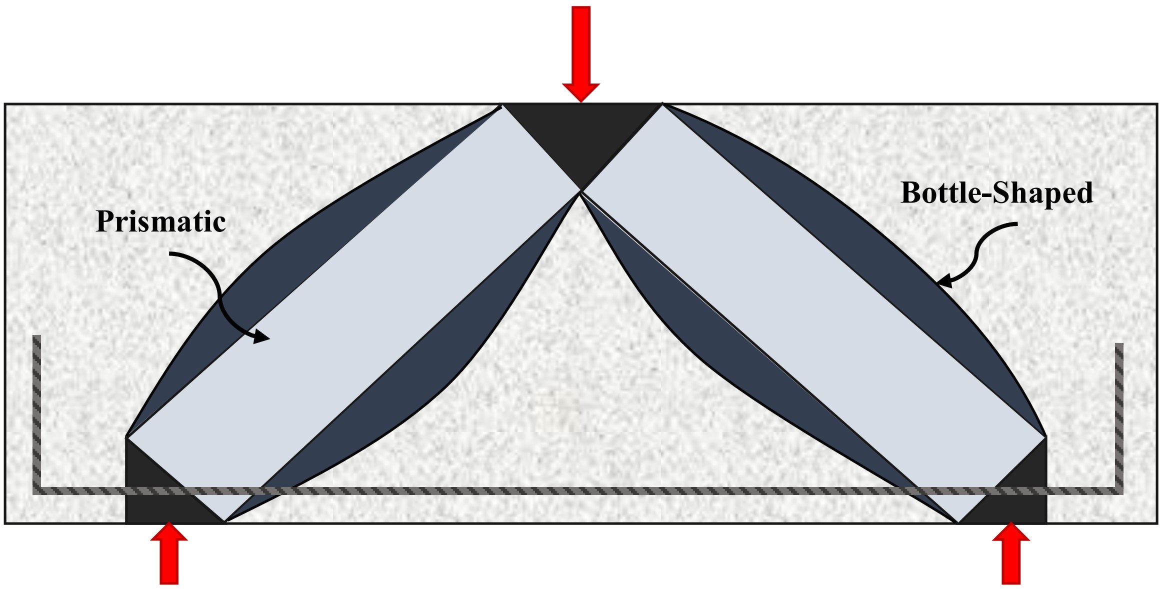

Figure 2-5: STM containing bottle-shaped and prismatic struts

As seen in Figure 2-5, the prismatic strut has a constant or linearly-varying cross-sectional area along its length. For simplicity, struts are often idealized as prismatic except for a uniform compression field such as that which occurs in a flexural compression zone, a bottle shape will form. Bottle-shaped struts spread laterally along their length. This dispersion of compressive stresses was first described by Guyon (1953) as shown in Figure 2-6.

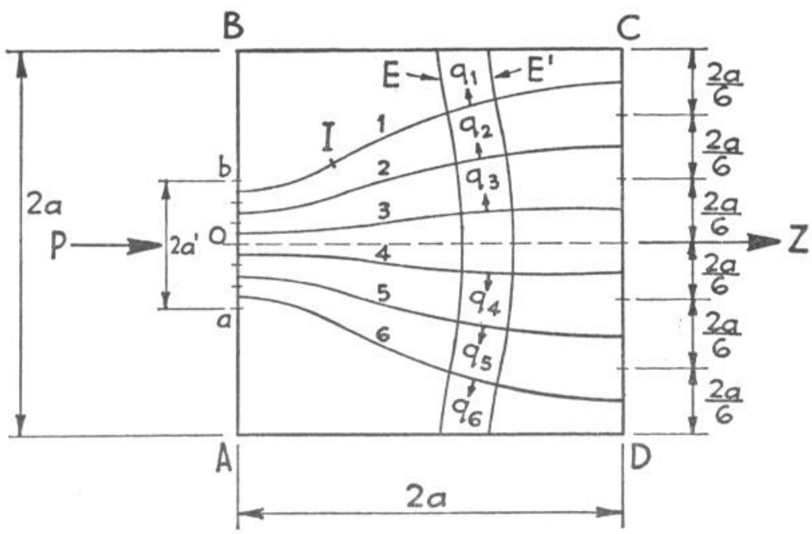

Figure 2-6: Dispersion of Compressive Stress (Guyon 1953)

Guyon applied St. Venant's principle to hypothesis that the lines of compression must be parallel to the applied force at a distance equal to one member depth away from the point of application. Figure 2-6 illustrates a spread of stresses at a maximum ratio of approximately 2:1 (length to width). The spread of stresses seen in a bottle-shaped strut introduces tensile stresses transverse to the strut. The presences of tensile stresses in the strut can potentially lead to cracking along the length (Figure 2-7), premature failure, or both.

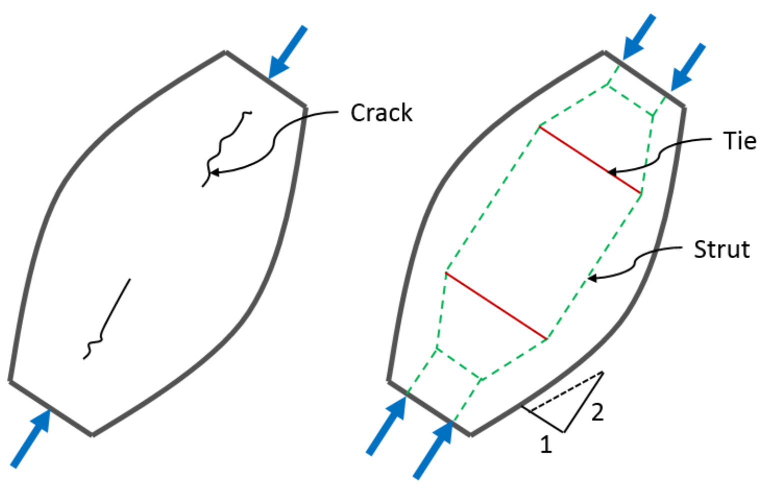

Figure 2-7: Bottle shaped strut adapted from (ACI 318 2014)

To control cracking in this area, transverse reinforcement should be provided. Current design recommendations are further discussed in Section 2.3.4.

2.3.2.3 Tie

Ties are the tensile members of an STM. Ties can include web and longitudinal reinforcement. In general, the centroid of reinforcing steel is placed at the tie locations in an STM. Anchorage of a tie is one of the most critical details designers need to consider as inadequate anchorage is a common source of failure. Current design recommendations are further discussed in Section 2.3.4.

2.3.2.4 Nodes

Struts and ties converge at nodes. They are analogous to joints in a truss. If more than three forces intersect at a node, the forces are often resolved into three resulting forces. There are different types of nodes depending on the elements framing into them. For example, a CCT ("C" stands for compression and "T" for tension) node is one which connects two struts and one tie. Figure 2-8 illustrates three different types of nodes.

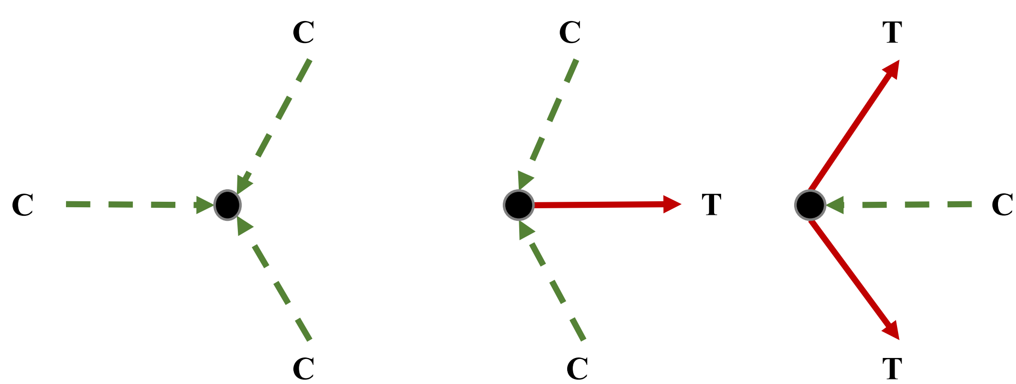

Figure 2-8: Classification of Nodes (ACI 318-14)

A node can be hydrostatic or non-hydrostatic. A node is hydrostatic if the stresses on all faces are equal. If stresses are equal on all sides, then principal stresses are equal, and shear stresses do not exist within the node. Stresses on the faces of non-hydrostatic nodes, on the other hand, are not equal thus causing shear stress within the node. These hydrostatic and non-hydrostatic states of stress are illustrated in Figure 2-9.

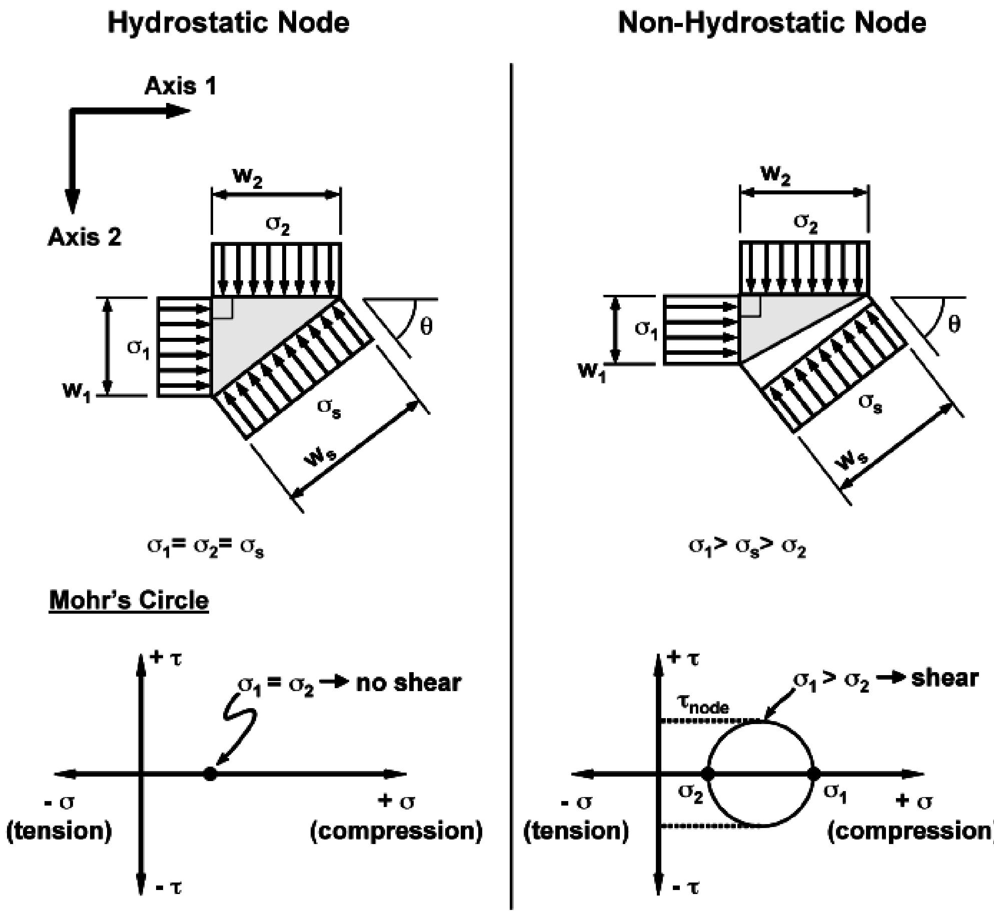

Figure 2-9: Stresses on Hydrostatic and Non-Hydrostatic Nodes (Thompson 2002)

In reality, the convergence of forces in an STM does not look exactly like and idealized node. The proportioning techniques available for nodes are established for consistency and ease of model creation. For hydrostatic nodes, the width of the interface (size of the strut) is based on the bearing stress which can result in an unrealistically large strut with shallow strut angles. Unlike hydrostatic, non-hydrostatic nodes are proportioned based on well-established guidelines which consider additional details such as location of longitudinal reinforcement and flexural capacity.

2.3.3 Nonlinear Analysis

Nonlinear finite element analysis of a D-region of concrete is a highly sophisticated method which combines the material properties of concrete and steel reinforcement with the load-deformation behavior of the reinforced concrete matrix. This results in a complex design procedure which is near impossible to analyze without computational software to aid in the calculations. This complexity in behavior stems from the nonlinear behavior of concrete, and the 'softening' of the modulus of elasticity due to tensile cracking.

An advantage to using the nonlinear analysis method for designing D-regions is, if executed properly, the procedure can predict load deformation behavior with good certainty (Park and Kuchma 2007). A disadvantage to using the nonlinear analysis method would be its dependency on model parameters and advanced experience of the user. It is difficult to model a B-Region of reinforced concrete due to the complex interaction of stresses between the reinforcing steel and concrete, let alone a region with more complexity with regard to plasticity and nonlinearity.

The procedure for developing a model divides the D-regions into a designated number of 'elements' which are then assigned parameters such as material properties, dimensions, and elasticity behavior. A general purpose model is typically based on two material models, concrete and steel, which are combined with models involving their interaction with each other for both short and long term behavior.

Given the limitations of strut and tie modeling, and the challenges associated with a nonlinear finite element analysis, researchers have attempted to combine and optimize these two approaches. Yun (2000) developed a nonlinear strut and tie model approach that can account for both limitations. The procedure requires the designer to iteratively assign and check geometric assumptions and elemental stresses.

Expanding on the combined approach, Liang et al. (2013) optimizes the STM model through a nonlinear analysis method called the "Performance-Based Optimization" technique. The technique attempts to minimize strain energy which in turn maximizes overall stiffness. This technique is made up of an algorithm which utilizes the finite element analysis method to identify elements in the model that are ineffectively carrying load. This results in the gradual removal of elements resulting in the "optimized model" essentially finding the path which minimizes the strain energy in the STM.

2.3.4 Strength Design Using an STM

Strut and tie modeling requires an understanding of basic member behavior and informed engineering judgement. This method is not a "cookbook" procedure but a design tool that requires experience. This process is illustrated by the flowchart shown in Figure 2-10.

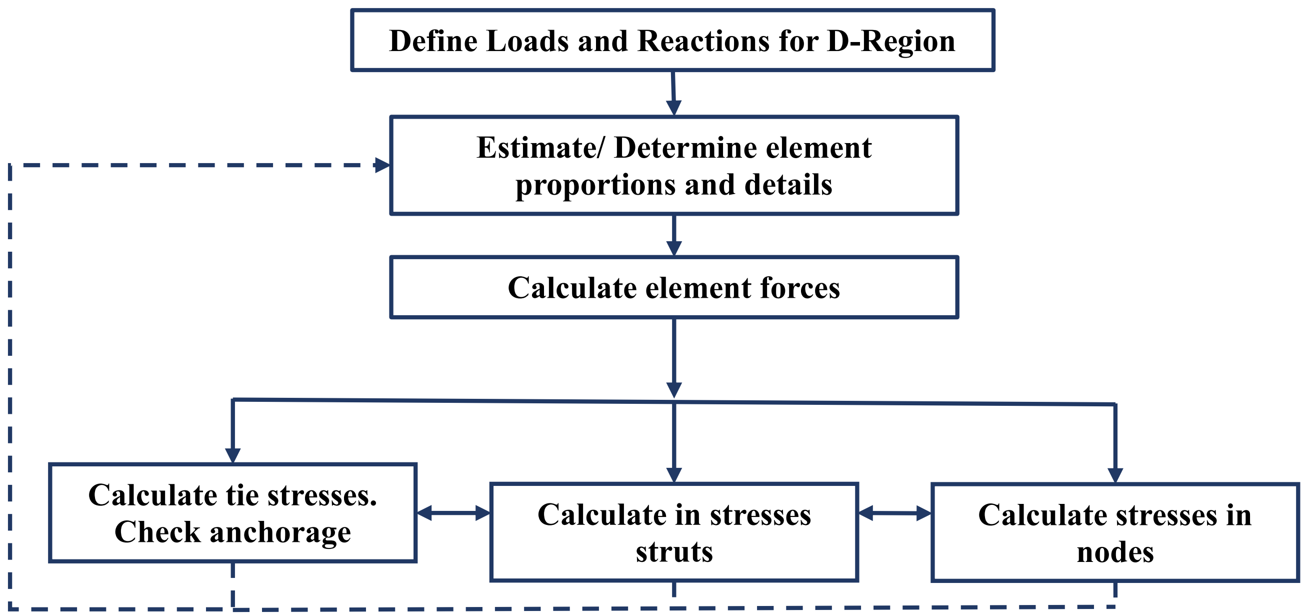

Figure 2-10: Strut and Tie Design Flowchart

Once a designer has assigned an STM to a D-region, proportioning the nodes and struts and selecting tie reinforcement to achieve equilibrium without exceeding the limiting stresses must satisfy Equation 2-1:

Equation 2-1

$$\varphi F_n > F_u$$

Where,

φ = Strength reduction factor

F_n = Nominal capacity of strut, tie, or node

F_u = Factored force resisted by strut tie or node

For concrete elements, F_n is taken as:

Equation 2-2

$$F_n = v * f_c' * A_n$$

Where,

v = Factor related to efficiency or effectiveness of concrete compressive strength in the presence of varying degrees of tension

f_c' = specified compressive strength of concrete

A_n = Effective area of concrete strut or node face

For steel reinforcement, F_n is taken as:

Equation 2-3

$$F_n = f_y * A_s$$

Where,

f_y = Specified tensile strength of steel reinforcement

A_s = Area of steel reinforcement

The efficiency of a strut is dependent on the amount of transverse reinforcement crossing its longitudinal axis. Struts that contain “minimum reinforcement” have a higher efficiency factor than those that do not. Per ACI 318-14, the minimum reinforcement crossing the strut axis can be satisfied by Equation 2-4.

Equation 2-4

$$\sum \frac{A_{si}}{b_s s_i} sin\alpha_i \geq 0.003$$

Where,

A_{si} = is the total area of disturbed reinforcement at spacing

s_i = The spacing in the *i*-th direction of reinforcement crossing a strut at angle to the axis of strut

α_i = The strut angle relative to the *i*-th axis

b_s = the width of the strut.

Nodal zone efficiencies are dependent on the presence of tensile strains caused by the anchorage of one or more ties within the node (Table 23.9.2 of ACI 318-14). Interfaces for these nodes can be proportioned per the commentary of ACI 318-14 (Figure 2-11). The nodal zone coefficient helps to ensure nodes anchoring one or more ties are sufficiently designed.

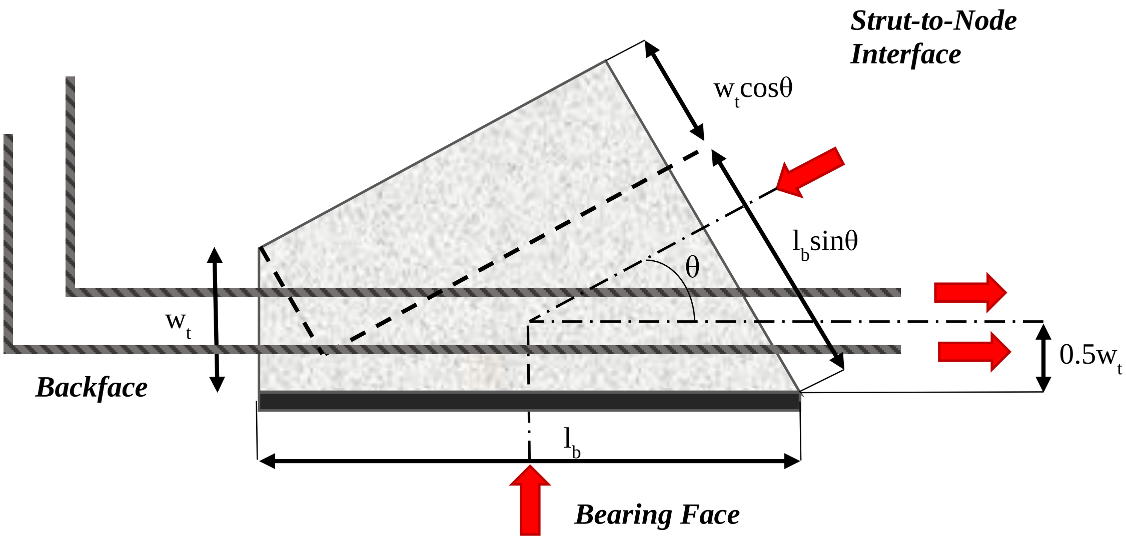

Figure 2-11: CCT Node

The strut-to-node interface, w_s, is determined by Equation 2-5.

Equation 2-5

$$w_s = l_b sin\theta + w_t * cos\theta$$

Where,

l_b = Length of bearing plate, in.

w_t = Height of backface of node equal to the minimum of two times the distance between centroid of tie and exterior surface, or $\frac{F_{nt}}{f_{ce}b_s}$, in.

θ = Angle of strut measure from the horizontal axis

Equation 2-5 is included in Figure R23.2.6b of ACI 318-14. The proportioning of the CCC node is show in Figure 2-12.

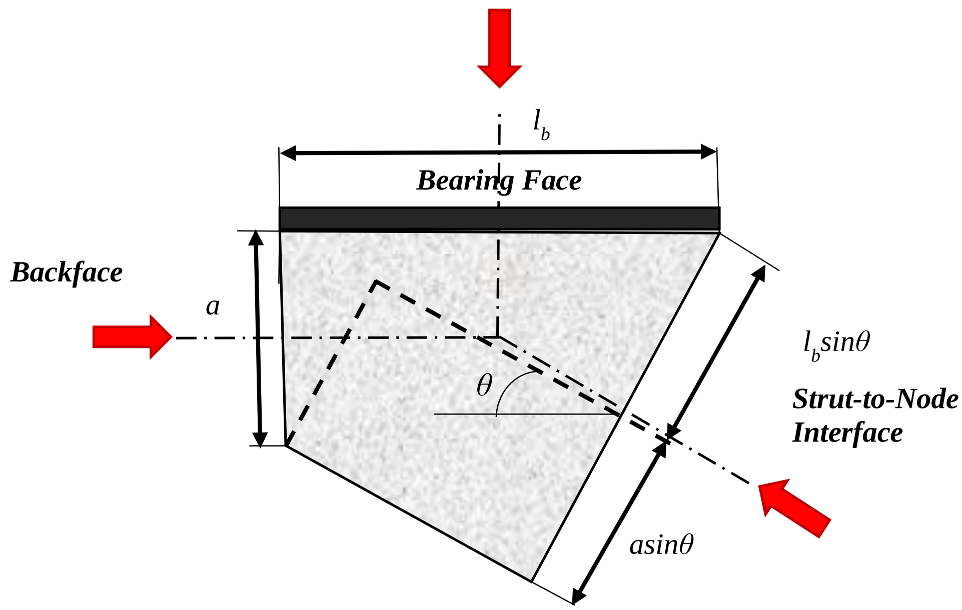

Figure 2-12: CCC Node

The depth of the backface, *a*, is equal to:

Equation 2-6

$$a = \frac{A_s f_s - A_s' f_s'}{0.85 f_c' b_w}$$

Where,

A_s = Area of tension reinforcement, in^2

A_s' = Area of compression reinforcement, in^2

b_w = Web width, in.

f_c' = Specified concrete compressive strength, psi

f_s = Stress in tension reinforcement, psi

f_s' = Stress in compression reinforcement, psi

CTT nodes, or nodal zones containing two tie anchorages can be classified as either "discrete" or "smeared". Discrete nodes are bounded by defined loading regions and their dimensions are straight-forward. Smeared nodes are typically interior and their dimensions required more subjective judgement. One type of CTT node of interest to this project is a "curved-bar node". While smeared, the dimensions of this node are theoretically established (Klein 2008). To develop the tie prior to concrete crushing, a bend radius as shown in Figure 2-13 and Equation 2-7 is recommended.

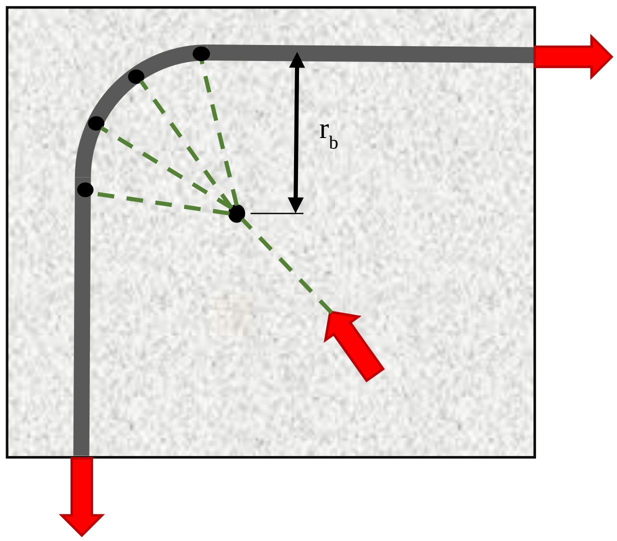

Figure 2-13: Curved Bar CTT Node

The radius of bend that is included in the nodal zone is explained by Equation 2-7.

Equation 2-7

$$r_b \geq \frac{A_{ts} f_y}{b_s f_{ce}}$$

Where,

A_{ts} = Area of non-prestressed tie reinforcement

f_y = the specified yield strength of tie reinforcement

b_s = The width of the strut transverse to the plane of the STM

f_{ce} = allowable nodal stress as specified by ACI 318-14

2.3.5 Serviceability Design using an STM

2.3.5.1 Overview

While an STM design will be conservative, it is entirely possible it will experience unacceptably large cracks or deflections while in service. Currently, serviceability limit states are satisfied via prescriptive requirements. By meeting these requirements, appropriate serviceability is presumed. This section will discuss the current state of practice with regard to serviceability in an STM.

2.3.5.2 Current Provisions

Current provisions related to serviceability in D-regions are assumed given the ACI 318-14 Chapter 24 requirements are satisfied. These provisions include the following:

- 9.9.3.1 Distributed reinforcement along the side faces of deep beams shall be at least that required in a) and b)
    a) The area of distributed reinforcement perpendicular to the longitudinal axis of the beam, A_v, shall be at least $0.0025b_ws$, where s is the spacing of the distributed transverse reinforcement.
    b) The area of distributed reinforcement parallel to the longitudinal axis of the beam, A_{vh}, shall be at least $0.0025b_ws_2$, where s_2 is the spacing of distributed longitudinal reinforcement.
- 9.9.4.3 Spacing of distributed reinforcement required in 9.9.3.1 shall not exceed the lesser of $d/5$ and 12 in.

The commentary for provision 9.9.3.1 states this requirement is to limit the width and propagation of cracks. By satisfying the above provisions, crack widths in service are generally assumed to be within allowable limits. Thus, service-level crack widths are indirectly controlled through minimum reinforcement requirements. While not stipulated by ACI 318-14, researchers and other codes of practice attempt to establish an "acceptable" maximum crack width. Oesterle (1997) surveyed practicing engineers on their opinion of a visually observed crack. The results of this study found that a crack width of 0.008-in. was acceptable by 100% of the observers; a width of 0.012-in. was acceptable by 50% of the observers; and width greater than 0.016-in. was unacceptable. ACI 224 provides a "guide to reasonable crack widths in reinforced concrete under service loads" which is summarized by Table 2-1.

Table 2-1: Guide to Reasonable Crack Widths for Reinforced Concrete Under Service Loads (ACI 224 2008)

	Crack Width (in.)	
Exposure Condition	(in.)	(mm)
Dry air or protective membrane	0.016	0.41
Humidity, moist air, soil	0.012	0.30
Deicing chemicals	0.007	0.18
Seawater and seawater spray, wetting and drying	0.006	0.15
Water-retaining structures	0.004	0.10

The *fib* Model Code (2010) contains explicit crack width equations and a limiting range between 0.008 and 0.012 in. depending on exposure classification.

2.3.5.3 Past Studies

After Kumar (1978) first introduced the principle of minimizing strain energy in an "associated truss" to optimize load transmission, the idea of improving serviceability performance through minimizing strain energy was discussed more closely by Schlaich et al. (1987). Schlaich et al. aimed to provide a consistent STM design approach for reinforced concrete structures with regard to safety and serviceability. Accordingly, they recommend selecting a truss model that most closely matches the elastic distribution of forces. Thus, the optimal model is that whose elemental paths require the least deformation and results in the smallest total strain energy. This is explained by Equation 2-8.

Equation 2-8

$$\int F * \Delta = \sum FL\varepsilon = minimum$$

Where,

F = Force in strut or tie

L = Length of member

Δ = Axial deformation of the strut or tie

ε = Mean strain in member

Equation 2-8 is derived from the principle of minimum strain energy for linear elastic materials. According to the conservation of energy, the external work done on a structure is transformed into internal strain energy (Equation 2-9)

Equation 2-9

$$W = U = \sum \frac{F^2 L}{2EA}$$

Where,

W = External work

U = Internal strain energy

E = Modulus of elasticity in strut or tie

A = Cross-sectional area of strut or tie

As the summation of internal strain energy is related to total deformation, it stands to reason that a relationship exists between the degree of cracking of a D-region and the internal strain energy estimated from a STM (i.e. Equation 2-9). Accordingly, minimizing the internal strain energy would minimize cracked area of concrete (Equation 2-10).

Equation 2-10

$$U_{total} \propto A_{cr} = \sum l_c * w_{avg}$$

Where,

U_{total} = Total strain energy in a representative STM

A_{cr} = Total area of cracked concrete

l_c = Length of crack

w_{avg} = Average crack width

The model with the least internal strain energy most closely matches the elastic stress distribution and, the model that most closely matches the elastic stresses will result in the least amount of cracking. For example, consider the "good" and "bad" model shown in Figure 2-14.

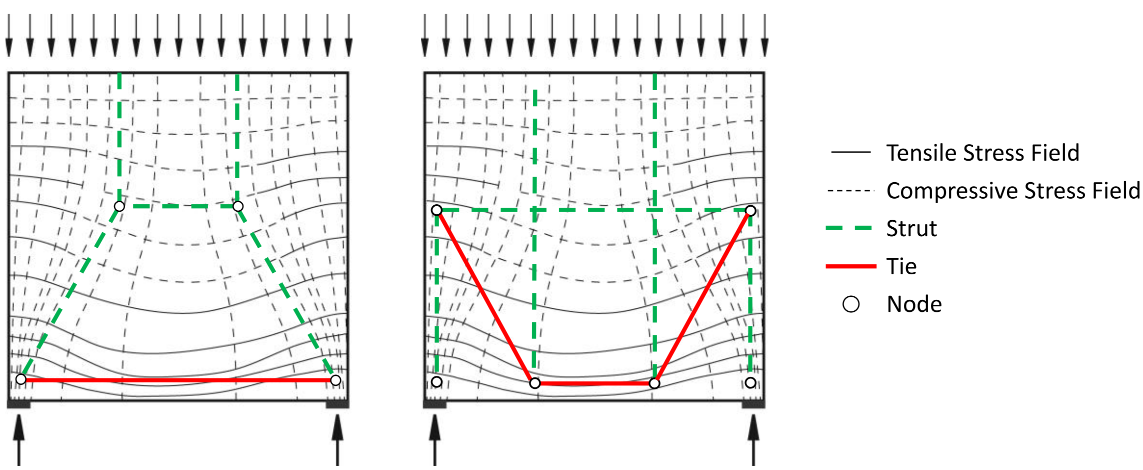

(a)"Good" model ***(b) "Bad" model***

Figure 2-14: Identical structures with force paths represented by a (a) "Good" and (b) "Bad" STM (Schlaich et al, 1987).

For the “good” model shown in Figure 2-14(a), the struts and ties are closely aligned with the resultants of the tension and compression fields and optimize the load transfer, whereas the elements of the “bad” model do not. Thus, the “bad” model would need to undergo larger deformations to transfer the same amount of force as the “good” model. As a result, the “bad” model will experience wider cracks than the “good” model when transferring the same amount of force.

It is important to note that the replacement of a set of smooth curves with discrete straight lines is, in itself, an approximation. There is no unique or singularly optimal solution, which, in turn, is another reason many practitioners lack confidence in the use of STM (Schlaich et al. 1987).

2.3.5.4 Limitations

As stated previously, strut and tie modeling is a lower bound estimate of a structures ultimate capacity. It does not predict or account for service limit states. Serviceability limit states are satisfied with prescriptive requirements.

It is good practice for a STM to agree with the dominant mechanism of force transfer in the structure. However, in many situations the “dominant mechanism of force transfer” may not be apparent. An STM satisfying equilibrium will always be valid but not all models are “good” models. An STM that forms a valid load path may potentially experience large cracks while in service, depending on its configuration. Because, if the orientation of the truss model varies significantly from the actual stress field, then the structure must undergo substantial deformation in order to develop the poorly assumed model; resulting in an unacceptable amount of wide cracking. To illustrate, consider the members shown in Figure 2-15.

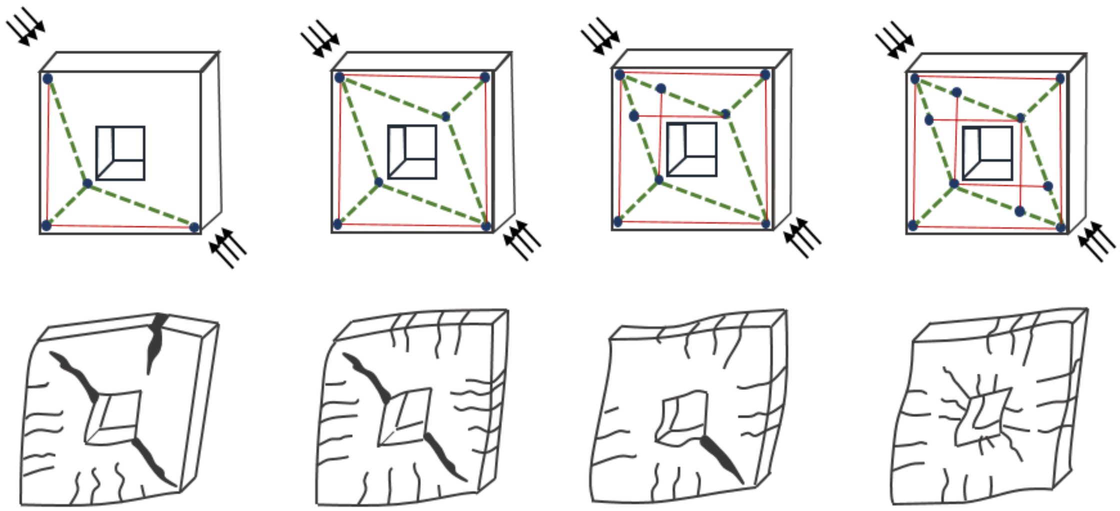

Figure 2-15: Procedure for Designing Suitable Stress Fields (Muttoni et al., 1997)

As seen in the Figure 2-15, a model satisfying equilibrium does not necessarily exhibit good cracking behavior. The best performing model aligns struts and ties with elastic fields. From a designer's standpoint, determining this best model is not always clear. This ambiguity can be considered a disadvantage as it relies on designer intuition.

2.4 Crack Width Database

2.4.1 Overview

In addition to the current program, a database of experimental data from past studies (Kong et al., 1970; Smith and Vantsiotis, 1982; Birrcher et al., 2009; and Deschenes, 2009) of D-regions was compiled. Generally, past studies provide little or no crack width information. Thus, the collected data are limited. The current database includes 100 beams. The relative cross-sections are shown in Figure 2-16. The studies involving those beams are further discussed in this section.

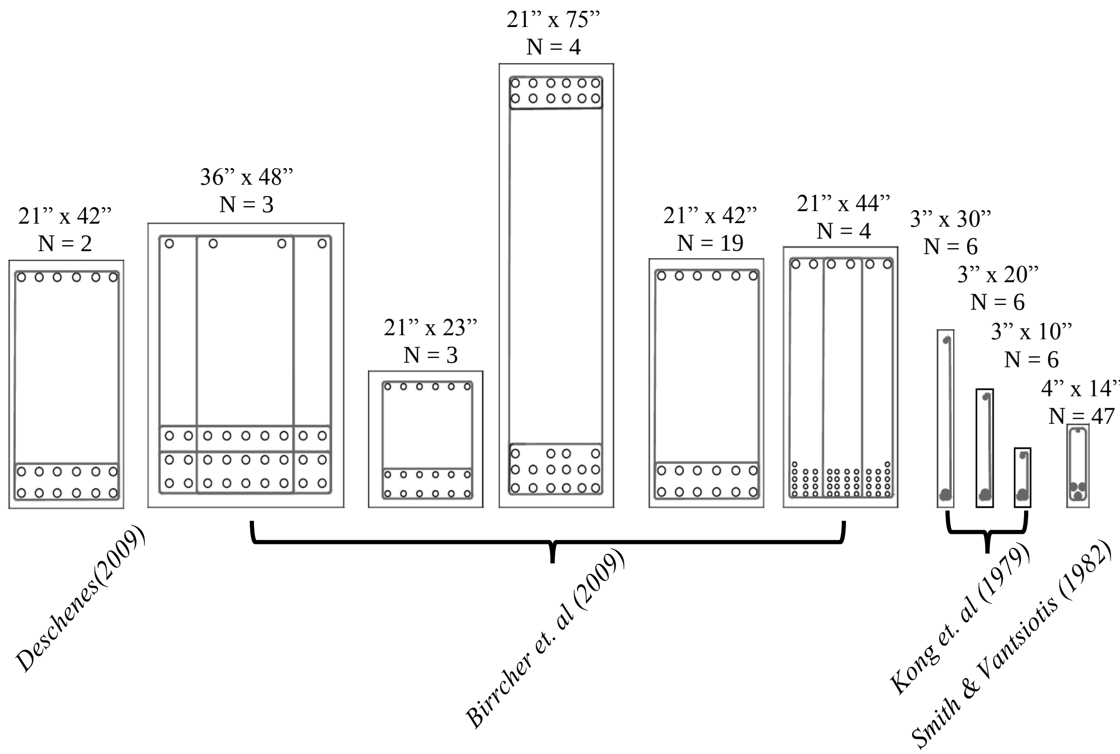

Figure 2-16: Cross-sectional dimensions and number of beams in the database

2.4.2 Kong et al., 1970

Kong et al. (1970) investigated the influence of various types of web reinforcement on the cracking behavior and strength of deep beams. Their testing program included 35 rectangular deep beams with widths of 3 in. and heights ranging from 10 in. to 30 in. The *a/d* ranged from 1 to 3. Transverse web reinforcement was used throughout the testing program. Seven series containing a different configurations of web reinforcement spacing and orientation were investigated. The beams were simply supported and the test setup was consistent for all beams.

Average and maximum crack width data were collected at each load increment after the cracking load using a hand microscope of 20 magnifications and the crack pattern was mapped. To facilitate crack observations, beams were white-washed before testing. To establish locations of cracks, a grid was drawn on the beam. Because of space limitations, only the crack widths for beams with heights of 30, 20, and 10 in. for each series were provided.

Kong et al. (1970) observed that average crack width increased with larger *a/d*. The average crack widths did not exceed 0.5 mm (0.02 in) even for the some beams which contained no web reinforcement. Also, it was observed that flexural cracks generally stop growing after the formation of diagonal cracks. The primary cause of failure was from diagonal cracking with concrete crushing at the bearing surface. Lastly, the test results indicate the influence of web reinforcement on max crack followed the same pattern as the influence on average crack.

Of the 35 beams tested, series 7, which contained no web reinforcement were omitted from the database because they did not contain either sufficient load or crack width data.

2.4.3 Smith and Vantsiotis, 1982

This study investigated the influence of web reinforcement and *a/d* on the inclined shear cracking behavior and ultimate shear strength, midspan deflection, tension reinforcement strain and maximum crack width of deep beams. The testing program included 52 rectangular deep beams with 4 x 14-in. cross-section. The testing program, consisted of four series with different *a/d* (0.77, 1.01, 1.34, and 2.01). Web reinforcement was provided for all but 5 beams. Web reinforcement included both horizontal and vertical #2 deformed bar. Steel reinforcement was used throughout the testing program. Another variable in the testing program was the spacing and orientation of the web reinforcing. The beams were simply supported and the test setup was consistent for all beams.

All beams were made with Type III cement and cured for 7-8 days before white-washing and testing. Beams were loaded monotonically at 10-kip increments. At each load increment, applied load, end reactions, midspan deflection, maximum crack width and longitudinal steel strain at midspan and points of application were measured. Photographs were taken to document the cracking pattern at each increment. The means of collecting crack widths is not specified. Crack widths reported are only maximum diagonal cracking.

It was observed that none of the beams crack under 20% of the ultimate load. Between 50 to 60% of ultimate, a diagonal crack formed in all tests. For some beams, the diagonal crack appeared to be initiated by a flexural crack which originated in approximately the same location. The most stable propagation of cracks (i.e. no large increase of crack widths for increases in load) was observed at approximately 60 to 70% ultimate load. At this point, the maximum crack width did not exceed 0.012 in. At about 85 to 90% of ultimate load, new diagonal cracks formed parallel to the existing diagonal cracks. The maximum crack width for all beams never exceeded 0.03 in. Failure occurred in either reduced compression zone in the nodal region or by fracture of concrete due to diagonal crack.

2.4.4 Birrcher et al., 2009

The purpose of this study was to study the effects of distribution of stirrup legs transversely through the web, triaxial confinement, quantity of web reinforcement, member depth, and *a/d* on the strength and serviceability behavior of D-regions. The testing program included 37 reinforced deep beams with varying cross-sectional areas with a width of 21 in. and depths ranging from 23 to 75 in. All beams contained steel reinforcement and 36 of 37 beams contained web reinforcement.

The testing procedure consisted of loading the beam monotonically in increments of 50-150 kip (approximately 10% of the expected capacity depending on specimen size). At each load increment, cracks were marked and the width of the largest diagonal crack was measured using a crack comparator card. Photographs were also taking at each increment to document crack propagation.

It was observed that diagonal cracks first form between 20 to 35% of the ultimate capacity, regardless of the *a/d*. Also, the increase of depth between the 42- and 75-inch deep beams did not have an effect on the maximum width of diagonal cracks. However, the 23-in deep beams had consistently narrower diagonal crack widths. The maximum diagonal crack widths at approximately 50% of ultimate capacity did not exceed 0.06 in. The largest cracks measured near 95% of ultimate capacity ranged were as large as 0.16 in. The researchers noted a minimum amount of web reinforcement of approximately 0.2% is needed for maintaining the integrity of the strut and a minimum amount of approximately 0.3% is needed for limiting service-level crack widths to less than 0.016 in.

Of the 37 beams tested, four were omitted from the database because they did not contain either sufficient load or crack width data.

2.4.5 Deschenes, 2009

The purpose of this study was to investigate the structural safety of deep beams subject to alkali-silica reaction (ASR) and delayed ettringite formation (DEF). The testing program included six reactive specimens along with one "validation" beam and one non-reactive control beam. The validation beam was also non-reactive and is included in the database for the current study. The cross-sections of all beams were 21 x 42-in. and all beams contained steel reinforcement and web reinforcement.

During testing, each beam was monotonically loaded to failure in increments of 15 to 100 kips. At each load increment, cracks were documented. All cracks were marked for later mapping, photographs were taken to track the crack propagation, and the largest diagonal crack's width was measured. A crack comparator card was used for the measuring of cracks during testing.

The first observed diagonal cracks formed at 25 to 30% of the ultimate capacity. A single web-shear crack then formed and grew towards the point of applied load between 40 to 80% of ultimate capacity. The failure of the two nonreactive beams occurred from splitting of the strut on the inside edge near the load bearing plate. No recommendations with regards to serviceability were made.

2.4.6 Summary

Crack width data was collected from past research (Kong, Robins, and Cole 1970; Smith and Vantsiotis 1982; Birrcher et al. 2009; Deschenes 2009). Along with this data collection, predictive models in the literature are also gathered (Walraven 1981; Mihaylov et. al. 2014) and further discussed in Section 2.5. Table 2-2 provides a summary of the characteristics of the beams in the database.

Table 2-2: Beams in Crack Width Database

Reference	*Year*	*No. of Beams Tested*	*a/d*	$b_w d$ (in^2)	*Reinforcement Ratio* ρ_h	ρ_v
Kong et al	1970	6	0.35 - 1.18	26-86	0.61%-0.86%	0.0%-0.61%
Smith & Vantsiotis	1982	47	0.94 – 1.96	51	0.23%-0.91%	0.18%-1.25%
Birrcher et. al.	2009	33	1.84 - 2.50	410-1450	0.0%-0.3%	0.0%-0.45%
Deschenes	2009	2	1.85	760	0.58%	0.30%

The entire database including measure crack widths at service loads (50% ultimate) and ultimate loads is in Appendix A.

2.5 CRACK WIDTH PREDICTION MODELS

2.5.1 Overview

This section presents models proposed by others for predicting the maximum diagonal width of serviceability cracks for D-regions. Though crack width prediction models exist for slender beams (Frosh 1999; Gergely and Lutz 1968), this section only includes those applicable to D-regions.

2.5.2 Walraven, 1981

This study was the first to explore the mechanism of force transmission across cracks which are subject to shear displacement. The testing program included pre-cracked shear specimens (0.01 to 0.03-mm initial cracks). The variables were type of reinforcement (internal reinforcement versus external restraints), concrete strength ($12 < f_c' < 60$ MPa), continuity of concrete (B- versus D-region), type of concrete (normalweight versus lightweight) maximum size of aggregate (16 and 32 mm) and initial crack width. The cross-sectional dimensions were approximately 16 in. x 24 in. During testing, shear displacements and crack widths were measured using instrumentation with an accuracy of 0.01mm (0.003 in.). Crack widths were measured at a pre-determined location at about mid-depth of the test specimen. Specimens were loaded at a constant rate and shear displacement and crack width data were collected. The results of the study suggest a relationship between the shear displacements of cracked faces (Δ) and the width of crack (w). The relationship is shown in Equation 2-11.

Equation 2-11

$$\frac{d\Delta}{dw} = w^{0.18}(1.65 + 2.10w) - 1.5\Delta$$

This study provided insight into the role of aggregate interlock as a mechanism to transfer force across cracks. It was concluded all available results during the time of testing were “satisfactorily predictable” by Equation 2-11.

2.5.3 Mihaylov et. al., 2014

Mihaylov et al. developed a method for predicting the shear capacity of deep beams using a two parameter kinematic theory. The two parameters, rotation about the top of the crack and a vertical translation, are combined with equilibrium equations and stress-strain relationships to form a theory to predict the shear strength of deep beams. Thus, their expression for maximum shear capacity is a function of the maximum diagonal crack width and can be rearranged in terms of the maximum diagonal crack width. The total shear resistance of a beams found using Equation 2-12.

Equation 2-12

$$\boldsymbol{V = V_{CLZ} + V_{ci} + V_s + V_d}$$

Where,

V_{CLZ} = Shear force resisted by the critical loading zone

V_{ci} = Shear force resisted by aggregate interlock

V_s = Shear force resisted by stirrups

V_d = *Shear force resisted by dowel action*

The shear force contributed by the aggregate interlock V_{ci} is a function of crack width and is given in Equation 2-13.

Equation 2-13

$$V_{ci} = \frac{0.18\sqrt{f_C'}}{0.31 + (\frac{24w_{cr}}{a_g + 16})} bd$$

Where,

w_{cr} = Maximum crack width (mm)

f_c' = Compressive strength of concrete (MPa)

b = Beam width (mm)

d = effective depth of section (mm)

The equation provide to calculate the maximum crack with is given in Equation 2-14.

Equation 2-14

$$\boldsymbol{w_{cr} = \Delta_c * cos\theta + \frac{\varepsilon_t l_k}{2sin\theta}}$$

Where,

Δ_c = Ultimate shear displacement (Equation 2-15)

s_{max} = Maximum spacing of radial cracks (Equation 2-16)

l_k = Length of bottom reinforcement's elongation contributing to crack width (Equation 2-17 and Equation 2-18)

ε_t = Strain along bottom longitudinal reinforcement (Equation 2-19)

θ = Angle of diagonal cracks in uniform stress field

The above variables are calculated using the following equations.

Equation 2-15

$$\boldsymbol{\Delta_c = 0.0105 l_{b1e} cot\alpha}$$

Where,

l_{b1e} = Effective width of bearing plate parallel to longitudinal axis of member

α = Angle of line extending from inner edge of support plate to far edge of tributary area of loading plate responsible for shear force (V).

Equation 2-16

$$\boldsymbol{s_{max} = 0.28d_b \frac{2.5(h-d)}{\rho_l d}}$$

Where,

d_b = Diameter of longitudinal reinforcing steel bars

ρ_l = ratio of bottom longitudinal reinforcement

h = Total depth of section

d = Effective depth of section

Equation 2-17

$$\boldsymbol{l_k = l_0 + d(cot\alpha - cot\alpha_1)}$$

Where,

l_0 = Length of heavily cracked zone at bottom of critical diagonal crack

α_1 = Angle of critical diagonal crack

Equation 2-18

$$\boldsymbol{l_0 = 1.5(h-d)cot\alpha_1 \geq s_{max}}$$

It should be noted that α is approximately equal to α_1 and thus, l_0 is equal to l_k.

Equation 2-19

$$\boldsymbol{\varepsilon_t = \frac{T_{max}}{E_s A_s} = \frac{Va}{E_s A_s(0.9d)}}$$

Where,

T_{max} = Maximum tensile force in bottom reinforcement

a = Shear span

A_s = Area of longitudinal reinforcing bar on flexural tension side

E_s = Specified modulus of elasticity of steel reinforcing bars

V = The total shear resistance of deep beams

The calculation for both shear strength is iterative since the total shear capacity depends on crack width which is depended on tie strain which is dependent on shear. This circular referencing goes on until equilibrium satisfied. Though the authors' original intention was not to predict service load cracking, it is of interest to compare their equation against the database. So, this method was applied to the beams to the crack width database. Max load was multiplied by 50% to simulate service level loading. The results of this analysis are shown in Figure 2-17.

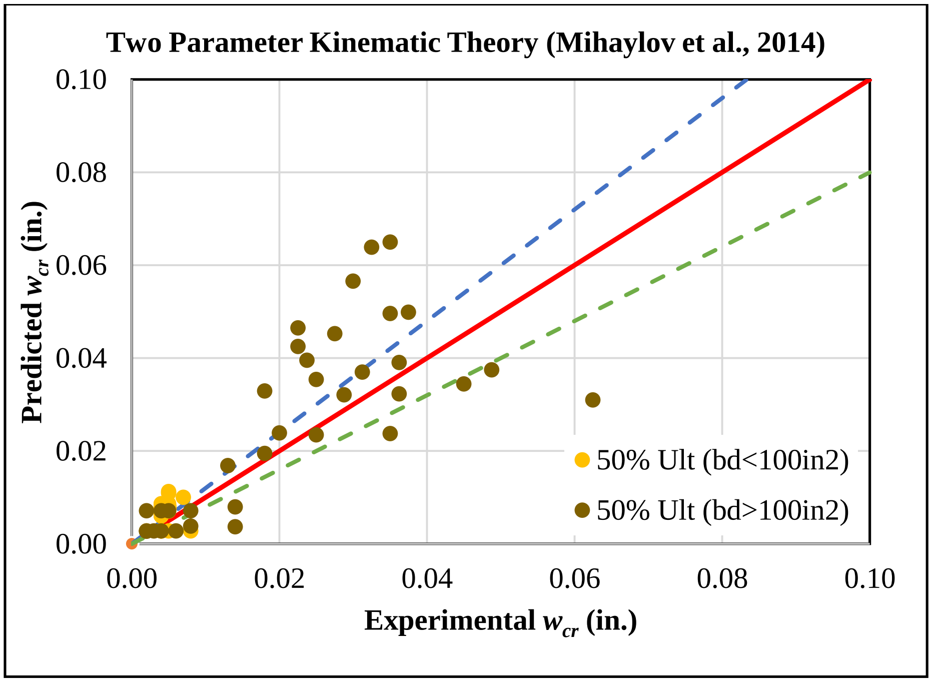

Statistics $\left(\frac{predicted}{experimental}\right)$

N = 100

Min. = 0.27

Mean = 1.48

Max. = 3.51

CoV = 0.37

Figure 2-17: Predicted versus experimental crack widths predicted per Mihaylov et al., 2014

Figure 2-17 shows the majority of the results indicate the predicted values for crack width are larger than the experimental values. This suggests the two parameter kinematic theory could be used as a conservative estimation of service-level crack width. To date, this is the only known approach for predicting crack widths in discontinuity regions.

2.6 CRACK COLLECTION

Methods of collecting crack widths in concrete structures have traditionally been limited to the use of a crack comparator cards (Figure 2-18a), calipers (Figure 2-18b), or microscope (Figure 2-18c).

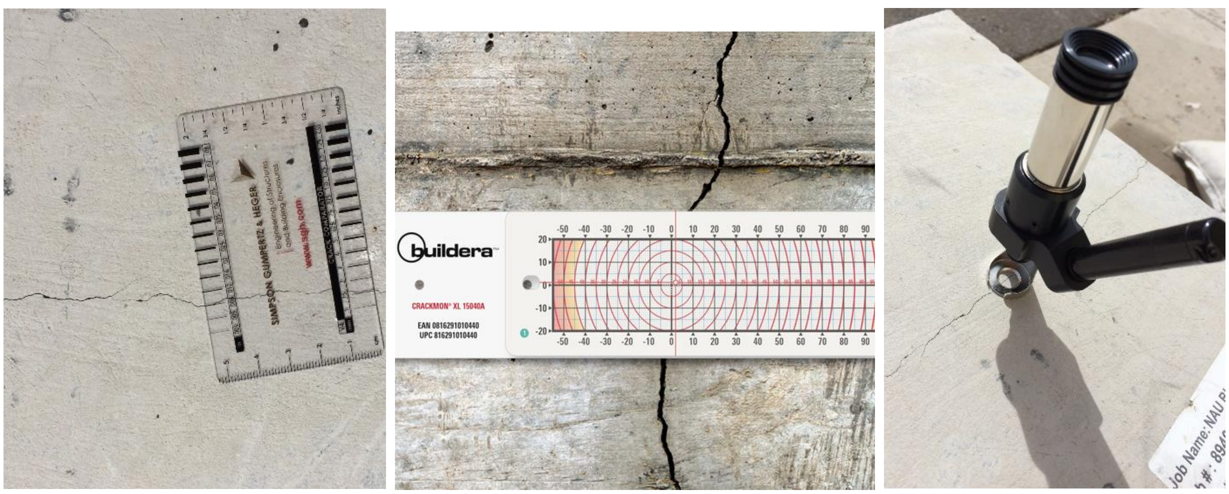

a) *b)* *c)*

Figure 2-18: a) Crack comparator card; b) Calipers and; c) Microscope

Rivera et al (2015) developed an automated procedure that used digital images and an algorithm to collect and process crack data which includes the length, width and areal density of cracks. This study was employed in part, to assist with the current labor intensive process of collecting data. The new process uses a non-contact method that is both faster and more precise, given the removal of inconsistencies of using the human eye. The results of the study show an average percent difference of 31% (with a minimum of 0% and maximum of 97%) between the new method and comparator card when measuring crack widths.

Ballard et al. (2016) also investigated a technique using digital images. This method utilized photogrammetric software (*Photomodeler*) to collect crack width measurements and compared results to crack comparator card and microscope measurements. The results of the study compared three crack collection techniques and found approximately 8-22% difference when comparing photogrammetry to crack comparator cards and 4-21% when comparing to microscopes. Consider microscopes as being the "gold standard" of crack width collection given they allow for a magnification and therefore a better visualization of crack edges. This would indicate the use of photogrammetry when comparing to microscopes, is better than the use of crack comparator cards.

2.7 NEED FOR CURRENT RESEARCH

Current design of D-regions is limited to two methods: strut and tie modeling and nonlinear analysis. Given strut and tie modeling is the predominant choice for strength design, there is a need to adapt the method for serviceability design. Currently, design provisions related to the service-limit state of D-regions are prescriptive and make no allowance for expected performance. Thus, there is a need for a serviceability design procedure that better reflects the expected in-service performance of D-regions.

Crack width data collected from past studies only includes maximum crack widths. This study will consider crack area (in addition to maximum crack widths) to represent the serviceability behavior. To date, there are no studies that contain crack area data for D-regions.

The recommendations of Schlaich et al. (1987) and the principle of minimum strain energy suggest two things. First, there is a quantitative way to determine whether a model is deemed ‘good’ or ‘bad’ (Equation 2-8). Secondly, there is likely a relationship between deformation and estimated strain energy in a representative STM (Equation 2-10). Though this relationship has merit, is has not been explored with experimental results.

Lastly, existing methods for crack width collection are labor intensive and provide limited information. Methods involving the use of digital images for the use of crack width and crack area collection have been investigated by Ballard et al. (2016) and Rivera et al., (2015). Both studies found acceptable crack measurements when using digital images in comparison with existing methods. To better inform future serviceability studies, there is a need for more comprehensive crack data. Digital imaging serves this need.

CHAPTER 3

Experimental Program

3.1 OVERVIEW

To accomplish the goals of this study, twelve concrete deep beams were designed, fabricated, and tested at Northern Arizona University. The testing program uses parameters within comparable range of past studies (Section 2.4) and uses novel approaches to measure beam deformations, crack width propagation, and area of crack surface. The variables tested include the web reinforcement, tie configuration, *a/d*, and spacing of web reinforcement. This chapter outlines the specimens' details, fabrication, instrumentation, test setup, data collected and the methods used to conduct the experimental program.

3.2 TESTING PROGRAM

3.2.1 Overview

Specimens tested for this study were proportioned and designed to fit within the range of variables tested as part of past studies (Section 2.4). In addition, the testing program was developed to investigate the serviceability behavior of concrete in terms of crack widths, crack area, and strain energy estimated in representative STM. The variables within the program included the following:

1) The configuration of the tie
2) Amount of shear reinforcement
3) Spacing of stirrups
4) Shear span-to-depth ratio

A secondary goal of this project is to refine existing methods for processing digital images and automating the collection of crack and displacement data. The procedure and instrumentation used to achieve this goal is outlined in Section 3.7.

The author developed a short hand notation for the test specimens to assist with the identification and comparison of results. The notation is given in Figure 3-1 and the test specimens are subsequently denoted.

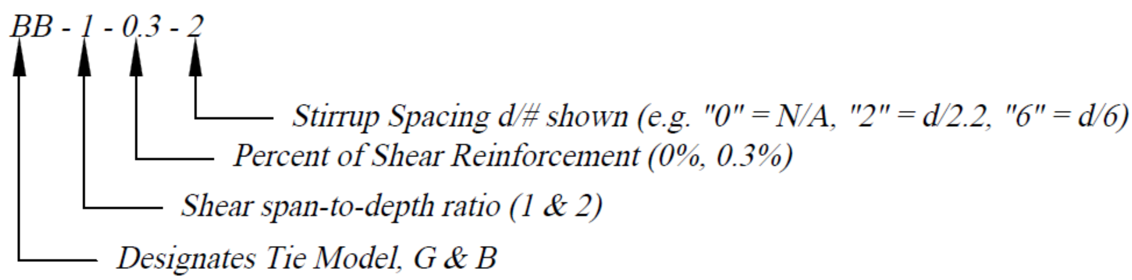

Figure 3-1: Testing Program Notation

Design constraints for test specimens stemmed from the capacities of laboratory equipment, ease of moving the beams, acceptable range in the existing database, and ensuring the specimens were “realistically-scaled”. These constraints include the following:

1) A cross-sectional area greater than or equal to approximately 100 in^2;
2) Total weight less than approximately 2000 lbs; and
3) Cross-sectional area appropriate for attaining minimum reinforcement ratios with #2 or #3 stirrups.

The testing program was divided into two series of six beams to isolate variables and allow for efficient testing. Series 1 and 2 have *a/d* ratios of 1 and 2, respectively. All other variables including web reinforcement (ρ_h and ρ_v), stirrup spacing (s_h and s_v) and size, and configuration of tie were analogous among the series. Table 3-1 provides a summary of specimen details.

Table 3-1: Testing Program

	Beam ID	Tie Model	a/d	$\rho_v = \rho_h = A_v/bd$	$s_h = s_v$
Series 1	BG-1-0.3-6	G	0.99	0.30%	d/6
	BG-1-0.3-2	G	0.99	0.30%	d/2.2
	BG-1-0-0	G	0.99	0.00%	0
	BB-1-0.3-6	B	0.99	0.30%	d/6
	BB-1-0.3-2	B	0.99	0.30%	d/2.2
	BB-1-0-0	B	0.99	0.00%	0
Series 2	BG-2-0.3-6	G	1.98	0.30%	d/6
	BG-2-0.3-2	G	1.98	0.30%	d/2.2
	BG-2-0-0	G	1.98	0.00%	0
	BB-2-0.3-6	B	1.98	0.30%	d/6
	BB-2-0.3-2	B	1.98	0.30%	d/2.2
	BB-2-0-0	B	1.98	0.00%	0

The tie models shown in Table 3-1 indicates two types: G and B. These model names are based on the recommendations of Schlaich et al. (1987). Schlaich et al. (1987) state when comparing two models identical in capacity, the model with the shorter length of ties is considered a "good" model (G) and the other a "bad" model (B). Given this suggestion, the tie configuration is labeled as "good" and "bad" based on the estimated strain energy in the STM.

3.2.2 Specimen Details

This section outlines the details of each beam tested for this project. Each series, regardless of the tie configuration, reinforcement or stirrup spacing, is designed to attain the same nominal capacity. All beam dimensional and reinforcement details are shown Figure 3-2 through Figure 3-7.

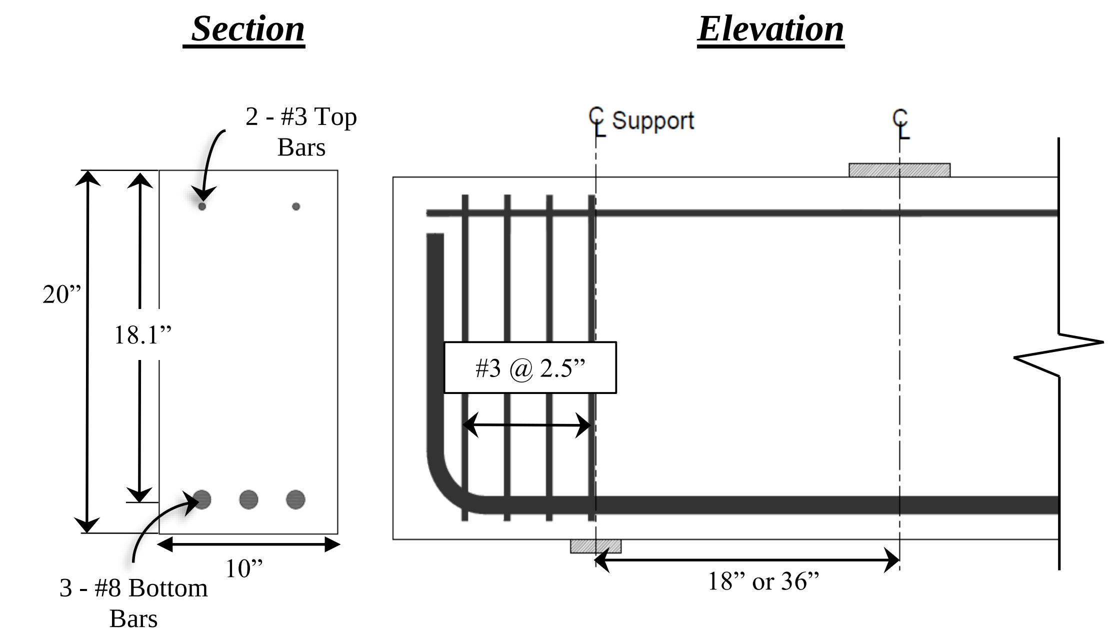

Figure 3-2: Specimens BG-1-0-0 & BG-2-0-0

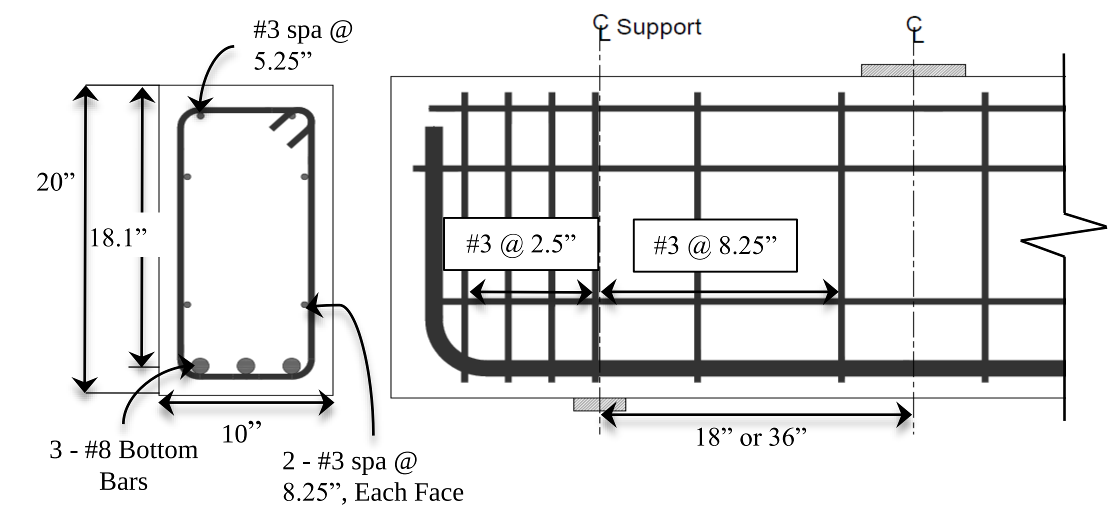

Figure 3-3: Specimen BG-1-0.3-2 & BG-2-0.3-2

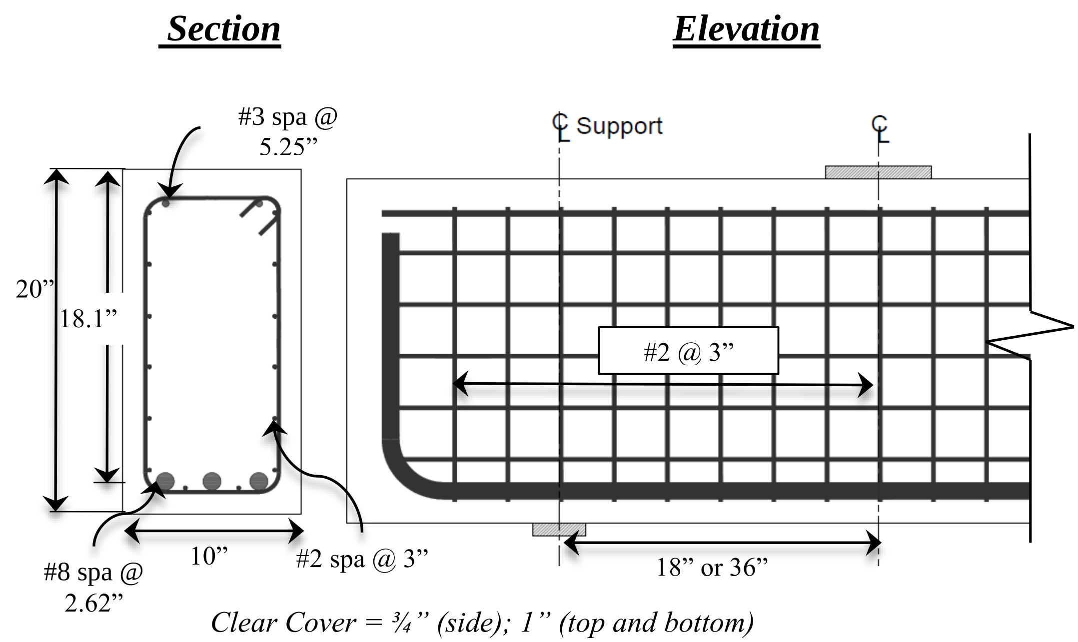

Figure 3-4: Specimens BG-1-0.3-6 & BG-2-0.3-6

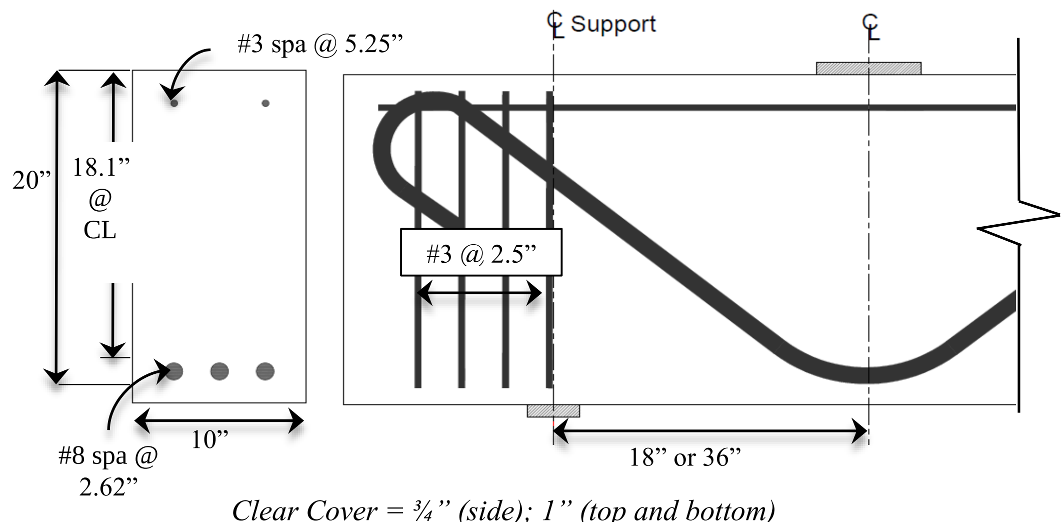

Figure 3-5: Specimens BB-1-0-0 & BB-2-0-0

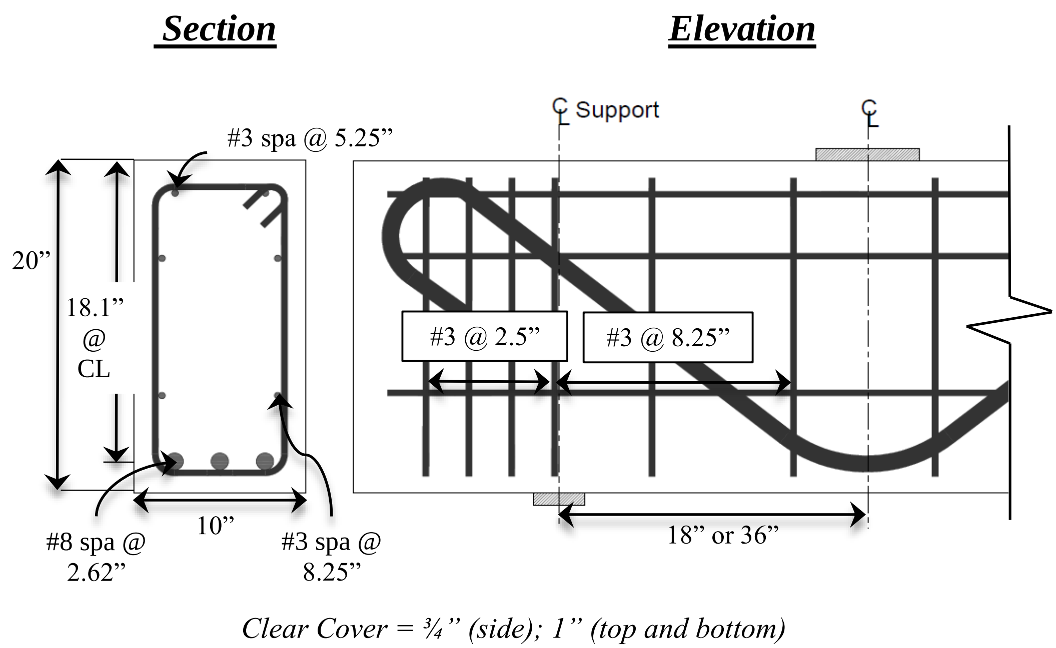

Figure 3-6: Specimens BB-1-0.3-2 & BB-2-0.3-2

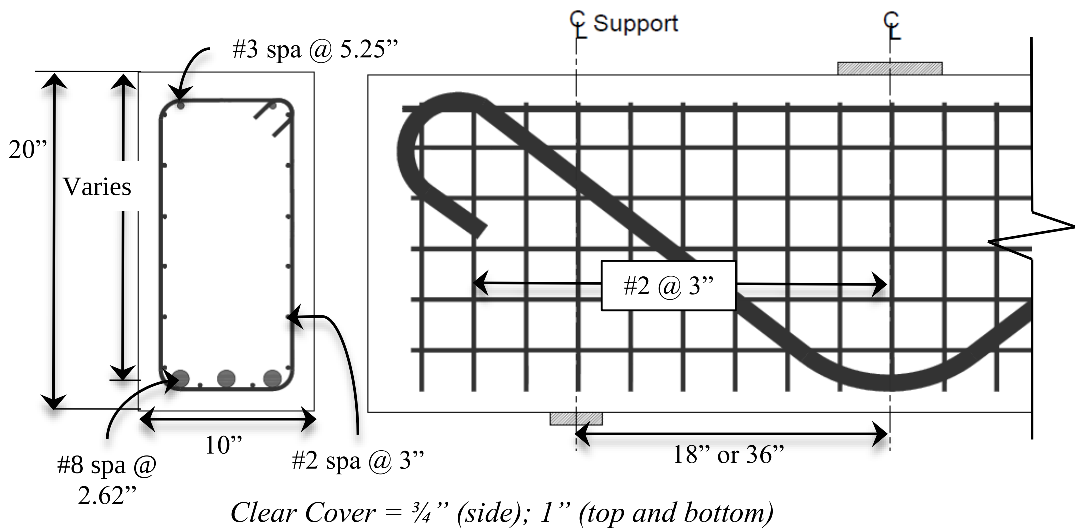

Figure 3-7: Specimens BB-1-0.3-6 & BB-2-0.3-6

It can be seen in Figure 3-2 through 3-7, the tie configuration for the model B beams contains a depth value (*d*) that varies throughout the testing region. When establishing *a/d*, the depth at the centerline of the span (18.1 in.) was the selected value of *d*. Complete shop drawings for all twelve beams are located in Appendix B.

3.3 Strut and Tie Model

3.3.1 Overview

The strut and tie modeling used for the design of both beams is proportioned according to ACI 318-14, Chapter 23. Strut and ties are labeled as shown in Figure 3-8.

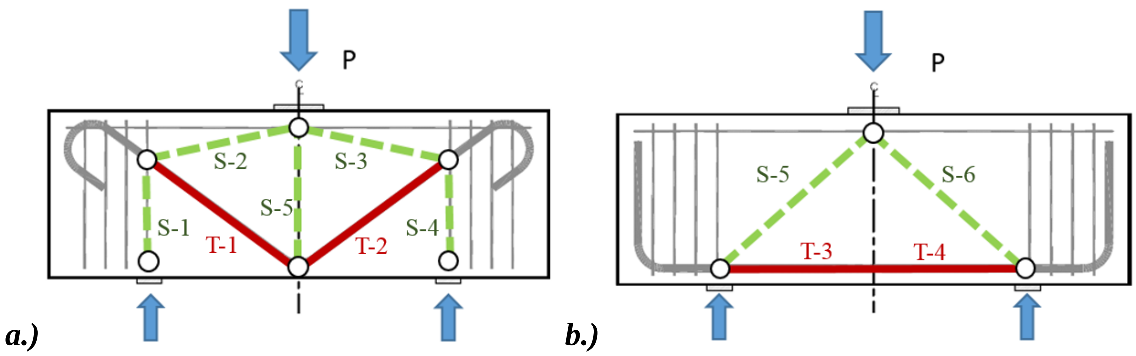

Figure 3-8: Strut and Tie Label Notation for a.) Model B and b.) Model G Beams

The geometric assumptions of the elements shown above are explained in the subsequent section.

3.3.2 Geometric Assumptions

Strut proportions and model configurations were selected based on conventional methods and standards of design practice. These simplifying assumptions are intentionally employed to keep the findings and recommendations relevant to design practice. Scaled drawings of all STM models can be found in Appendix C. Figure 3-9 illustrates the locations of each nodal face. Table 3-2 provides corresponding dimensions.

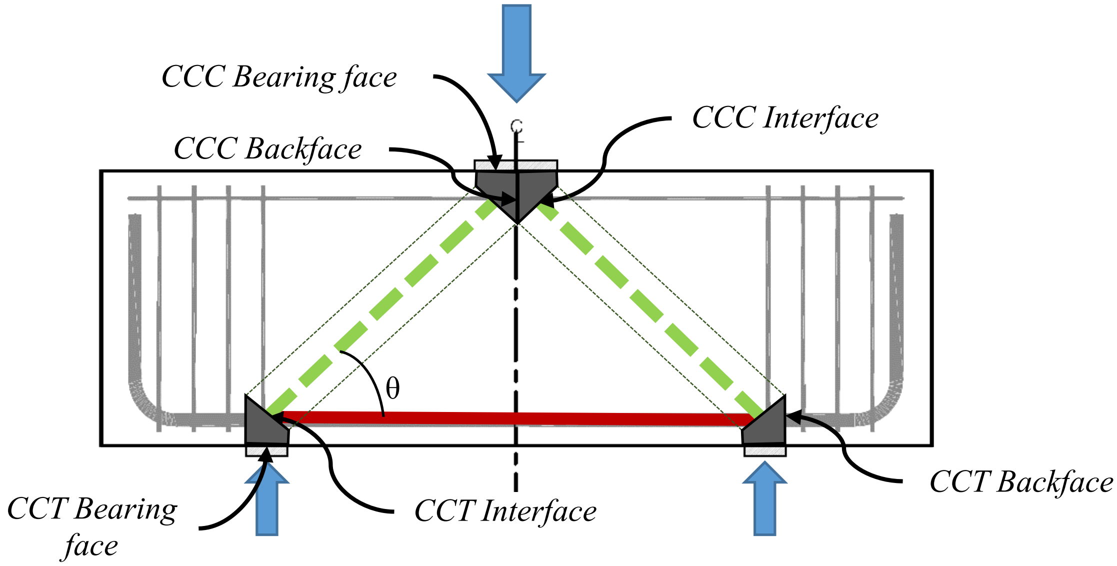

Figure 3-9: Model G Node Locations

Table 3-2: Model G Nodal Widths

	Model G	*θ* (deg)	Backface (in)	Interface (in)	Bearing Face (in)
Series 1	CCT	42.60	3.60	4.68	3.00
	CCC	42.60	4.06	5.00	3.00
Series 2	CCT	24.60	3.60	4.52	3.00
	CCC	24.60	4.06	4.90	3.00

Model B geometries are not as straight forward as model G because of its unconventional design. Strut widths were assumed to spread at a ratio of 2 to 1 (ACI 318-14, Figure R23.4.3). Figure 3-10 illustrates the geometry of the struts and nodes. Table 3-3 provides the values for the nodal widths.

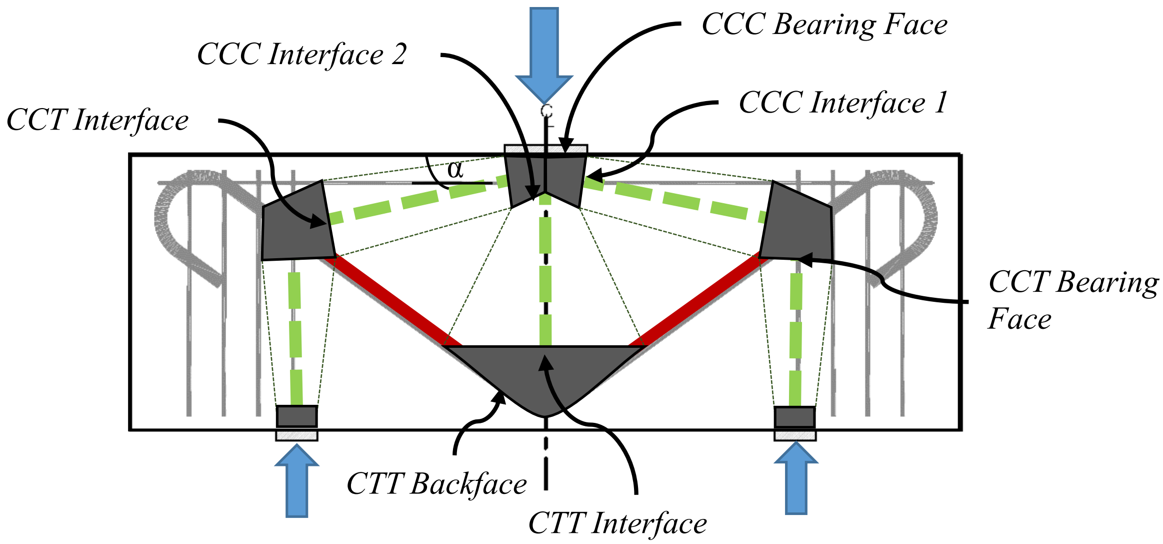

Figure 3-10: Model B Nodal Geometry

Table 3-3: Model B Nodal Widths

	Model B	α (deg)	Backface (in)	Interface 1 / 2 (in)	Bearing Face (in)
	CCC	12	4.06	4.6 / 2.11	3.00
Series 1	CCT	12	-	5.00	6.25
	CTT	12	15.5	6.16	10.65
	CCC	5.6	4.06	5.42 / 5.60	6.00
Series 2	CCT	5.6	-	5.90	7.52
	CTT	5.6	16.5	7.1	10.12

The width of the CCC bearing face is determined by subdividing the node under the point load into two symmetric nodes. The width of the CCT interface is determined based on the dimensions of a singular node. The length of all struts is defined from the centroid of each nodal region. Estimated proportions of strut and ties are listed in Table 3-4.

Table 3-4: Strut and Tie Proportioning

Series 1				Series 2			
Beam ID	**Member ID**	**Length (in)**	**Area (in^2)**	**Beam ID**	**Member ID**	**Length (in)**	**Area (in^2)**
BG-1-0.3-6 *BG-1-0.3-2* *BG-1-0-0*	S-5 & S-6	24.2	48.5	*BG-2-0.3-6* *BG-2-0.3-2* *BG-2-0-0*	S-5 & S-6	39.5	47.3
BG-1-0.3-6 *BG-1-0.3-2* *BG-1-0-0*	T-3 & T-4	18	2.37	*BG-2-0.3-6* *BG-2-0.3-2* *BG-2-0-0*	T-3 & T-4	36.0	2.37
BB-1-0.3-6 *BB-1-0.3-2* *BB-1-0-0*	S-1 & S-4	12.3	46.3	*BB-2-0.3-6* *BB-2-0.3-2* *BB-2-0-0*	S-1 & S-4	13.0	52.6
BB-1-0.3-6 *BB-1-0.3-2* *BB-1-0-0*	S-2 & S-3	18.4	50.0	*BB-2-0.3-6* *BB-2-0.3-2* *BB-2-0-0*	S-2 & S-3	35.5	56.7
BB-1-0.3-6 *BB-1-0.3-2* *BB-1-0-0*	S-5	16	82.7	*BB-2-0.3-6* *BB-2-0.3-2* *BB-2-0-0*	S-5	15.5	99.0
BB-1-0.3-6 *BB-1-0.3-2* *BB-1-0-0*	T-1 & T-2	21.7	2.37	*BB-2-0.3-6* *BB-2-0.3-2* *BB-2-0-0*	T-1 & T-2	38.0	2.37

The shape of the strut was assumed to be prismatic to maintain consistency with design practice.

3.4 FABRICATION

3.4.1 Overview

The fabrication of twelve reinforced concrete beams was done at Northern Arizona University's Engineering building. The fabrication included the building of formwork, assembly of steel reinforcement cages, installation of internal strain gauges and placement of concrete. The beams were designed and constructed using conventional materials. Fabrication and material specifications are outlined in this section.

3.4.2 Longitudinal Reinforcement for Flexure

3.4.2.1 Material Properties

The primary flexural reinforcement met the requirements of ASTM A615 Grade 60 deformed bar. The bar bend radii specified were in accordance with ACI Chapter 25. Control coupons were not tested. The yield strength, f_y, is assumed to be 60 ksi and the modulus of elasticity, E_s, is assumed to be equal to 29,000 ksi.

3.4.2.2 Tension stiffening

Tension stiffening is the result of tensile stresses in cracked concrete whose friction between cracks and deformed rebar accounts for a slight increase in the effective modulus of elasticity of reinforcement surrounded by concrete. MC 2010 provides for the strain caused by tension stiffening, ε_{ts}, as given in Equation 3-1.

Equation 3-1

$$\varepsilon_{ts} = \frac{\beta \sigma_{sr}}{E_s}$$

Where,

β = empirical coefficient to assess mean strain over length which slip between steel and concrete occur (MC 2010 Table 7.6-2)

σ_{sr} = Max steel stress in the crack formation stage (MC 2010 Equation 7.6-6).

E_s = Specified modulus of elasticity of longitudinal reinforcement

The strain caused by tension stiffening can be added to the strain energy, provided the total does not exceed the yield strain of the bar. After applying this factor, a range of 6 to 15% increase in U_{tie} was observed for estimated strain energy calculations depending on the percentage of ultimate load (approximately 15% for an applied load below $0.5P_u$ and 6% for an applied load near P_u).

3.4.3 Web Reinforcement

The web reinforcement was either ASTM A36 #2 smooth bar or #3 deformed bar meeting requirements of ASTM A615 Grade 60. Bar bending radii met requirements of ACI 318-14, Chapter 25. Control coupons were not tested.

3.4.4 Concrete Mixture

The concrete mixture used for this project was provided by a local “ready-mix’ supplier. The mixture design is provided in in Table 3-5.

Table 3-5: Mix Design (Cemex, 2015)

Material	Volume (ft^3)	Weight (lb)	% of Mix by Volume
Cement	2.84	558	11%
Fly Ash	0.87	118	3%
1" Course Agg.	6.71	1174	26%
1/2" Course Agg.	1.92	335	8%
3/8" course Agg	0.96	168	4%
Fine Agg.	7.54	1238	30%
Water	4.54	283	18%
Admixtures	N/A	N/A	N/A
Total	**27**	**3874**	**100%**
Air entrainment	6%		
Specified f_c'	4000 psi		
Unit weight	143.5 lb/ft^3		

3.4.5 Formwork

Formwork was constructed of lumber using nominally sized 2x2 and 2x4 studs and ½-in. and ¾-in. thick plywood. Formwork was built so that concrete for all twelve specimens (six 5-ft. long and six 8-ft. long) could be placed at the same time. Figure 3-11 shows formwork prior to placing concrete (wall bracing not shown for clarity).

Figure 3-11: Formwork Platforms for Twelve Concrete Beam (wall bracing not shown for clarity).

Formwork walls were braced using diagonal 2x4 "kickers" placed on both sides of the formwork and near the center of each beam.

3.4.6 Reinforcement Cages

Reinforcement cages were assembled in the concrete laboratory. Longitudinal Rebar and stirrups were attached to each other using 17-Gauge tie wire. Once assembled (Figure 3-12a), spacers were attached to the sides and bottom to ensure clear distance requirements were satisfied during casting. Steel strain gauges were also installed on reinforcement at targeted locations. This will be further explained in Section 3.5.2. With spacers and strain gauges attached, the cages were placed in the formwork (Figure 3-12b).

a) ***b)***

Figure 3-12: a) Rebar Cage for BB-2-0.3-6 and b) Assembled Cages in Formwork

3.4.7 Concrete Placement

Concrete for the beams was placed on June 16, 2015 at Northern Arizona University. During placement, concrete was consolidated using a 2-in diameter concrete vibrator. Prior to concrete setting, two steel lifting loops with a 2400-lb capacity each (EMI Supplies 2016) were inserted in the top of each beam to facilitate moving. During casting, standard 4-in. x 8-in. cylinders were cast in accordance with ASTM C31 (2015), and placed adjacent to the beams as they cured. After concrete placement and finishing, test specimens were covered with an insulated tarp. The tarp remained in place for 20-days. After which formwork was removed and beams were made ready for testing. Beams and cylinders are shown in Figure 3-13.

Figure 3-13: Concrete Beams and Cylinders after 28 days of Curing

Before testing a beam, a minimum of three cylinders were tested to collect compressive stress and strain data. The results of all control cylinder tests are in Appendix D. Table 3-6 presents a summary of results.

Table 3-6: Concrete Cylinder Data

	No. of Tests	Min.	Max.	Average	Std. Deviation
f_c' (ksi)	15	4.62	5.75	5.22	0.37
E_c (ksi) ($57\sqrt{f_c'}$)	15	3873	4322	4115	146
E_c (ksi) measured	15	3185	4651	3842	391

***All specimens were tested between 50 to 155 days after concrete placement.*

As seen in Table 3-6, there is little variation between cylinder tests with respect to f_c' and E_c ($57\sqrt{f_c'}$). This is likely due to the age of the cylinders, all which were older than 50 days old. Since there was little change in strength, and because the statistical reliability of fifteen tests is greater than for three tests, the average value for all fifteen compressive strength and modulus of elasticity ($57\sqrt{f_c'}$) tests were used to calculate STM capacities.

3.5 EXPERIMENTAL TEST SETUP

3.5.1 Overview

The instrumentation used during the testing of all twelve beams provided redundancy and consistency. These instruments include steel and concrete strain gauges, hydraulic cylinders, load cells, string potentiometers, data acquisition unit and photogrammetry. Figure 3-14 provides an overview. This section provides further details.

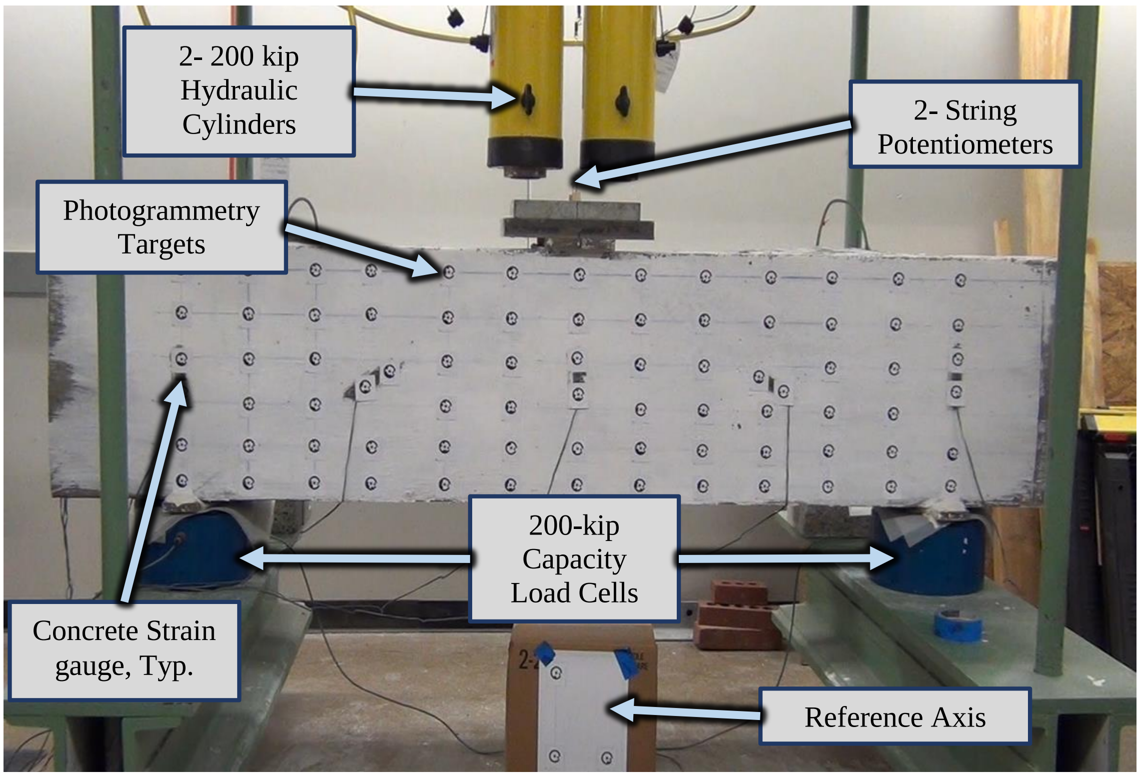

Figure 3-14: Beam Test Setup

3.5.2 Steel Reinforcement Strain Gauges

Uniaxial strain gauges were attached to the main longitudinal reinforcement during the fabrication process in order to measure the change in strain during testing. The gauge type was

FLA-3-11-1LT manufactured by *Tokyo Sokki Kenkyujo Co*. (Tokyo Sokki Kenkyujo, 2015) Specifications regarding this gauge can be seen in Table 3-7.

Table 3-7: Steel Strain Gauge Specifications

Strain Gauge Type	**Material Applications**	**Gauge Factor**	**Gauge Length**	**Gauge Resistance**
FLA-3-11-1LT	Mild Steel	2.12 ± 1%	3 mm	120 ± 0.5 Ω

The locations of all strain gauges were determined based on the assumed strut locations in the truss model. Results obtained from strain gauges are dependent on their proximity to a crack location. Since cracks often form at stirrup locations, gauges were placed in close proximity to a stirrup and when possible, mirrored about the centerline of the beam to add a level of redundancy. An example of strain gauge locations is shown in Figure 3-15.

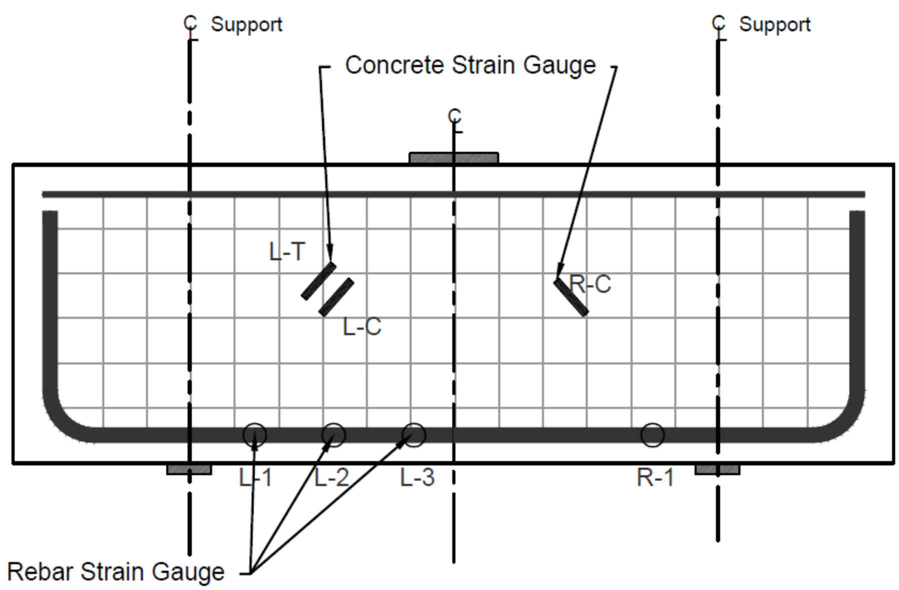

Figure 3-15: Strain Gauge Locations for BG-1-0.3-6

A complete map of all the strain gauge locations for all twelve beams is provided in Appendix E.

The installation of the rebar strain gauges was completed using the protective coating kit (M-Coat F) materials and specifications from *MicroMeasurements* (Vishay Precision Group, Inc 2014). This included the following steps:

1) Grind down the rebar until smooth at the designated locations,
2) Clean and neutralize the surface,
3) Glue the strain gauge to the rebar with cyanoacrylate,
4) Coat the gauge with a nitrile rubber coating,
5) Cover with a butyl rubber sealant,
6) Cover with a neoprene rubber sheet, then
7) Wrap the installation in aluminum foil tape.

Figure 3-16 shows an example of two installed steel strain gauges on BG-2-0.3-2.

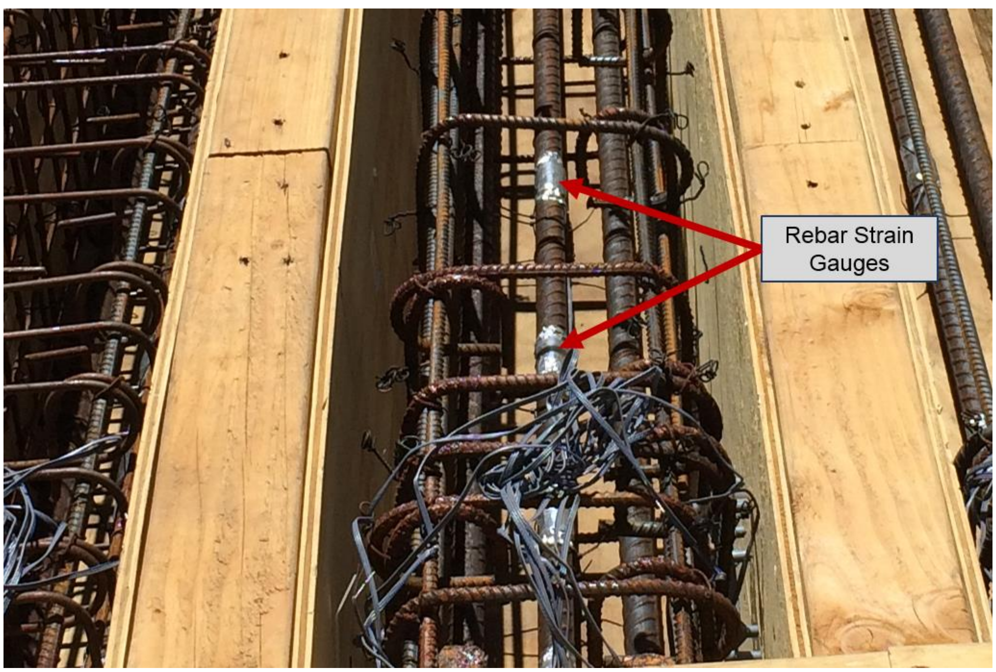

Figure 3-16: Rebar Strain Gauges

3.5.3 Concrete Strain Gauge

Uniaxial strain gauges were attached to the surface of the finished concrete one to three days prior to testing to measure the change in concrete strain during testing. The gauge type was PL-60-11-3LT manufactured by *Tokyo Sokki Kenkyujo Co* (Tokyo Sokki Kenkyyujo 2016). Specifications regarding this gauge are given in Table 3-8.

Table 3-8: Concrete Strain Gauge Specifications

Strain Gauge Type	**Material Applications**	**Gauge Factor**	**Gauge Length**	**Gauge Resistance**
PL-60-11-3LT	Concrete	2.13 ± 1%	60 mm	120 ± 0.5 Ω

The locations of all concrete strain gauges were determined based on the assumed strut locations in the truss model. Strain gauges were placed near mid depth of beam in strut locations and when possible, mirrored about the centerline of the beam to add a level of redundancy. To illustrate, a test specimen with concrete gauges installed is shown in Figure 3-17.

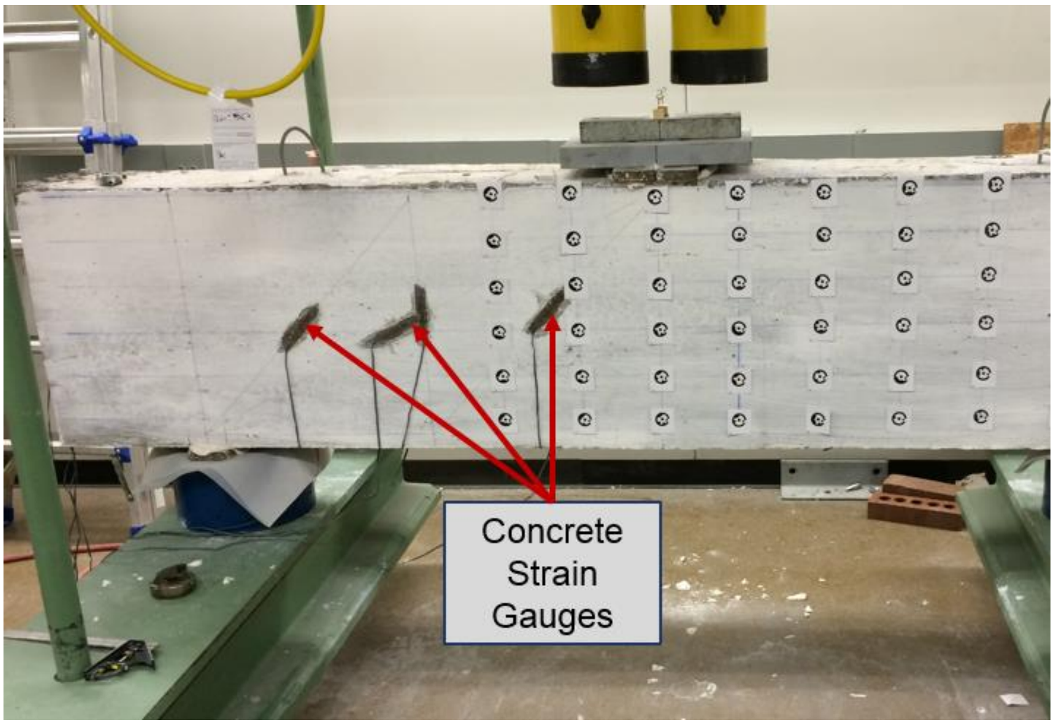

Figure 3-17: Example of Concrete Strain Gauges on Beam

The procedure used during installation was as follows:

1) Grind concrete surface to remove paste and expose fine aggregate (less than 1/8th inch)
2) Spread a thin layer of epoxy over the ground surface and dry for approximately 24 hours.
3) Roughen the epoxied surface by sanding to ensure complete adhesion of gauge.
4) Glue the gauge to the epoxied location according to manufacturer's instructions.

3.5.4 Hydraulic Cylinders

Test specimens were monotonically loaded at the top surface via two 200-kip capacity hydraulic cylinders. Each cylinder was an *Enerpac* RC-10010 (Enerpac 2016), see Figure 3-18.

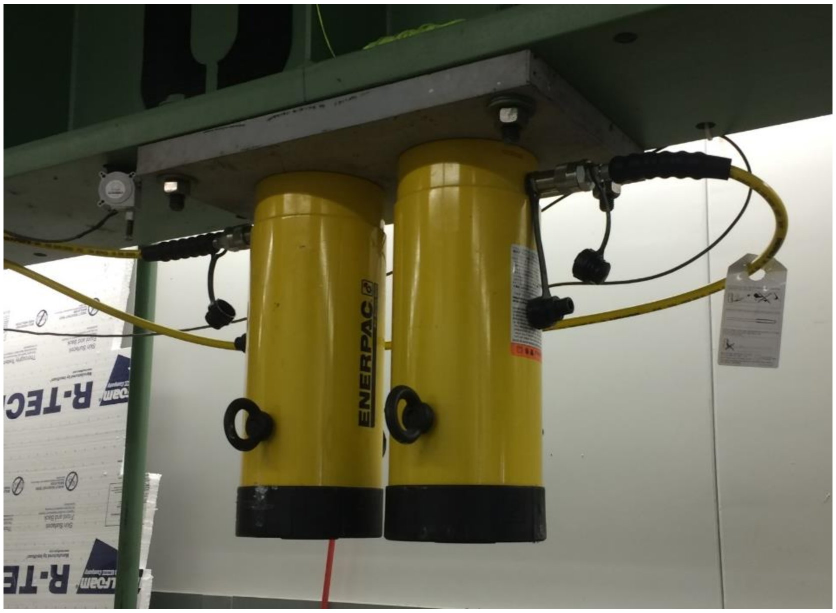

Figure 3-18: Hydraulic Cylinders

The cylinders were operated by a 10,000 psi pneumatically-controlled hydraulic pump with a 5-gallon capacity reservoir. Two hydraulic cylinders were used in series resulting in a maximum testing capacity of 400 kip. The specifications for the hydraulic cylinders are given in Table 3-9.

Table 3-9: Hydraulic Cylinder Specifications

Model Number	**Stroke**	**Max Capacity**	**Effective Area**
ENERPAC RC-10010	10.25 in	200 kip	20.63 in^2

3.5.5 Load Cells

Two 200-kip capacity load cells were centered on each support. The load cells used to collect the force reading during testing were Interface model 1240AF-200k-B (Interface 2016).

3.5.6 String Potentiometer

Displacement data was collected during testing using two string potentiometers with 12-in maximum stroke. The potentiometers were positioned on the centerline on the beam in front and behind the hydraulic rams to measure deflection downward of the top surface. The string potentiometers used in testing were *Celesco* SP2-12 (Celesco 2013), see Figure 3-19.

Figure 3-19: String Potentiometers

3.5.7 Data Acquisition (DAQ)

Voltage data collected from the load cells, string potentiometers, and strain gauges were routed to a National Instrument signal conditioning platform (Model SCXI-1000). This platform utilized a SCXI-1314 universal terminal block, SCXI 1320 universal terminal block, and a SCXI-1520 universal strain/bridge module to collect the various load, displacement and strain data (National Instruments 2000), see Figure 3-20.

Figure 3-20: Data Acquisition

This platform was connected to a computer running *LabView* which is system-design software for the visual programming language from National Instruments (National Instruments 2003). *Labview* is used to collect, sort, record, and save the data for later analysis.

3.5.8 Photogrammetry

3.5.8.1 Initial Setup

Photogrammetry is the science of making measurement from photographs. This technology was used to collect displacement measurements of the test specimens. Modeling software, *Photomodeler 14* (Photomodeler 2014), was used to process the data from the photographs. *Photomodeler* processes photographs to output relative displacements at target locations in the *x*, *y*, and *z* directions. Per the recommendations of the software manufacturer, three *Nikon* D7100 digital single-lens reflex (DSLR) cameras (Nikon 2013) were selected with a 24-mm fixed lens (Nikon 2016) for collection of displacement results. The specifications for these cameras are listed in Table 3-10.

Table 3-10: Camera and lens specifications

Camera Body	***Effective Megapixels***	***ISO***	***Shutter Speed***	***Lens***
Nikon D7100	24.1 Million	100-6400	1/8000-30 sec	AF *Nikkor* 24mm f/2.8D

The optimal size and number of targets is dependent on the distance the cameras are from the surface of the object being photographed. Each test required recalibration of the software's parameters, see Figure 3-21.

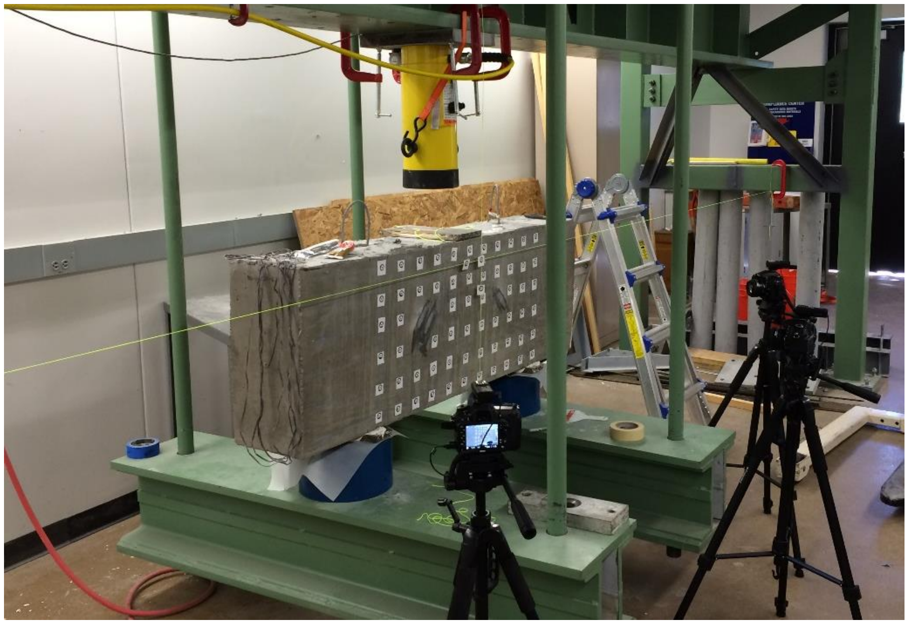

Figure 3-21: Set up of Camera for Photogrammetry

During each test, a reference axis is viewable to all cameras and does not move with respect to the beam. This allows for calibration of the Cartesian control and relative position of photogrammetric measurements. The accuracy of the measured displacement is dependent on lighting, camera resolution, and target reflectiveness. According to the manufacturer, the highest accuracy *Photomodeler* is capable of is 1:30,000 on a 3-m object. In this case, point positions would be accurate to 0.1-mm resolution within one standard deviation from the mean (i.e. 68% probability of occurrence). A number of camera settings were investigated to measure their effect on the total model error. The software calculates an error value based on the amount of agreeance between the cameras and their measured target displacements. A desired error value is less than 1 per the manufacture. The camera settings which yielded the smallest total model error most consistently (resulted in less than 0.65 consistently) are given in Table 3-11.

Table 3-11: Camera Settings for Photogrammetry

ISO	*Shutter Speed*	*f/Stop*	*Flash*
100	1/8	f/13	none

The above settings were used to measure the displacement of targets printed on white cardstock covering about 30% of the beam's surface. Before the targets were attached. The exterior surface of each beam was "white-washed" with a mixture of lime and water. White-washing the beams decreased the photo-modeling total error to approximately 0.6. An example of a photogrammetric model is shown in Figure 3-22.

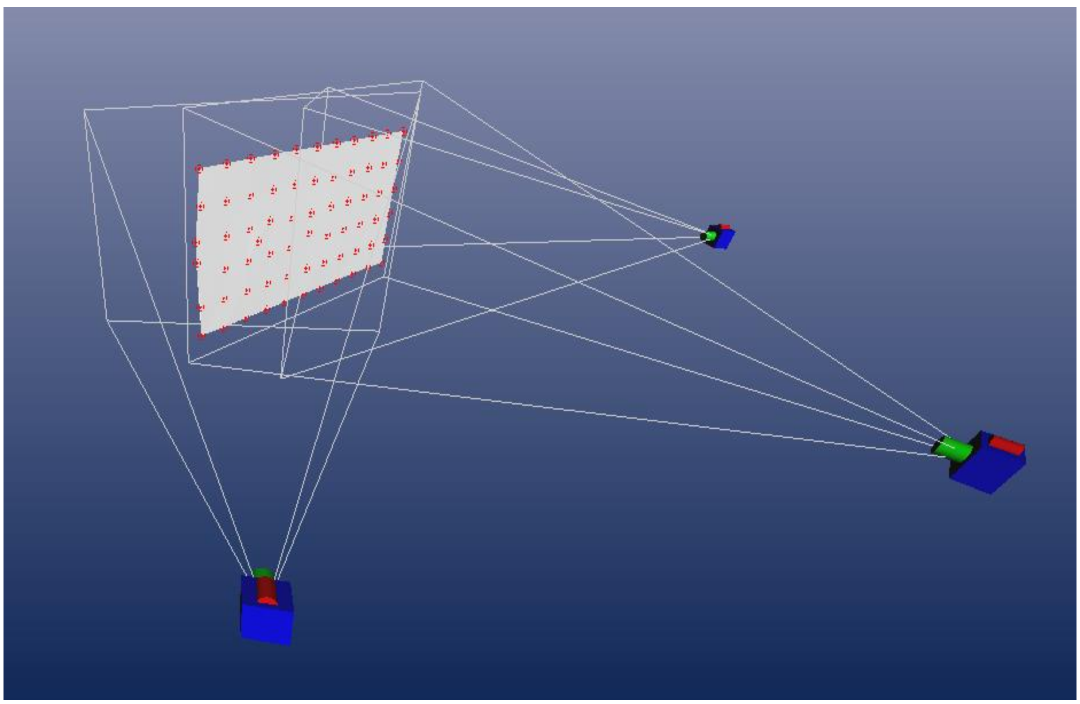

Figure 3-22: Resulting Photogrammetric Model using Photomodeler

As shown in Figure 3-22, only one side of the beam was modeled due to space restrictions in the laboratory. It was assumed both side would behave symmetrically.

3.5.8.2 Procedure for Camera Calibration

The initial position of the cameras was determined first by ensuring all three cameras covered the beam's testing region while getting as close as possible. First, the distance was measured from each tripod to the farthest location in the testing area of the beam to determine the farthest distance from camera to target. The farthest distance was then input into *Photomodeler* to determine the minimum required target diameter needed to ensure detection of all targets. Camera parameters and desired white space for each target were also input into *Photomodeler*. The software program automatically generates a digital file of targets which can be printed on cardstock. The total number of targets was based on the desired spacing and required area of coverage.

Once the targets were printed, they were glued to the beam in a grid layout for later ease of analysis of displacement data. The center of each target was placed on the intersection of chalk lines. The total number of targets used for each beam was 70 and 80 for *a/d* of 1 and 2, respectively. Targets were also placed at each end of the concrete strain gauges.

Once the beam was outfitted with targets, the cameras were field calibrated using the following steps:

1) Eight pictures were taken of the beam, moving the tripod to different locations, using different angles to the beam, and different frame orientation;
2) photos were imported into *Photomodeler* and a model was created;
3) the cameras were automatically calibrated using the *Photomodeler*'s software;
4) and the field calibrated settings were saved in *Photomodeler* to reduce future model error on objects in the same light setting.

3.5.8.3 Procedure for Test Setup

Once a beam was properly equipped with targets and in-place for testing, a trial and error processing of camera locations was executed before testing. The camera placement during testing is crucial to ensure a low error value for the model. A desired error value less than 1.0 is recommended by the manufacturer. Cameras were placed in locations so that at least two cameras cover any area in the testing region at one time. The maximum angles that could be used while still being able to capture all targets resulted in the least amount of error in the model. Pictures were taken at proposed camera locations of the unloaded deep beam. The pictures where then imported into *Photomodeler*, targets were checked for recognition and a model made. If the resulting model had an error value under 1.0, then the camera locations were marked and used for the subsequent beam test; if not, camera angles were adjusted and the process repeated. A summary of the above setup procedure is given in Figure 3-23.

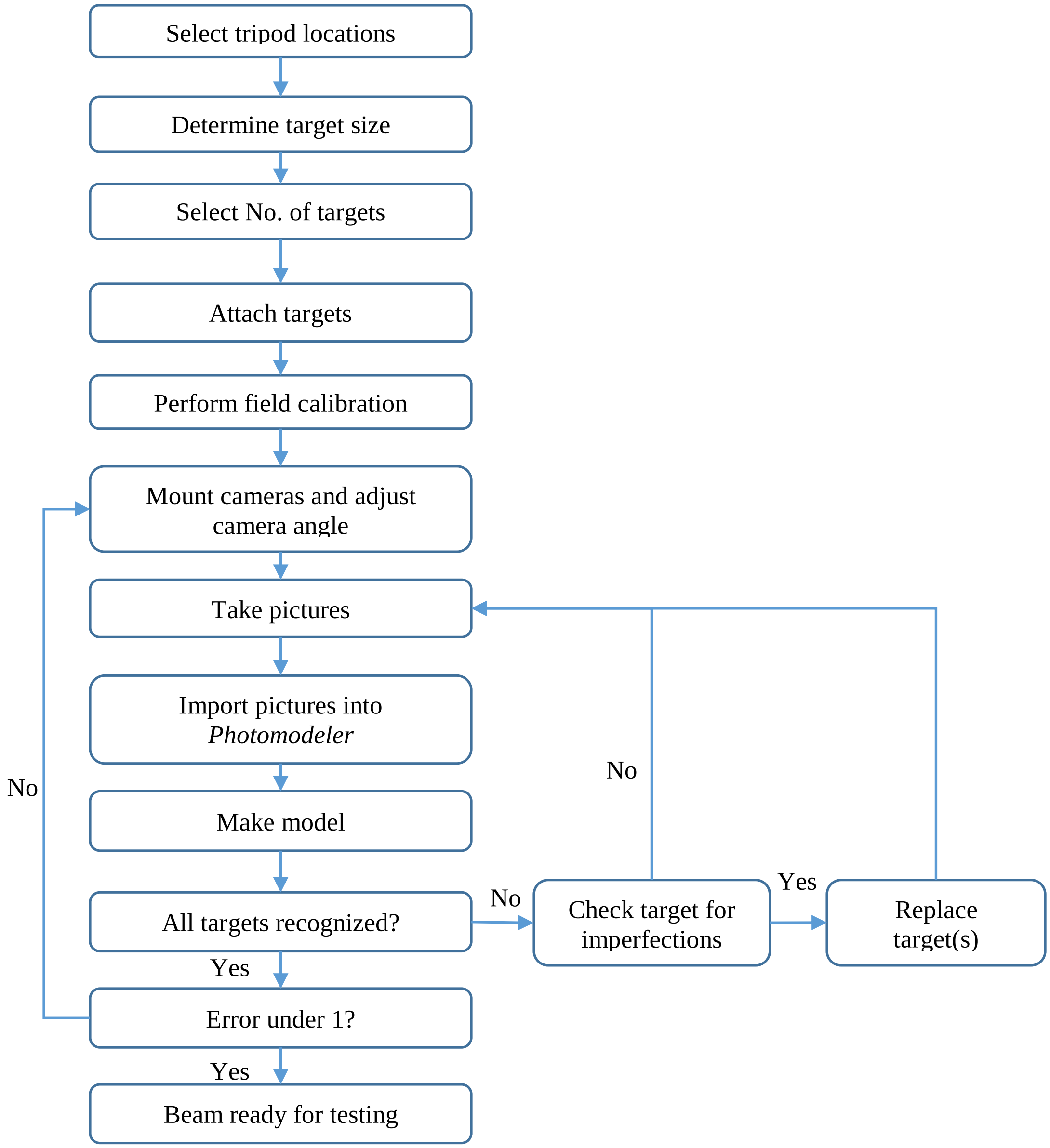

Figure 3-23: Photogrammetry Setup Flowchart

After an adequate model had been created for the unloaded beam, it was then tested using the procedure discussed in the following section. After testing, digital photographs were imported into *Photomodeler* and a model was created for each of the designated loading intervals.

3.6 TEST PROCEDURE

Concrete beams were tested at a minimum of 50 days after curing. Before testing, the beams were centered on the supports and under the applied load. A thin layer of self-leveling gypsum was placed between the bearing plates and beam to ensure an even bearing surface. Once in place, concrete strain gauges were installed, instrumentation placed, and all devices were wired to the DAQ.

During testing, beams were incrementally loaded depending on size of specimen and shear reinforcement. The loading increments were selected as approximately 10% of the expected capacity. During testing, cameras were equipped with a wireless remote shutter system to ensure all three cameras took pictures simultaneously at the pre-selected loading intervals. When the trigger was pressed, a comment within the data file was simultaneously inserted. This was so the strain, displacement, load, and photogrammetry data could be directly compared at similar instances. Once the beam had cracked, pictures were taken on the back side (i.e. side without targets) to collect crack measurements in the testing region. Finally, all beam tests were recorded on video.

3.7 CRACK MEASUREMENTS

3.7.1 Overview

The process of collecting crack measurements for this project was considerably more comprehensive than conventional methods. Generally, crack width measurements are visually collected using crack cards or microscopes during testing. In attempts to leverage advances in technology, maximum crack width and total cracked area were collected using high resolution cameras and modeling software. This section will outline the procedure used for both measurements.

3.7.2 Maximum Crack Width, w_{cr}

Maximum diagonal crack widths were collected for each beam at each load interval. Before testing, rulers were attached to the outside of the testing region to provide scale to the photographs after testing. During loading, at each interval, close range pictures (approximately 2-ft. from beam) were taken using a high resolution camera. After testing, pictures were orthorectified to remove lens distortion using *Adobe Photoshop Element*. After distortion was removed, photos were uploaded into *AutoCAD* and scaled using the rulers in each photograph. Once scaled, all diagonal crack widths were measured near mid depth of beam for all cracks wider than 0.002 in. The maximum diagonal crack for right and left of the beam centerline were averaged to mitigate any asymmetric effects that may have occurred during testing.

This procedure was investigated with respect to accuracy in an independent study done by Ballard et al. (2016), which collected crack width measurements for three separate crack width locations from ten independent participants on a concrete beam using microscopes, crack comparator cards, and the photogrammetry. The average crack widths for all three crack locations using three different methods of crack collection were found and plotted against each other. Figure 3-24 summarizes the results of the study in terms of crack width measurement using photogrammetry, crack comparator cards and microscopes.

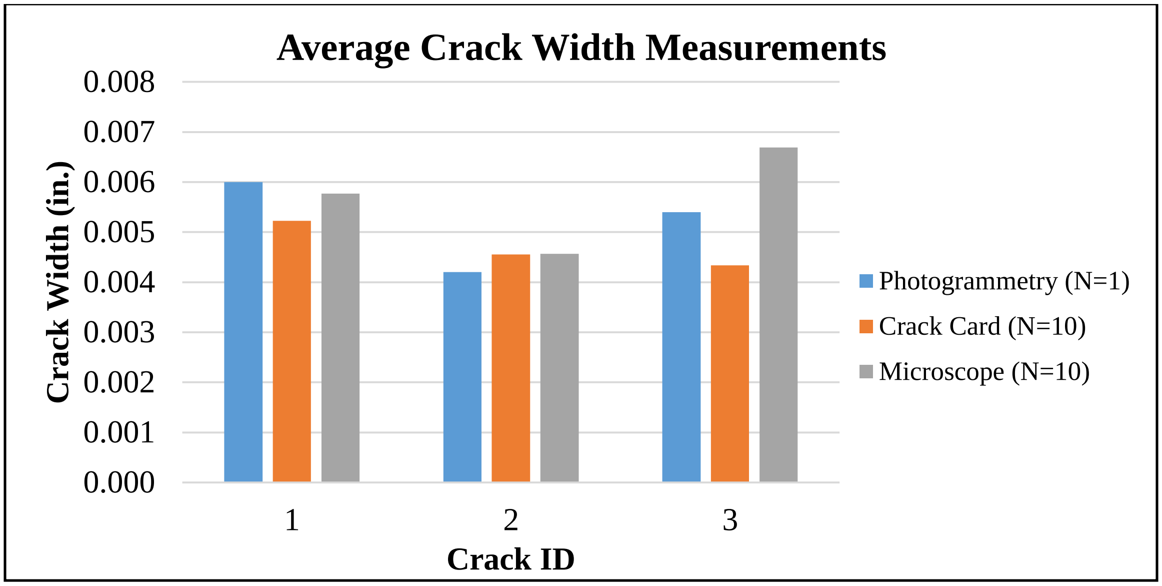

Figure 3-24: Results of Measured Crack Widths Using Three Different Methods

As shown in Figure 3-24, when comparing photogrammetry to microscopes or crack comparator cards, photogrammetric measurements are closer to those made with a microscope than with a crack comparator card.

3.7.3 Crack Area, A_{cr}

Area of cracked surface of concrete was collected for each beam at each load interval. The same photographs and process described in Section 3.7.2 was used to measure crack area. In this case, all cracks (not just diagonal) were collected. Length of each crack was traced using *AutoCAD*. The total length of cracks in each region was collected and recorded. A grid was then overlaid onto the beam in the modeling software to ensure crack widths were measured consistently. Any time a crack crossed a horizontal grid line, a crack width was measured and recorded. This was done for all cracks at all loading intervals with widths larger than 0.002 inches. An exaggerated example of a crack map with a grid overlay is shown in Figure 3-25.

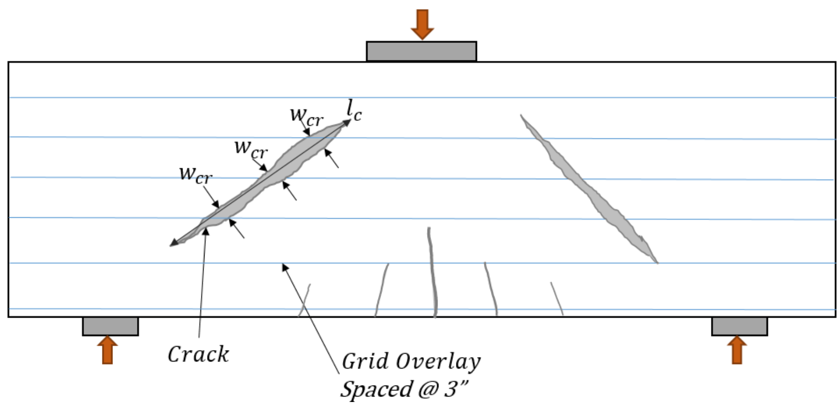

Figure 3-25: Crack Area Measurement

3.8 ALL SPECIMEN DETAILS

Details of all twelve test specimens are listed in Table 3-12.

Table 3-12: Summary of Specimen Details

	Beam ID	Tie Model	s_v (in.)	s_h (in.)	ρ_v	ρ_h	*a/d*	Stirrup size	θ
Series 1	*BG-1-0.3-6*	G	3	3	0.30%	0.30%	0.99	#2	42.6
	BG-1-0.3-2		8.25	8.25	0.30%	0.30%	0.99	#3	42.6
	BG-1-0-0		0	0	0.00%	0.00%	0.99	N/A	42.6
	BB-1-0.3-6	B	3	3	0.30%	0.30%	0.99	#2	42.6
	BB-1-0.3-2		8.25	8.25	0.30%	0.30%	0.99	#3	42.6
	BB-1-0-0		0	0	0.00%	0.00%	0.99	N/A	42.6
Series 2	*BG-2-0.3-6*	G	3	3	0.30%	0.30%	1.98	#2	24.6
	BG-2-0.3-2		8.25	8.25	0.30%	0.30%	1.98	#3	24.6
	BG-2-0-0		0	0	0.00%	0.00%	1.98	N/A	24.6
	BB-2-0.3-6	B	3	3	0.30%	0.30%	1.98	#2	24.6
	BB-2-0.3-2		8.25	8.25	0.30%	0.30%	1.98	#3	24.6
	BB-2-0-0		0	0	0.00%	0.00%	1.98	N/A	24.6

Constants for All Beams

Dimensions	b_{plate}	3	in.	Material Properties	f_c'	5.22	ksi
	b_w	10	in.		f_y	60	ksi
	d	18.2	in.		E_c	4115	ksi
	d_b	1	in.		E_s	29,000	ksi
	A_s	2.37	in^2		β_1	0.79	
	A'_s	0.22	in^2				

Material properties listed above were either collected by the author or provided by the manufacturer.

CHAPTER 4

Results

4.1 OVERVIEW

In this Chapter, the experimental measurements of the testing program are presented in detail. Discussion of results are presented in Chapter 5. The following data are presented:

1) Load versus displacement data;
2) Photogrammetry data;
3) Concrete and steel strain data;
4) Maximum diagonal crack width versus tie strain; and
5) Total crack area (Equation 2-10) versus strain energy (Equation 2-9).

4.2 SPECIMEN LEGEND

For the presentation of all results, each specimen is associated with a unique marker, for ease of identification. For Series 1 (*a/d* = 1), squares are used for the graphic markers. Series 2 (*a/d* = 2) are illustrated using circle markers. Tie configurations are denoted using blue and red colors for model G and B, respectively. Lastly, the reinforcement and spacing of reinforcement is displayed in shades of either red or blue. Unreinforced specimens (ρ = 0%) are shown in the lightest shades, and reinforced specimens with spacing of *d/6* are shown in the darkest shades. This is illustrated in Table 4-1.

Table 4-1: Specimen Legend

	a/d = 1	a/d = 2
Model G	BG-1-0-0	BG-2-0-0
	BG-1-0.3-2	BG-2-0.3-2
	BG-1-0.3-6	BG-2-0.3-6
Model B	BB-1-0-0	BB-2-0-0
	BB-1-0.3-2	BB-2-0.3-2
	BB-1-0.3-6	BB-2-0.3-6

4.3 Load versus Displacement

Load and displacement data was collected from a load cell at each support and two string potentiometers centered at the point of load application, respectively. Data are presented in terms of the applied load (i.e. self-weight is not included). The average value of the two string potentiometers is the reported centerline deflection. The results for Series 1 and Series 2 specimens are shown in Figure 4-1 and Figure 4-2, respectively.

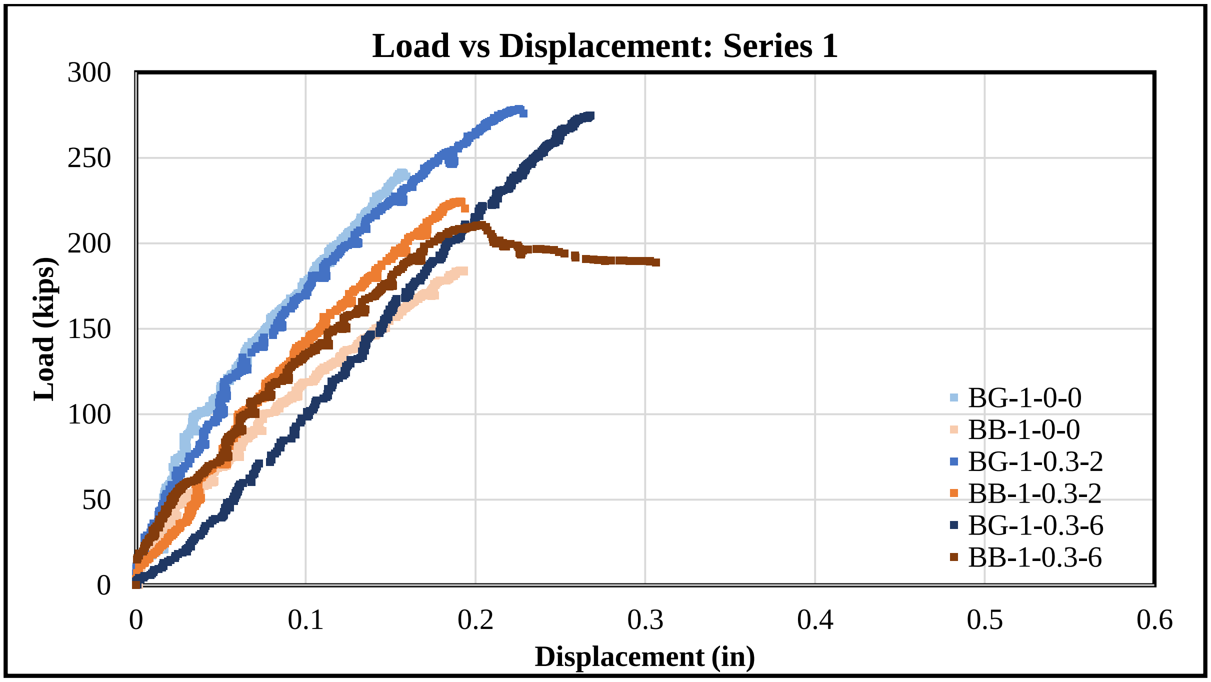

Figure 4-1: Series 1 Load vs. Displacement Data

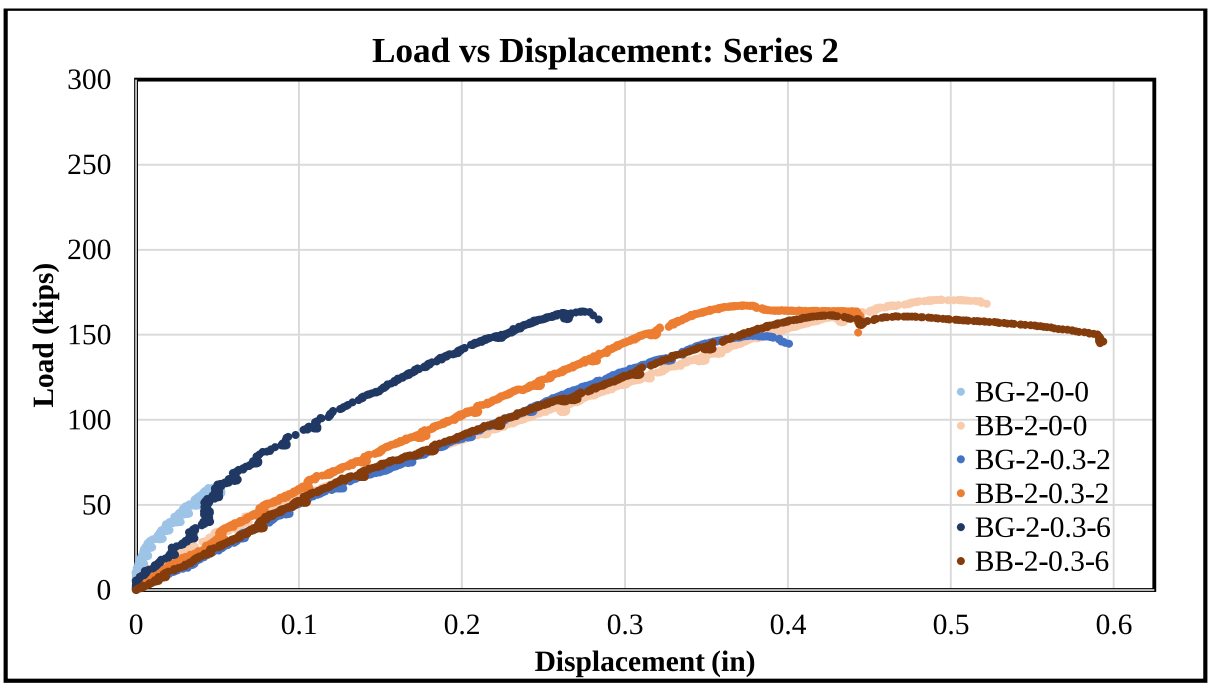

Figure 4-2: Series 2 Load vs. Displacement Data

The inconsistences in modulus during initial loading seen in the above can be attributed to the flexing of the loading plate atop the beam.

4.4 PHOTOGRAMMETRY DATA

Photogrammetric data were collected for each specimen to verify both displacement (i.e. string potentiometer) and concrete strain (i.e. strain gauge) data. This was done using the following steps:

1) Identify the target number which would best compare with string potentiometer data.
2) Make models of specimen at every loading interval
3) Calculated the change in target location (in inches) with respect to the reference axis in the Z direction.
4) Plot graph of target movement vs. load against string potentiometer vs. load (see Figure 4-3)

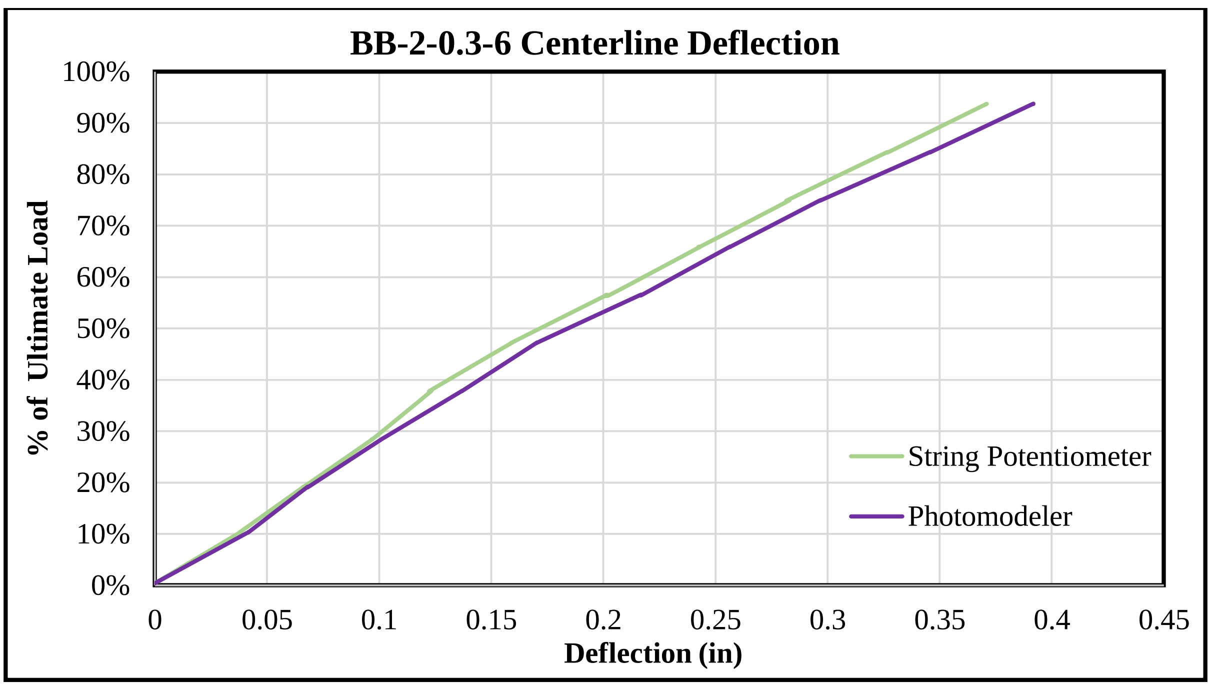

Figure 4-3: Photomodeler vs. String Potentiometer Centerline Deflection on BB-2-0.3-6

Figure 4-3 shows the difference between string potentiometer and *Photomodeler* data to be less than 12% for loading up to 95% of ultimate. This data accounts for frame flexibility measured by the string potentiometer, but not measured by photogrammetry. The data does not include the flexibility of the plate under the load (measured by string potentiometer). Thus the difference can likely be attributed to frame flexibility and not accuracy of one method versus another. Nonetheless, observed differences between photogrammetry and string potentiometers displacement measurements are within the expected degree of reliability, for the purpose of this study. For loads less than 50% ultimate, the difference is even smaller with a max of 6% difference. This data agrees with a study on the use of photogrammetry to measure the condition of existing structures done by Ballard et al. (2016) using the same equipment and setup as this testing program. In addition, targets were attached to concrete strain gauges to help verify concrete strain data. An example of this is shown in Figure 4-4.

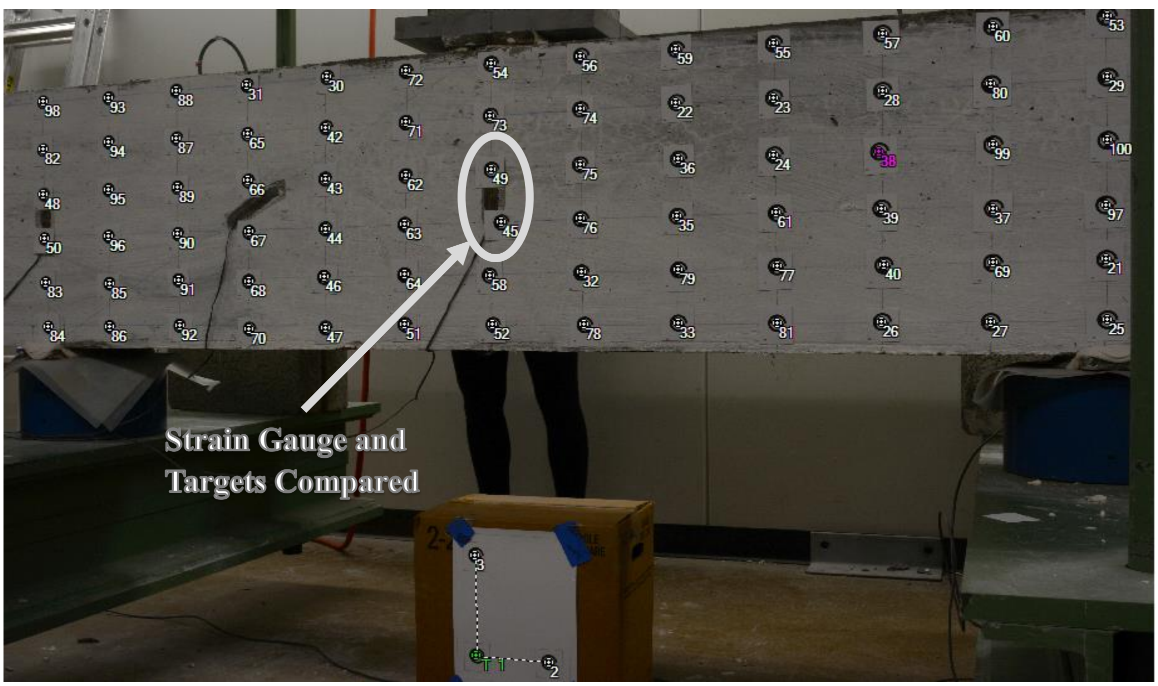

Figure 4-4: Target and Concrete Strain Gauge Location Used for Comparison on BB-2-0.3-6

As shown in Figure 4-4, the targets selected for comparison to concrete strain gauge are points 49 and 45. The results of the comparison are shown in Figure 4-5.

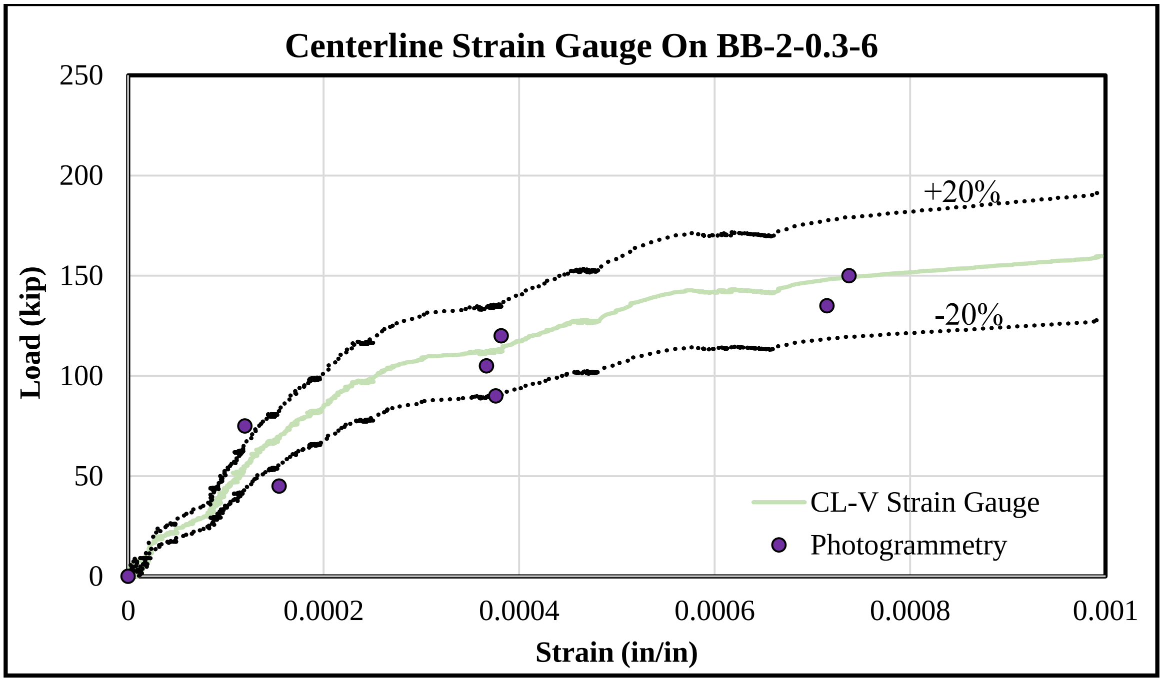

Figure 4-5: Photomodeler vs. Concrete Strain Gauge Data for locations shown in Figure 4-4

Figure 4-5 shows the majority of photogrammetry strain data fitting within a range of ± 20% of the strain gauge measurements. This data agrees with the results of Ballard et al. (2016) and follows similar trend of what has been studied.

While the wealth of photogrammetry and strain data is useful for verifying strut and tie modeling assumptions and experimental measurements; data collected from these tests are slated for future investigation not within the scope of this thesis.

4.5 STRAIN DATA

Strain gauges were attached to all specimens before testing. An average of seven total concrete and steel gauges were used for each test. The placement of these gauges were chosen based on the assumed STM. To illustrate, refer to Figure 4-6.

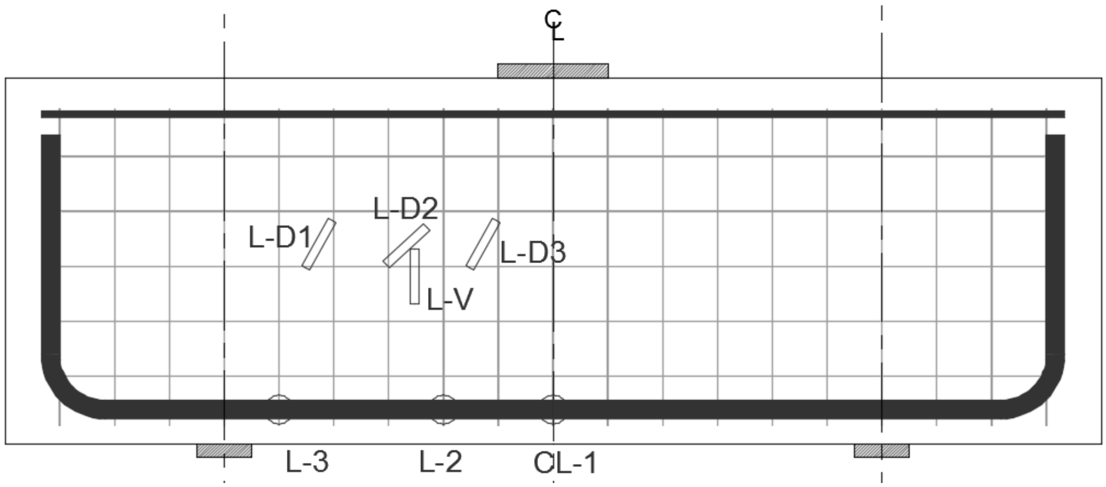

Figure 4-6: BG-2-0.3-6 Steel and Concrete Gauge Locations

Steel strain measurements are dependent on the proximity of the gauge to a crack. Similarly, concrete strain measurements are influenced by the proximity of the gauge to a crack. Figure 4-7 provides an example of the concrete strain data collected from the locations shown in Figure 4-6.

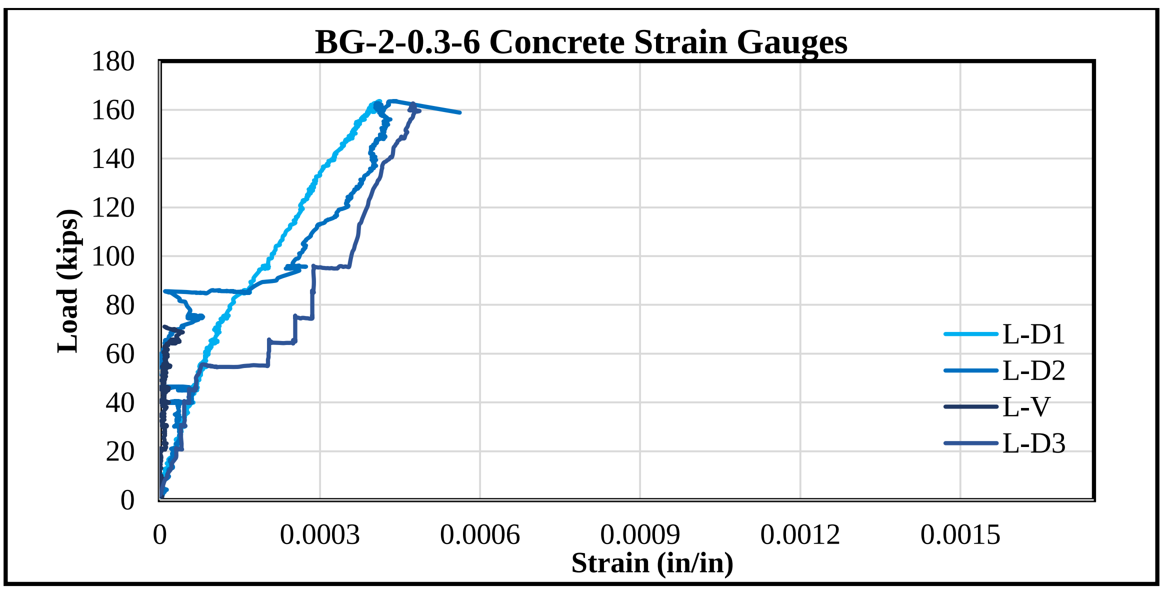

Figure 4-7: Concrete Strain Data for Gauges Shown in Figure 4-6

Figure 4-7 illustrates the influence of crack activity on concrete strain measurements. Gauge L-V data were lost at approximately 75 kips due to the close proximity to a diagonal crack.

Strain gauge L-D1, which was aligned along the left most indirect strut was not influenced by diagonal cracking.

The strain data for the steel strain gauges are shown in Figure 4-8.

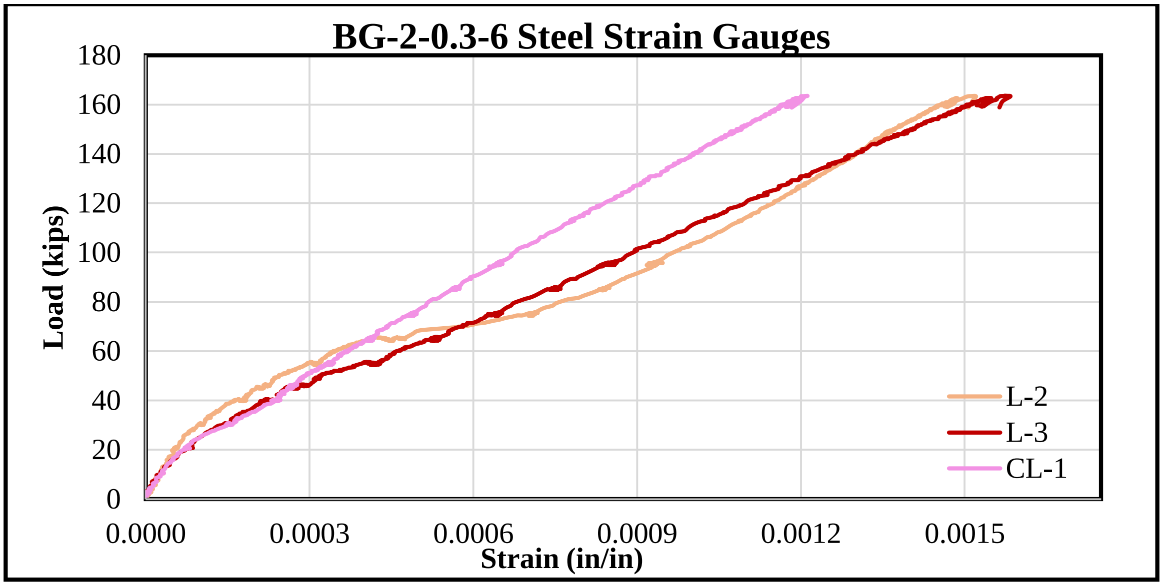

Figure 4-8: Steel Strain Data for Gauges Shown in Figure 4-6.

4.6 MAX CRACK WIDTH

Maximum diagonal crack width was collected using the procedure discussed in Section 3.7.2. The measured crack width for all specimens at a corresponding load is shown in Figure 4-9 and Figure 4-10.

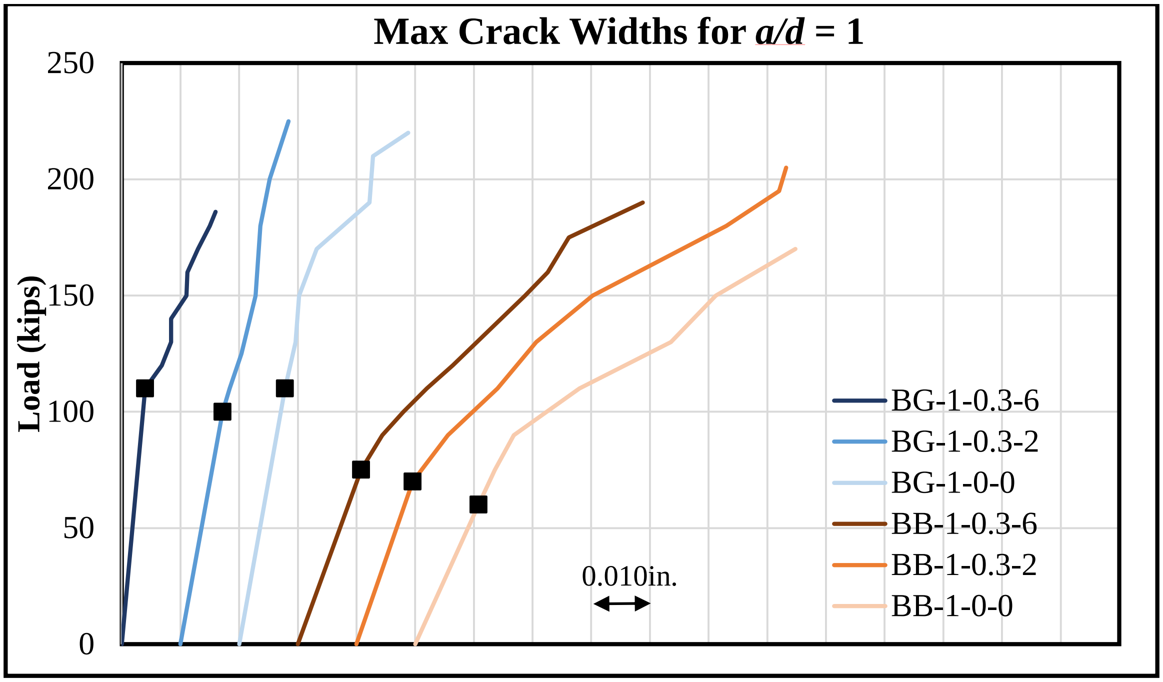

Figure 4-9: Maximum Crack Widths for Series 1 Specimens

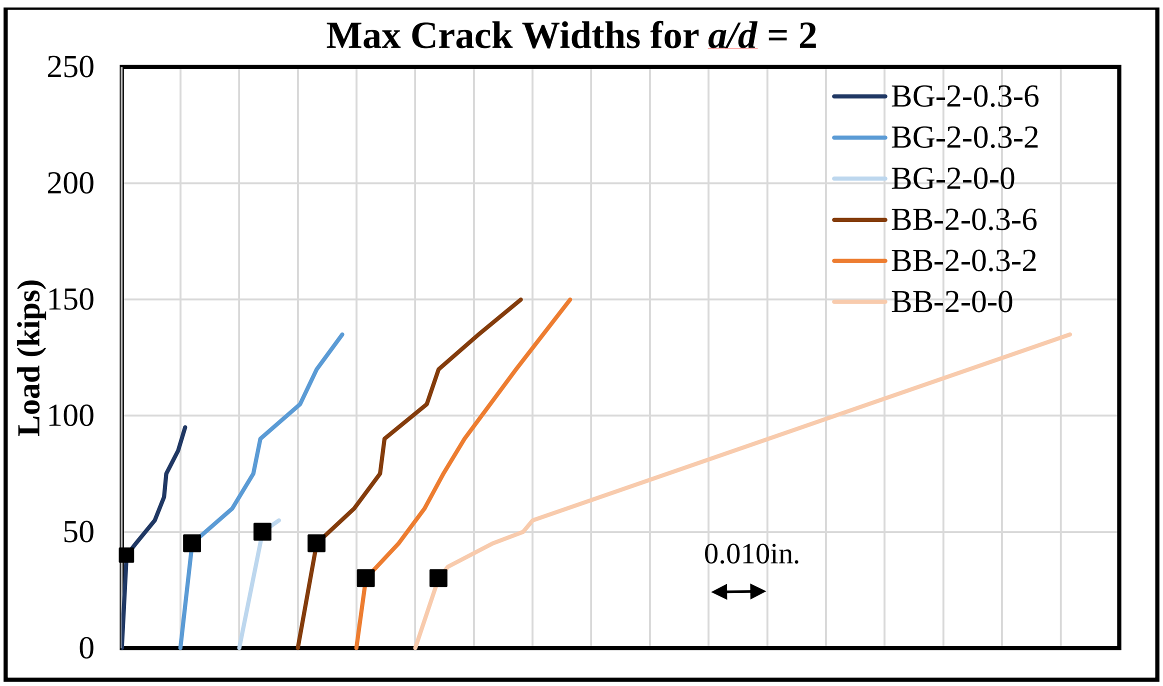

Figure 4-10: Maximum Crack Widths for Series 2 Specimens

The black squares show in Figure 4-9 and 4-10 indicate the first interval where cracks were measured.

Strain energy in the STM was calculated using Equation 2-9 and the values given in Section 3.3.2. The graphic legend mentioned in Section 4.2 is used to aid in visual analysis. The results for unreinforced (ρ = 0%, s = 0), and reinforced (ρ = 0.3%, s = $d/2$ and ρ = 0.3%, s = $d/6$) are shown in Figure 4-11 through 4 Figure 4-13, respectively.

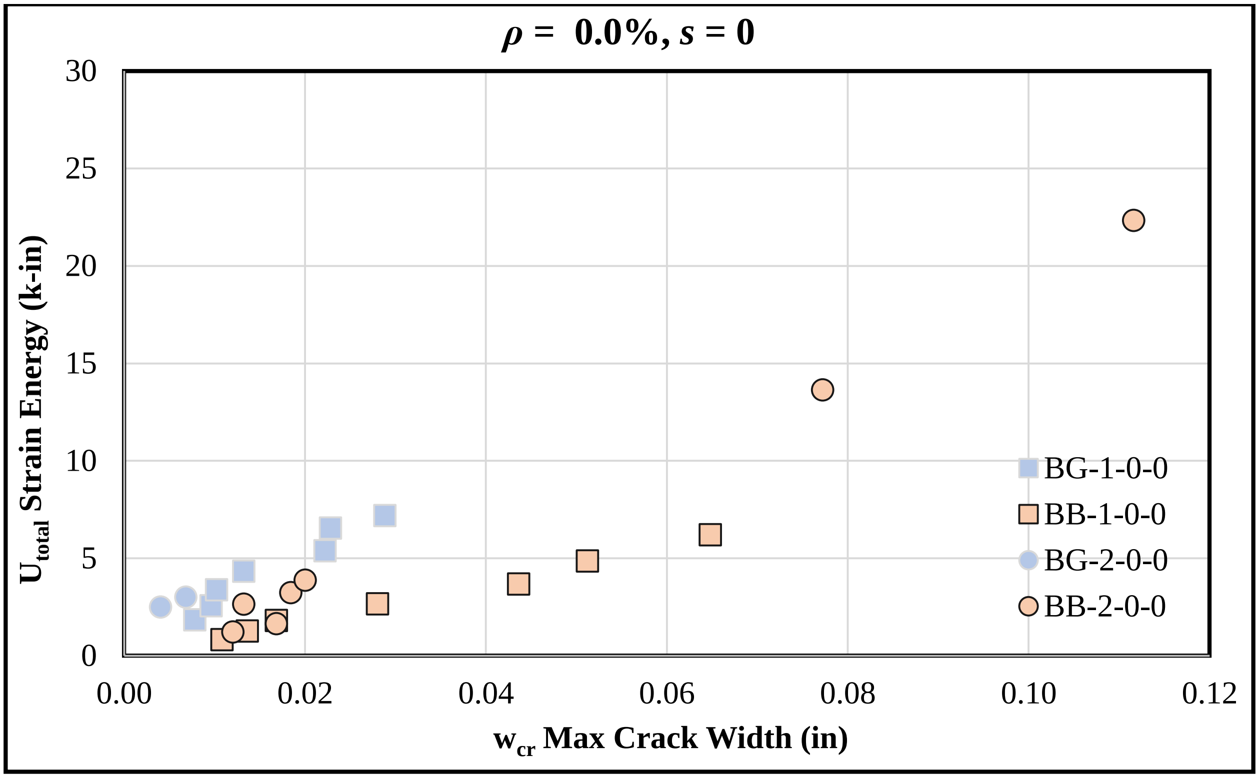

Figure 4-11: Max Diagonal Crack Width vs. Strain Energy for ρ = 0.0%, s = 0

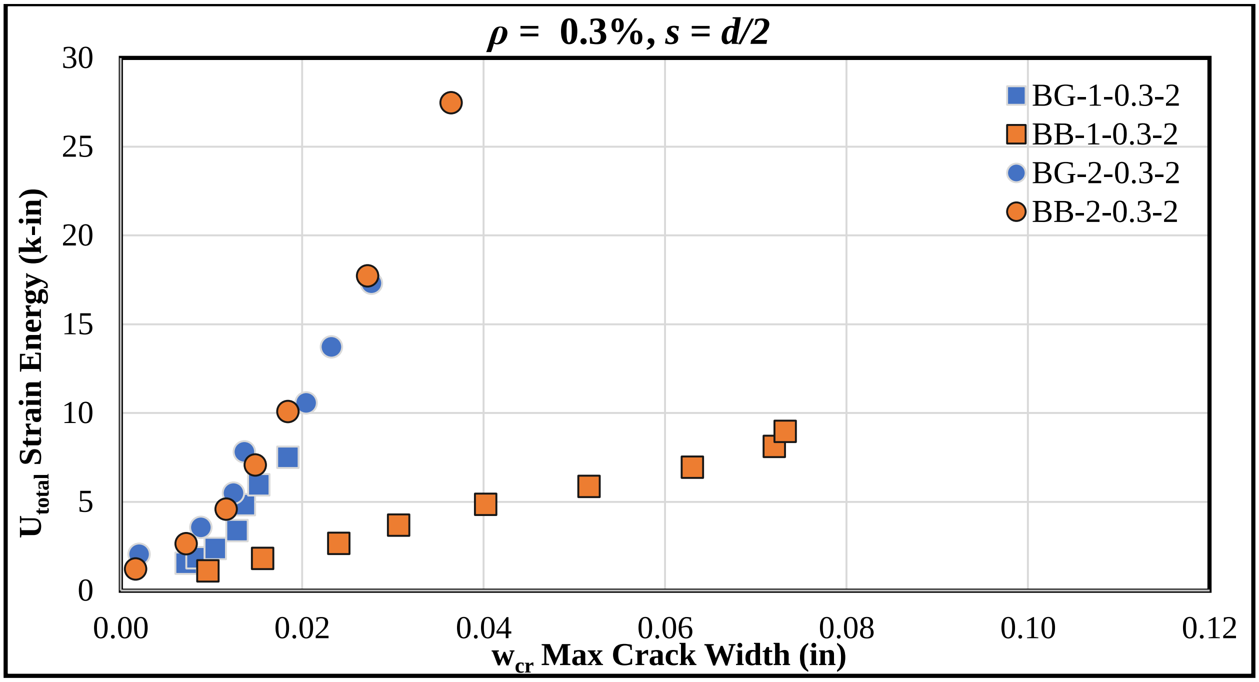

Figure 4-12: Max Diagonal Crack Width vs. Total Strain Energy for ρ = 0.3%, s = d/2

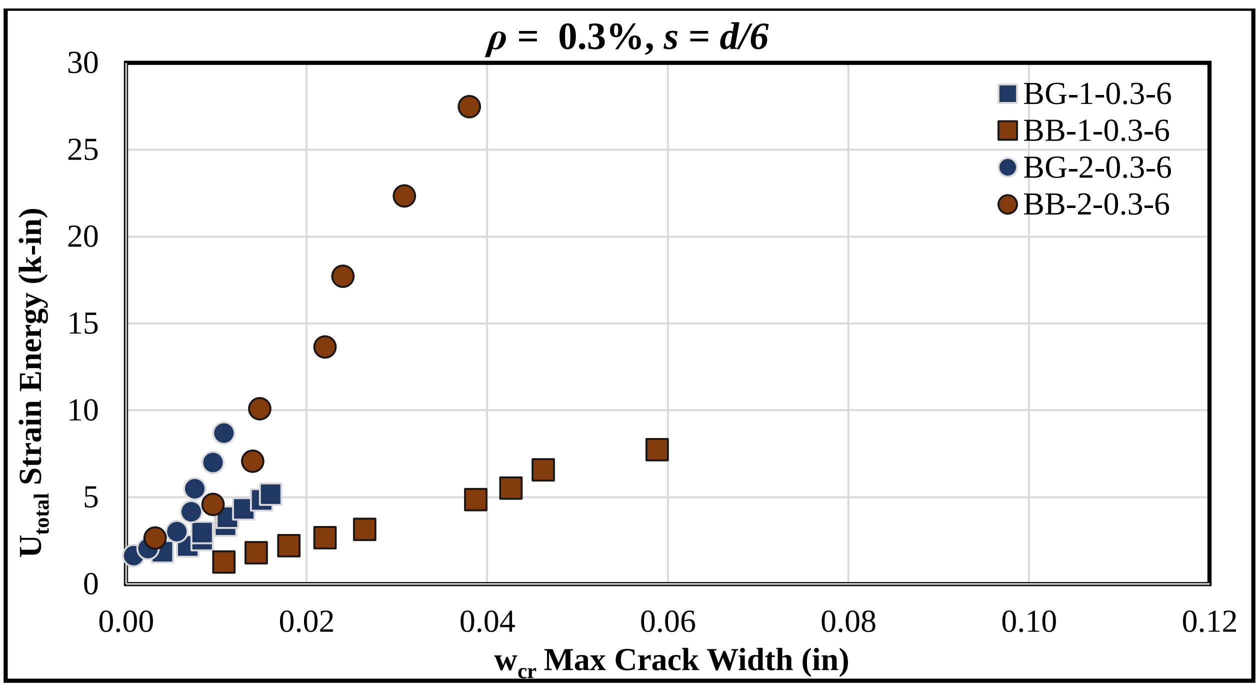

Figure 4-13: Max Diagonal Crack Width vs. Total Strain Energy for ρ = 0.3%, s = d/6

A complete table of all strain energy and crack measurements is located in Appendix F.

4.7 CRACK AREA

The total crack area was collected using the procedure discussed in Section 3.7.3. and calculated using Equation 2-10. The crack areas were then normalized by dividing out the total surface area in the testing region to create a percent of cracked area in testing region. Strain energy for the specimen STM was calculated using Equation 2-9 and the values given in Section 3.3.2. The graphic legend mentioned in Section 4.2 is used to aid in visual analysis. The results for unreinforced (ρ = 0%, *s* = 0), and reinforced (ρ = 0.3%, *s* = *d/2* and ρ = 0.3%, *s* = *d/6*) are shown in

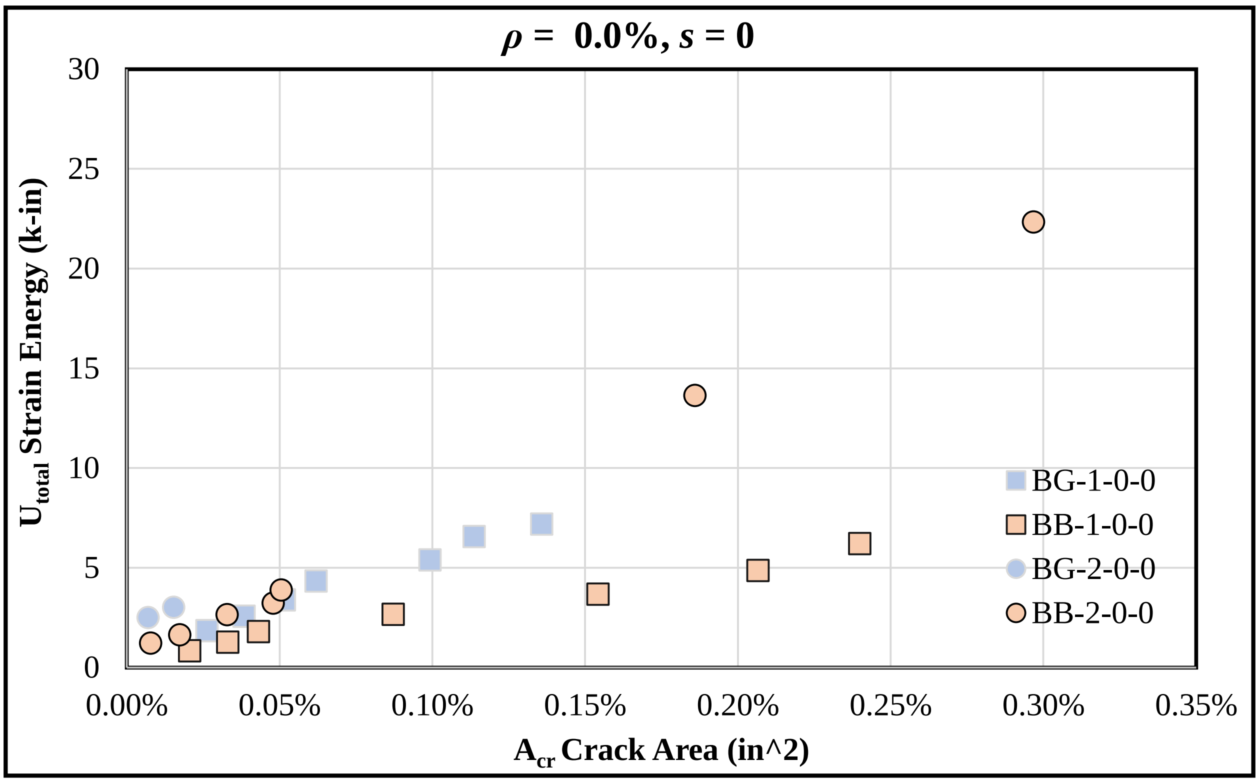

Figure 4-14 through Figure 4-16, respectively.

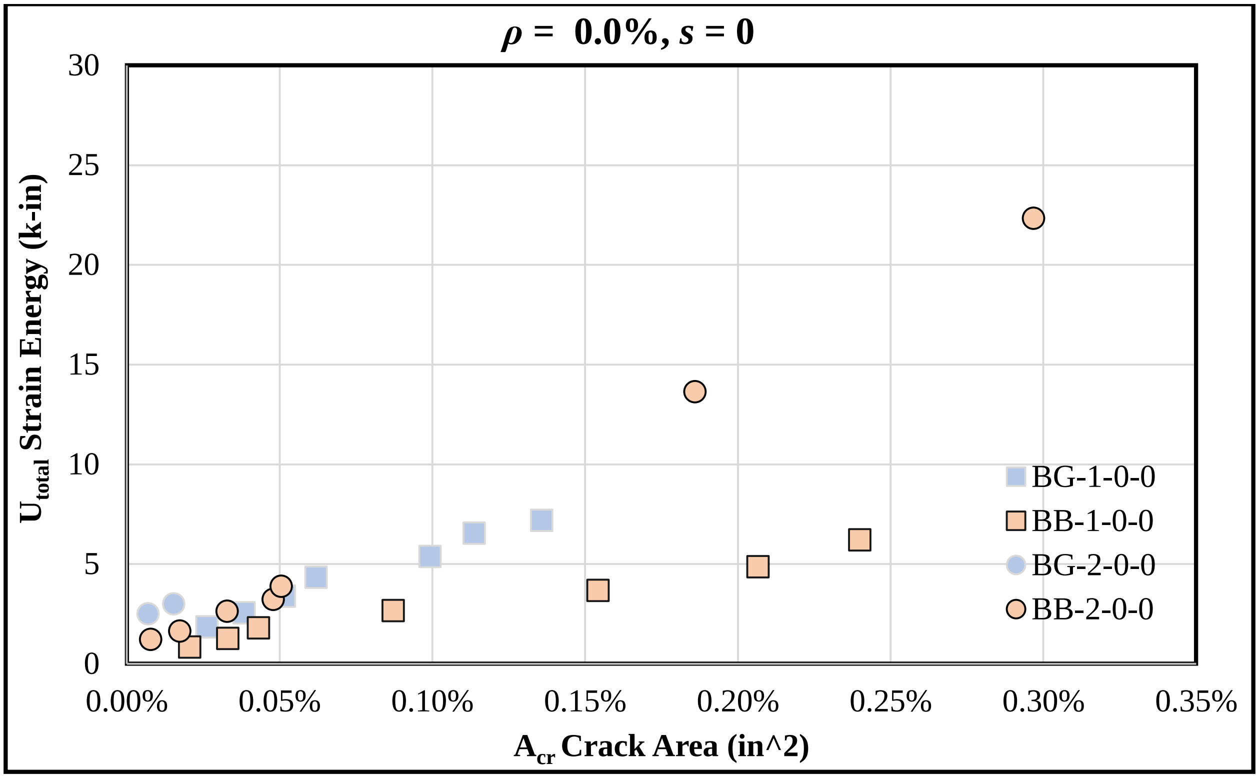

Figure 4-14: Normalized Crack Area vs. Strain Energy for ρ = 0.0%, s = 0

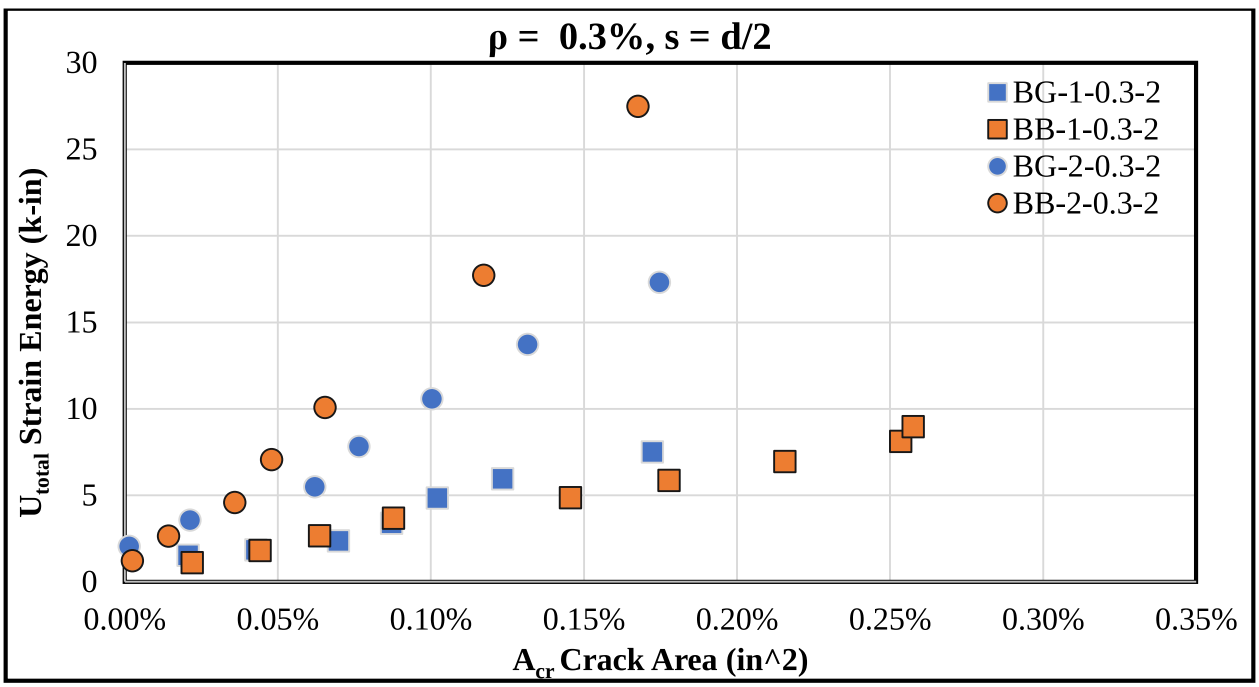

Figure 4-15: Normalized Crack Area vs. Total Strain Energy for ρ = 0.3%, s = d/2

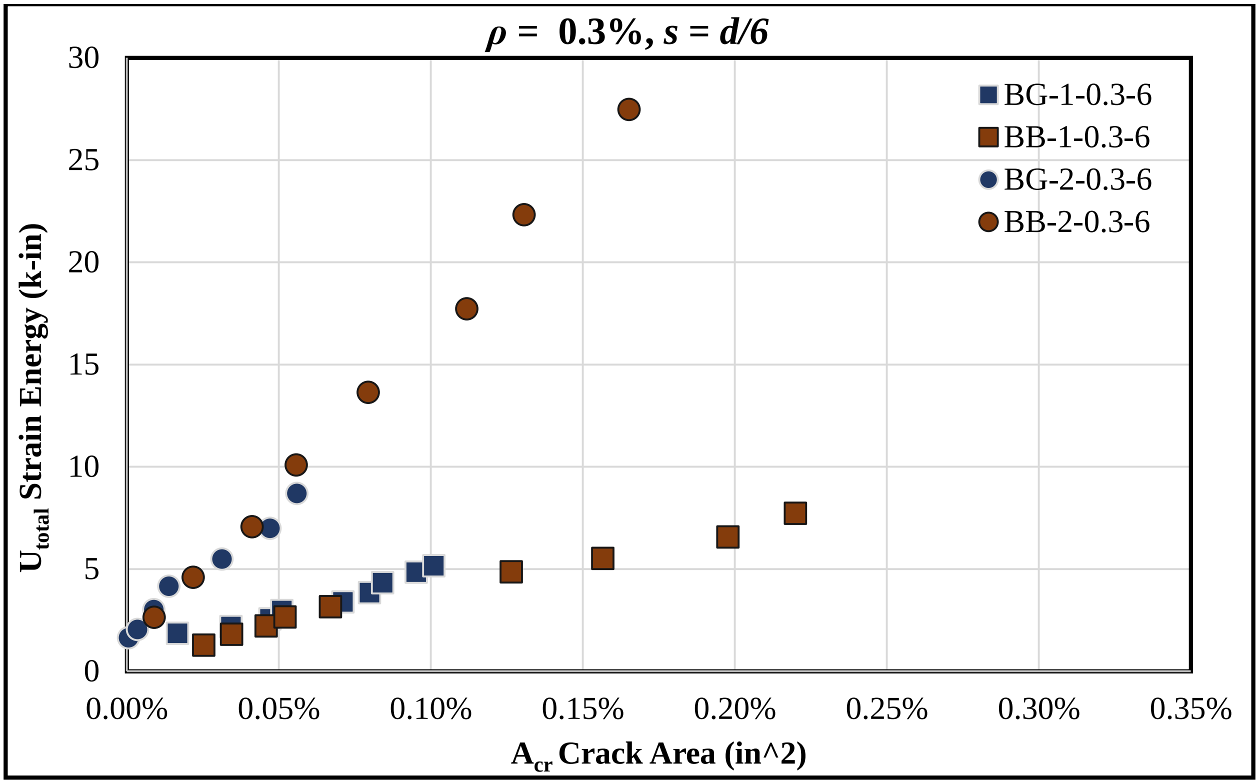

Figure 4-16: Normalized Crack Area vs. Total Strain Energy for ρ = 0.3%, s = d/6

Next, in Chapter 5, results are analyzed within the context of the project objectives.

CHAPTER 5

Discussion of Results

5.1 OVERVIEW

In this chapter, the results presented in Chapter 4 are discussed with respect to the three objectives of this study:

1) To investigate the serviceability behavior of concrete D-regions in terms of maximum crack width and tie strain estimated in representative STM;
2) To investigate the serviceability behavior of concrete D-regions in terms of total crack area and strain energy estimated in representative STM;
3) To recommend a procedure for distinguishing a ‘good’ STM from a ‘bad’ model.

The secondary goal of this project, to refine existing methods for collecting crack and displacement data by digital means, is also discussed.

To accomplish the above objectives, the following variables are isolated and their influence investigated:

1) Web Reinforcement (ρ = 0% and 0.3%)
2) Spacing of web reinforcement (d/2 and d/6)
3) Tie Model (Model G and B)
4) Shear span-to-depth ratio (a/d = 1 and 2)

5.2 MAX CRACK WIDTH VS STRAIN ENERGY

The influence of shear reinforcement, spacing of web reinforcement, tie model and shear span-to-depth ratio on maximum crack with are discussed in this section. The following figures are in terms of estimated tie strain and experimentally measured maximum crack width.

The y-intercept for all trendlines on Figure 5-1 through Figure 5-5 is equal to 0.0006 in/in due to the estimated initial strain in the tie before the beam noticeably cracks (cracks greater than 0.002 in.). This value was found by averaging the y-intercepts for all trendlines as suggested by the data. The y-intercept should not be zero because the specimen contains strain energy before it initially cracks.

5.2.1 Shear Reinforcement

Figure 5-1 and Figure 5-2 illustrate the influence of web reinforcement on maximum crack width for *a/d* 1 and 2.

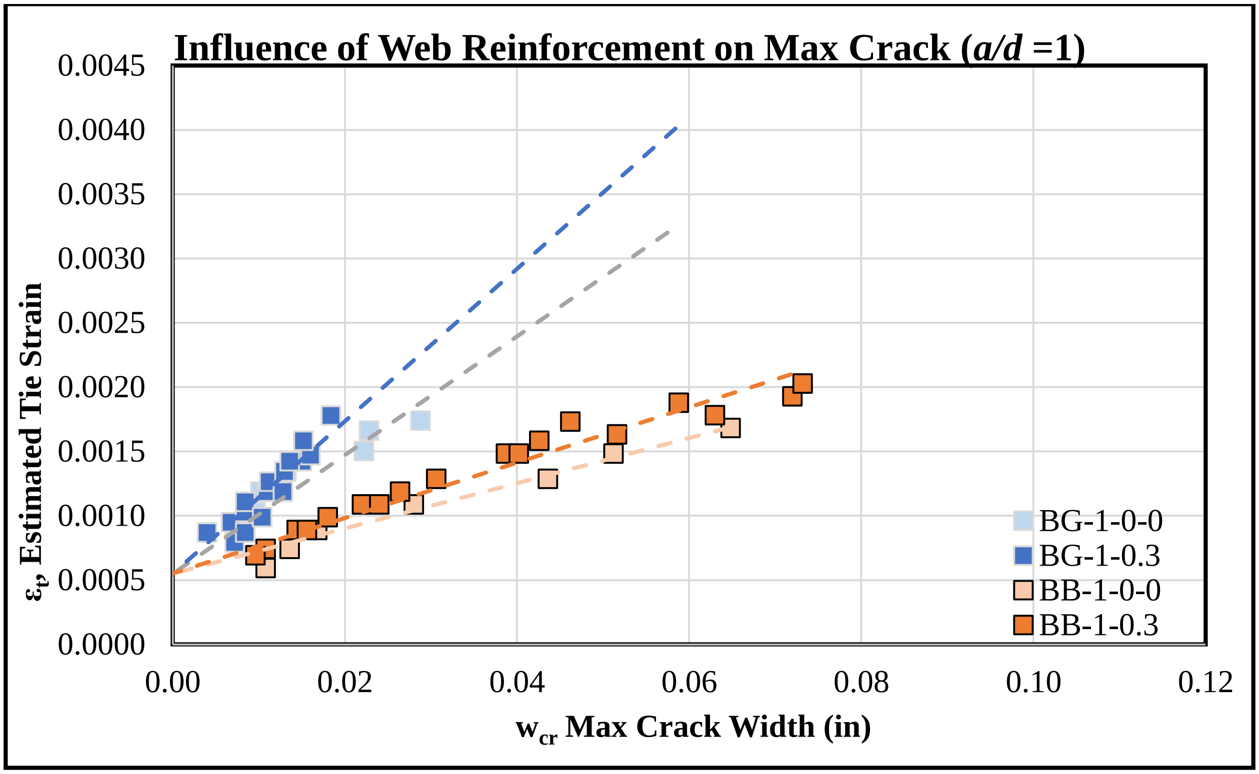

Figure 5-1: Influence of Web Reinforcement on Max Crack (a/d = 1)

The data labeled BG-1-0.3 and BB-1-0.3 include specimens with spacing of *d/2* and *d/6*. As seen in Figure 5-1, the influence of shear reinforcement at *a/d* equal to 1 is minimal. The addition of web reinforcement decreases maximum crack width by approximately 20%. This observation agrees with what has been observed by past research (Chapter 2).

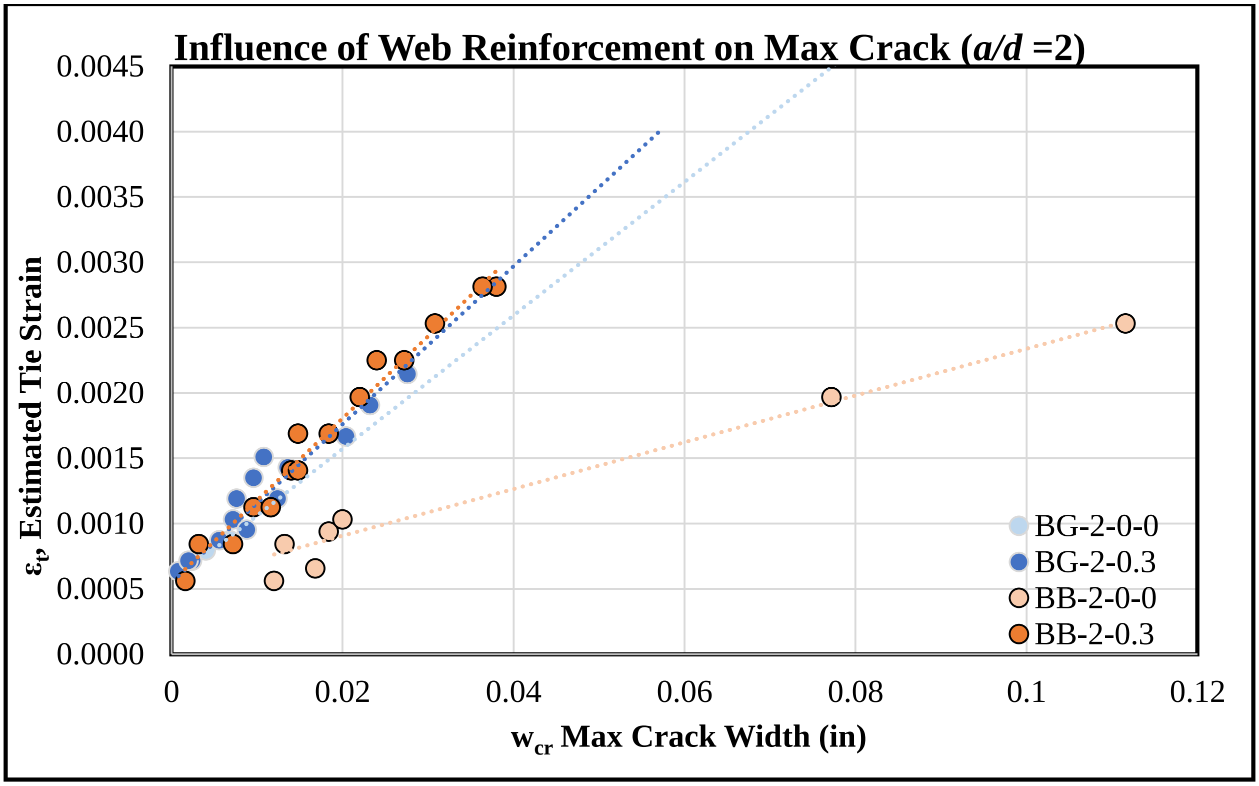

Figure 5-2: Influence of Web Reinforcement on Max Crack (a/d = 2)

The data labeled BG-2-0.3 and BB-2-0.3 include specimens with spacing of *d/2* and *d/6*. The influence in web reinforcement for *a/d* equal to 2 is significant. The Model G beams are somewhat inconclusive due to the small amount of data however, the influence expected would also be significant based on results from previous studies.

The results for both *a/d* suggest, if web reinforcement equal to 0.3% of the cross-section is provided, the relationship between tie strain and crack width is constant regardless of model configuration for both *a/d* equal to 1 and 2.

5.2.2 Shear Stirrup Spacing

Figure 5-3 and Figure 5-4 illustrate the influence of web reinforcement spacing on maximum crack width for *a/d* equal to 1 and 2, respectively.

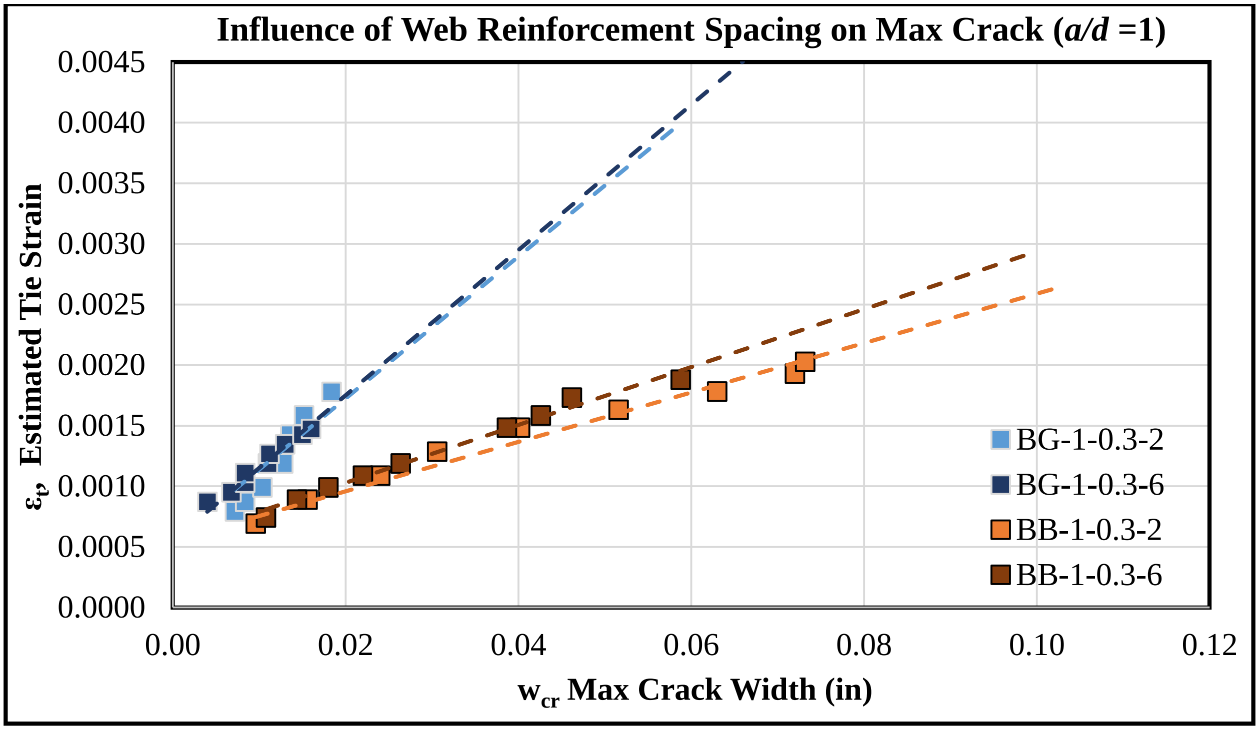

Figure 5-3: Influence of Web Reinforcement Spacing on Max Crack (a/d = 1)

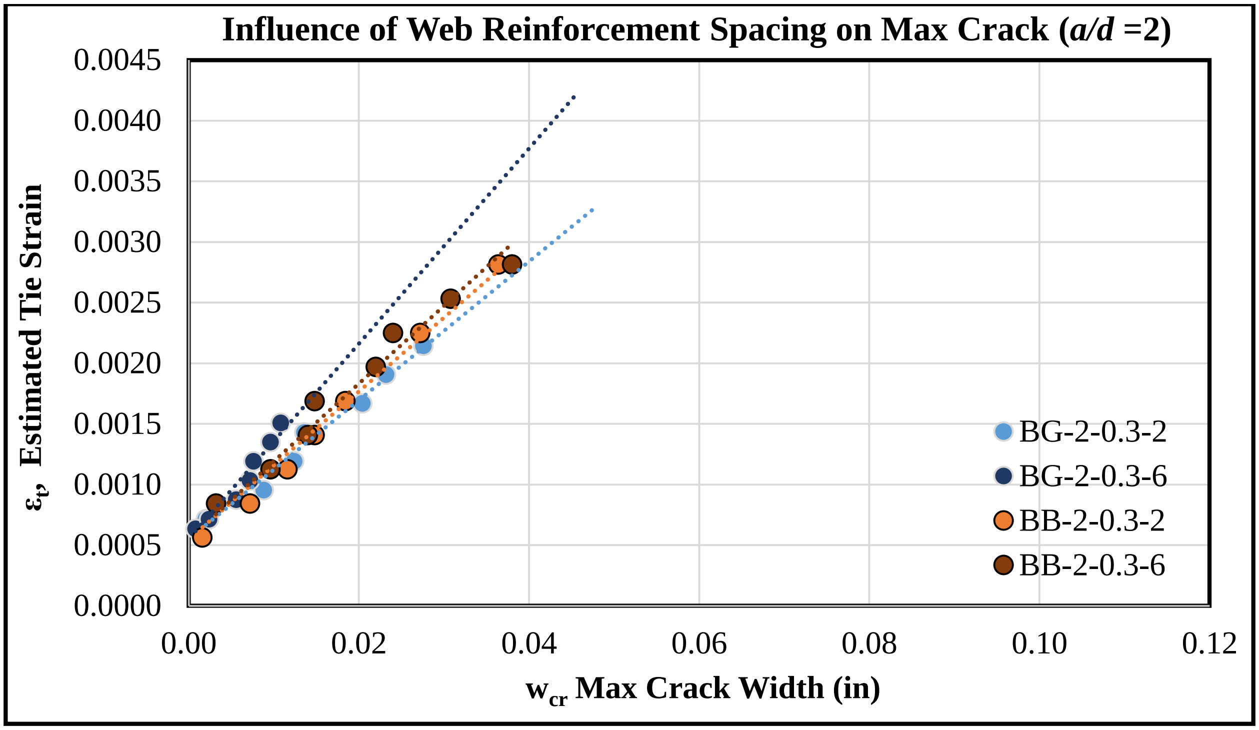

Figure 5-4: Influence of Web Reinforcement Spacing on Max Crack (a/d =2)

For both figures shown, insignificant influence of web reinforcement spacing is observed, regardless of model configuration or *a/d*.

5.2.3 Tie Model and Shear Span-to-Depth Ratio

Figure 5-5 illustrates the influence of tie model and *a/d* on maximum crack width.

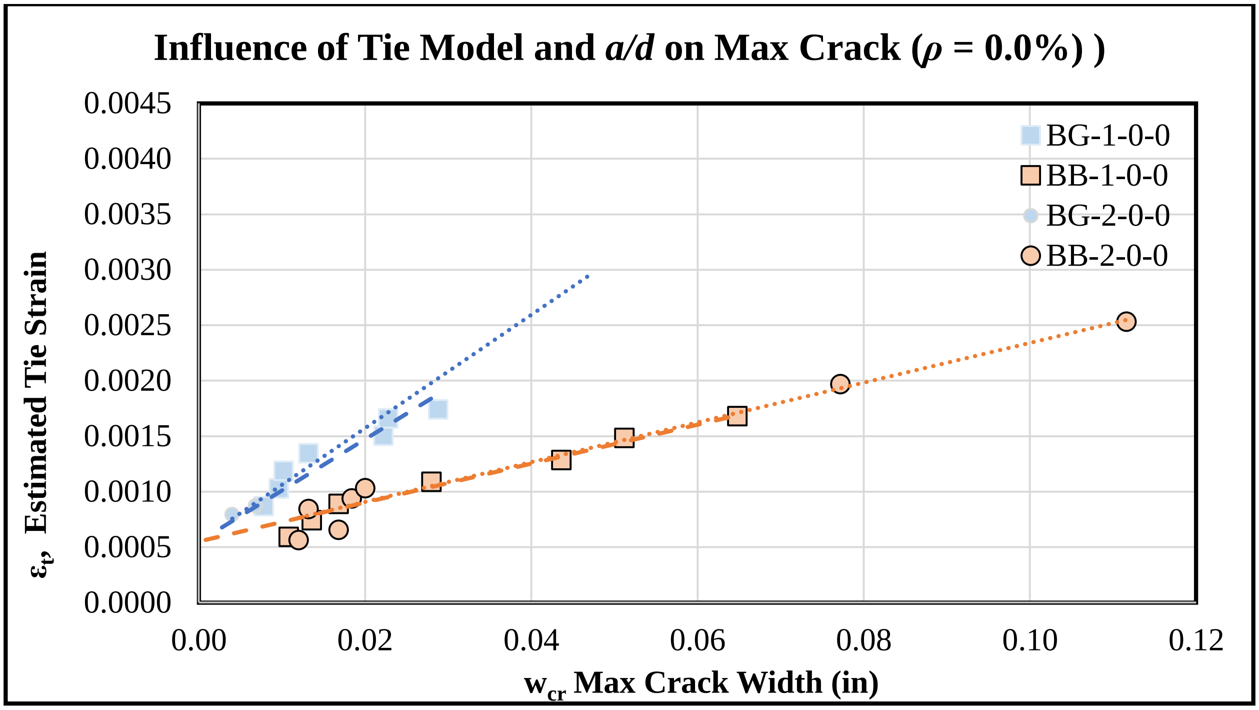

Figure 5-5: Influence of Tie Design on Max Crack (ρ = 0.0%)

Figure 5-5 indicates the chosen tie model has a significant influence on maximum crack. This may be explained by the orientation of the tie and principal tension with respect to the orientation of the diagonal cracks. For example, for Model B specimens, both principal tension and the tie are normal to the diagonal crack (i.e. the tie is parallel to the principal tension). On the other hand, Model G specimens have a tie that is approximately 45° from the crack's orientation leaving only principal tension normal to the maximum crack. Based on the above results, orienting the tie parallel to principal tension increased crack widths by 90%. One caveat is this assumes principal tension is not influenced by shear strains. Figure 5-5 also indicates, for a given tie model, tie strain is proportional to max crack width with no observable influence on *a/d* ratio.

5.3 CRACK AREA VS STRAIN ENERGY

The influence of shear reinforcement, spacing of web reinforcement, tie model and shear span-to-depth ratio on crack area are discussed in this section. The following figures are in terms of estimated total strain in STM (U_{total}) calculated by Equation 2-9 and experimentally measured crack area (Section 3.7.3) which has been normalize by the total area of testing region.

The y-intercept for all trendlines on Figure 5-6 through Figure 5-12 is equal to 1 due to the estimated initial strain energy in STM before the specimen noticeably cracks (cracks greater than 0.002 in.). This intercept was found by taking the average of all intercepts of best fit lines. The reason it is not equal to zero is because the beam can absorb work before cracking due to elastic straining of concrete.

5.3.1 Web Reinforcement

The influence of shear reinforcement on normalized total cracked area of concrete is discussed in this section. Figure 5-6 and Figure 5-7 illustrate the influence of web reinforcement for specimens with *a/d* equal to 1 and 2.

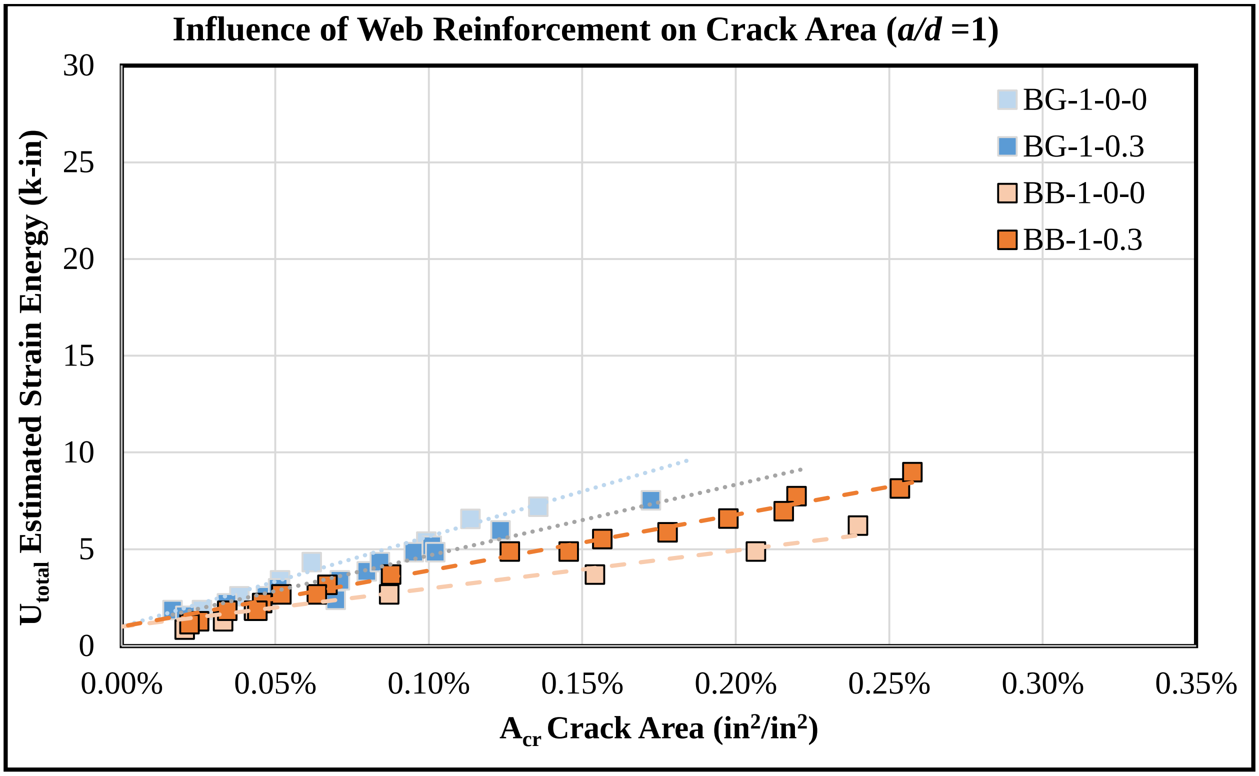

Figure 5-6: Influence of Web Reinforcement on Crack Area (a/d =1)

The data labeled BG-1-0.3 and BB-1-0.3 include specimens with spacing of *d/2* and *d/6*. Similar to its influence on maximum crack width, Figure 5-6 indicates there is minimal influence of web reinforcement for specimens with *a/d* equal to one.

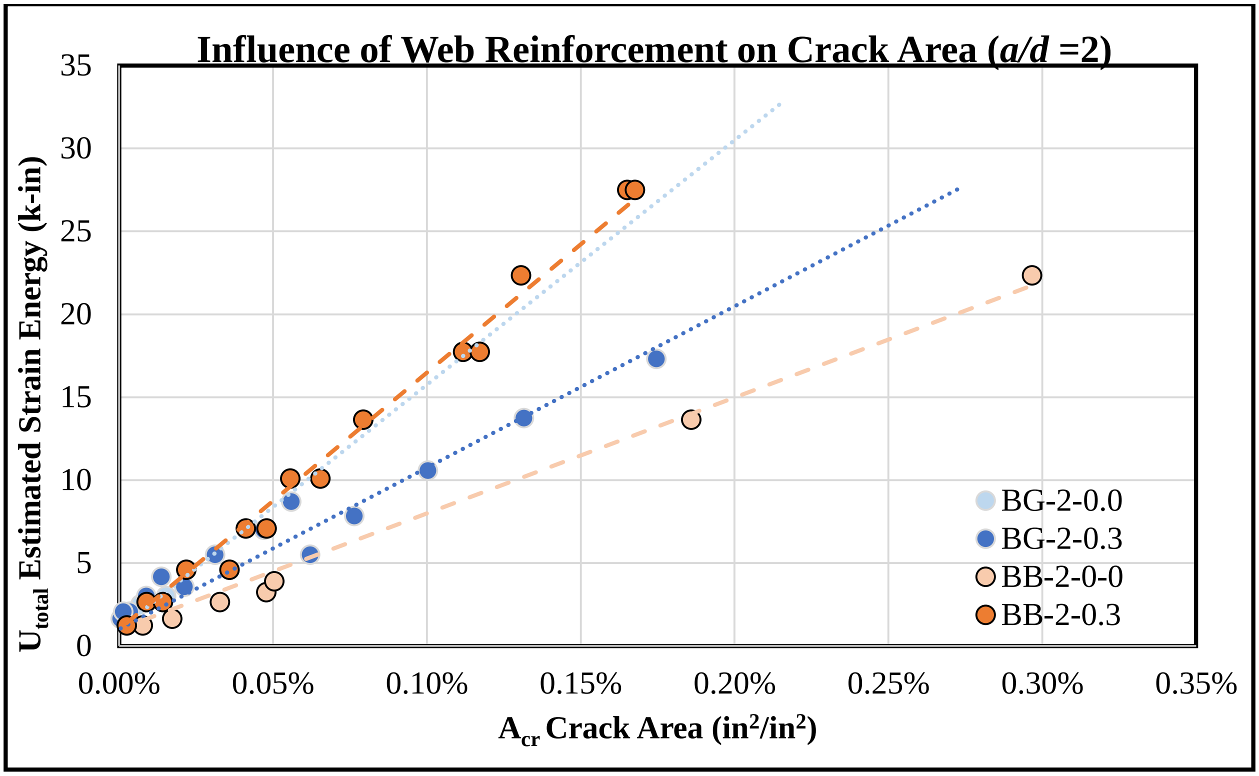

Figure 5-7: Influence of Web Reinforcement on Crack Area (a/d = 2)

The data labeled BG-2-0.3 and BB-2-0.3 include specimens with spacing of *d/2* and *d/6*. Again, for Models G specimens, the results are inconclusive due to the small amount of experimental data collected for specimen BG-2-0-0. However, there is a significant influence shown in the model B specimens. The reason for this is most likely because the selected modeled used in the calculation of U_{total} is a poor representation of the actual load path when web reinforcing is present.

5.3.2 Shear Stirrup Spacing

The influence of web reinforcement spacing on normalized total cracked area of concrete is discussed in this section. Figure 5-8 and Figure 5-9 illustrate the influence of web reinforcement spacing for specimens with *a/d* equal to 1 and 2.

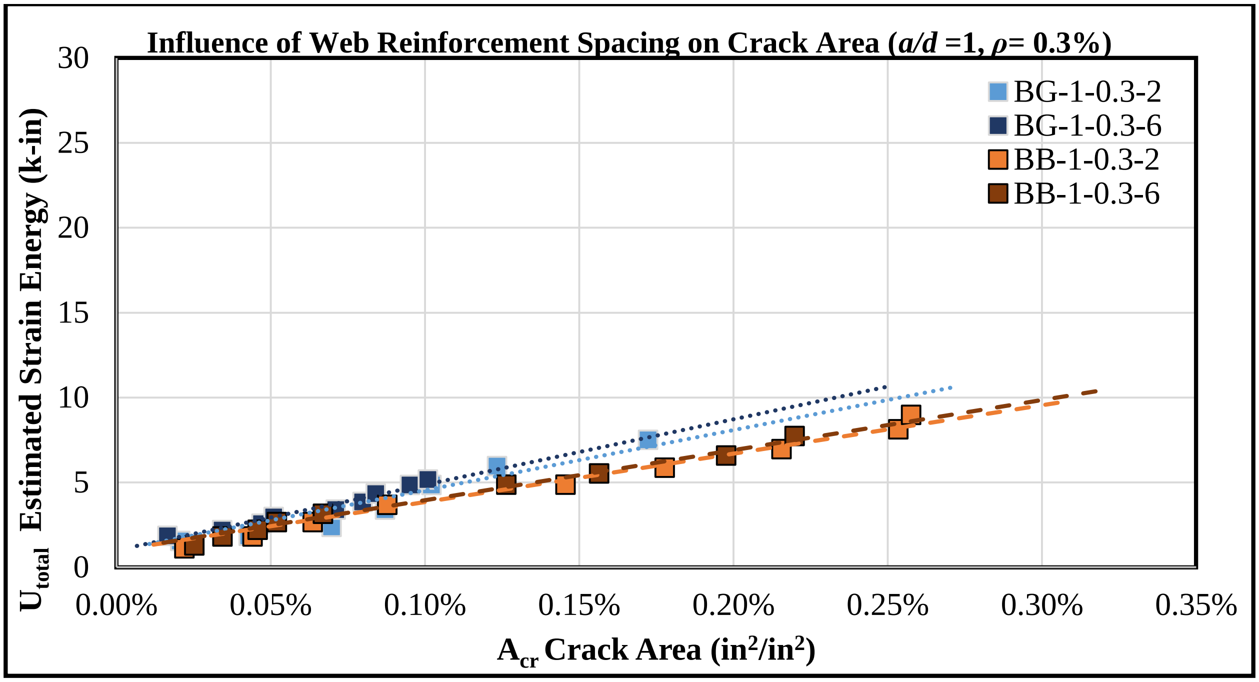

Figure 5-8: Influence of Web Reinforcement Spacing on Crack Area (a/d = 1, ρ = 0.3%)

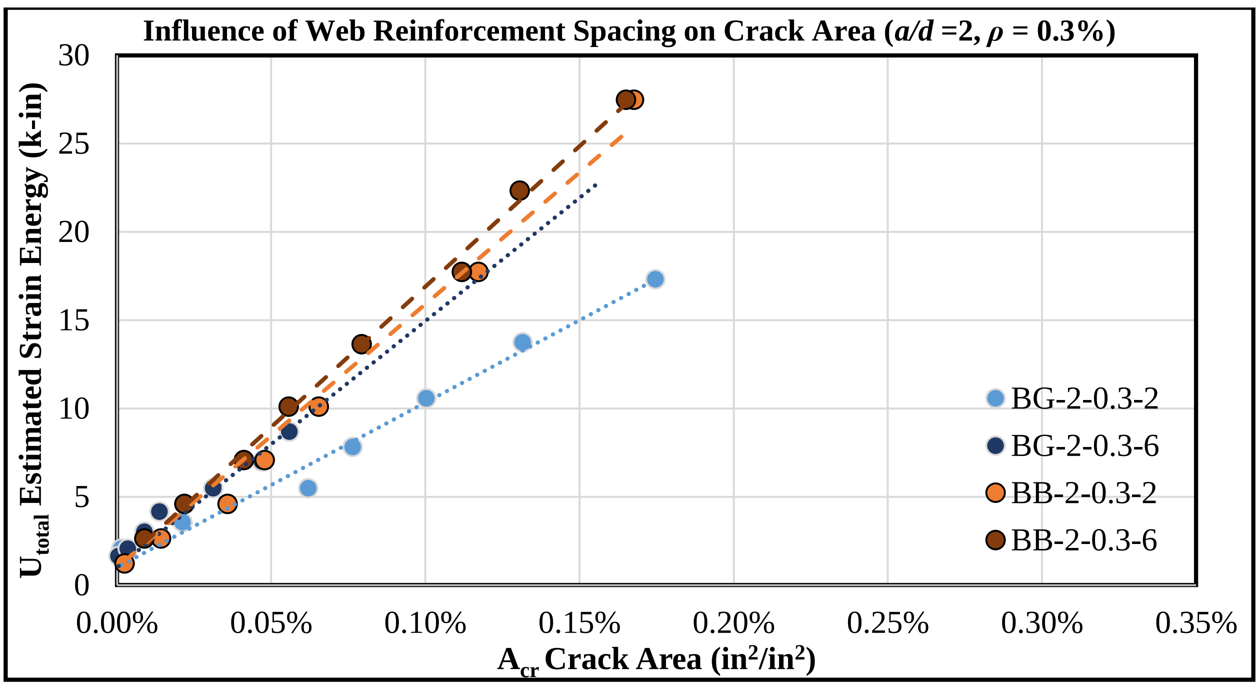

Figure 5-9: Influence of Web Reinforcement Spacing on Crack Area (a/d = 2, ρ = 0.3%)

As seen in the above figures, there is not a significant influence of spacing of web reinforcement on total crack area. With one exception, the model G specimens at *a/d* equal to two show a slight influence, this could be due the actual shear transfer. This is not seen in the Model B specimens because of the interaction between shear transfer and the tie.

5.3.3 Tie Model

Figure 5-10 illustrates the influence of tie model on total crack area for specimens with *a/d* equal to one, and no web reinforcement.

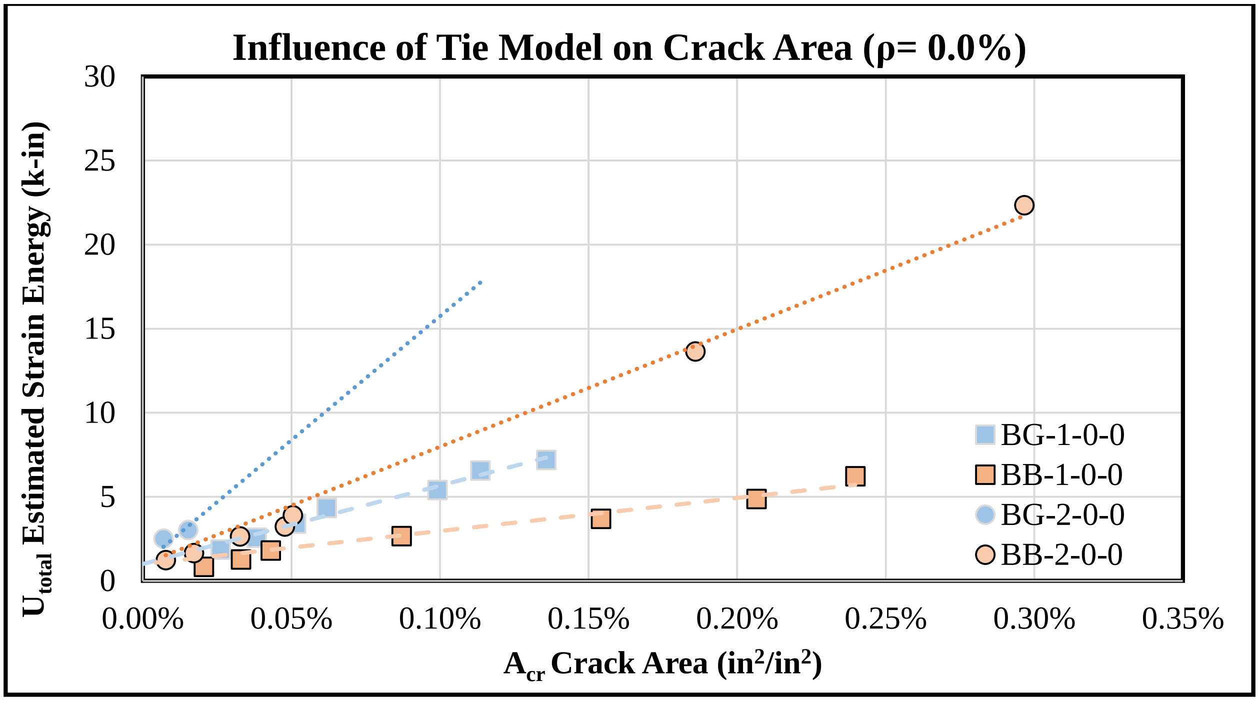

Figure 5-10: Influence of Tie Model on Crack Area (ρ = 0.0%)

As shown in Figure 5-5, there is a small difference between for *a/d* equal to 1 and inconclusive for *a/d* equal to 2, when comparing Models B and G.

5.3.4 Shear Span-to-Depth Ratio

The influence of shear span-to depth ratio on normalized total crack area is discussed in this section. Figure 5-11 illustrates the influence of *a/d* on crack area for both reinforced and unreinforced model G specimens. Figure 5-12 illustrates the same influence for model B specimens.

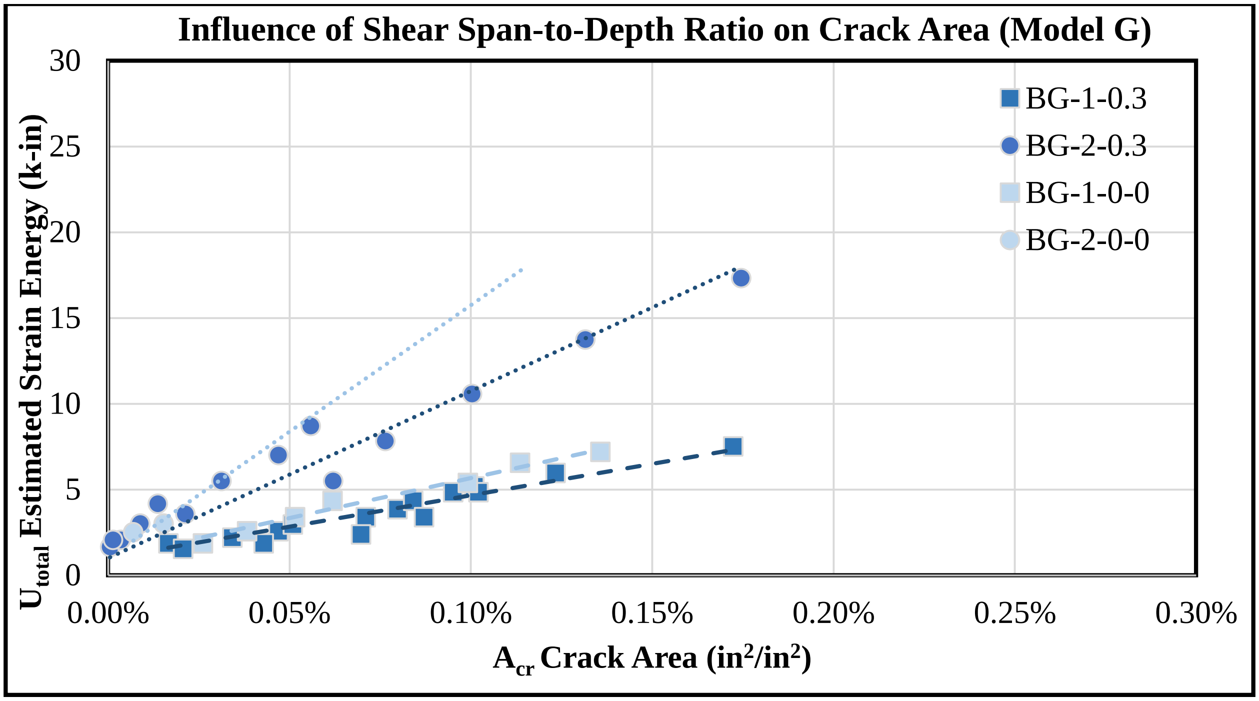

Figure 5-11: Influence on Shear Span-to-Depth Ratio on Crack Area (Model G)

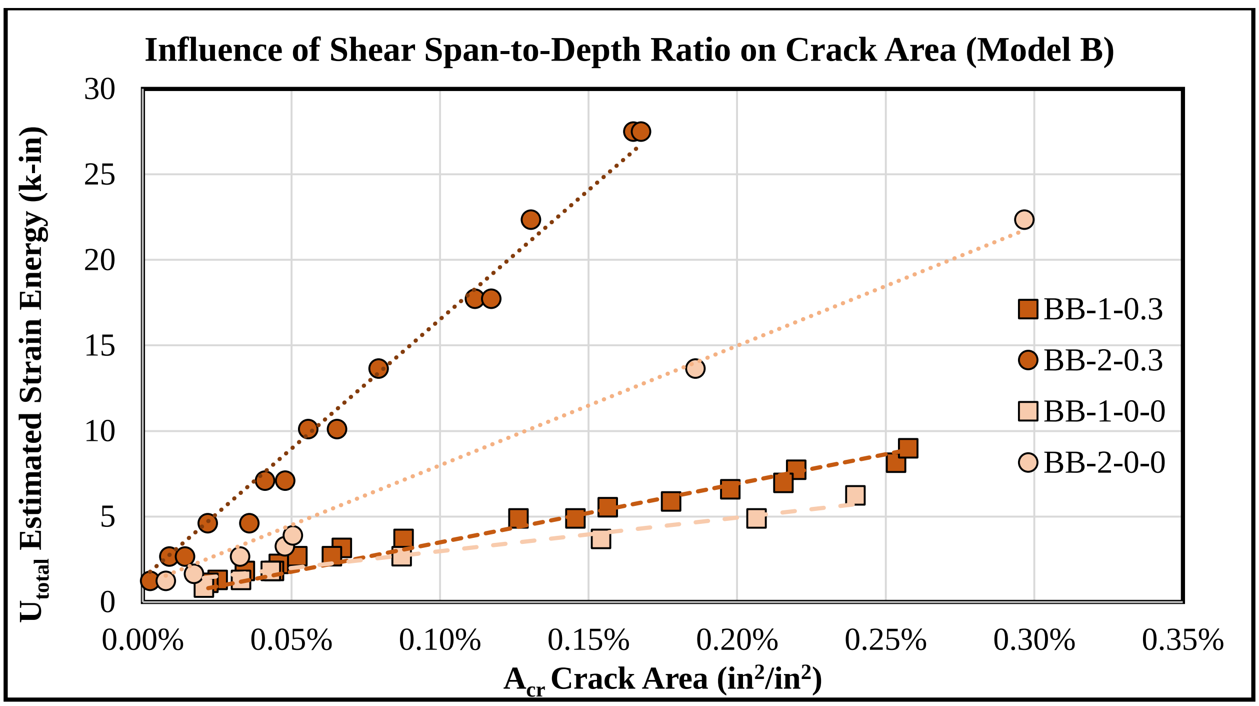

Figure 5-12: Influence of Shear Span-to-Depth Ratio on Crack Area (Model B)

The results shown in Figure 5-11 and Figure 5-12 provide insight as to how well the estimated STM is actually modeling the load path. For *a/d* equal to 1, the strain energy calculation collected from the assumed STM models the load path fairly well for both the Model G and Model B. For *a/d* equal to 2, the presence of web reinforcement allows alternate load paths which, in turn, indicates the assumed STM used to calculate strain energy is, likely, less than an ideal representation.

5.4 DESIGN PROCEDURE

5.4.1 Predicting Maximum Crack Width, w_{cr}

The first objective of this study is to investigate the relationship between the strain in the tie and maximum crack width. The results indicate there is a relationship between tie strain and maximum crack width provided the beam contains web reinforcement equal to 0.3% of the cross-section. However, the orientation of the tie with respect to principle tension is also an important factor to consider. Figure 5-13 illustrates this relationship.

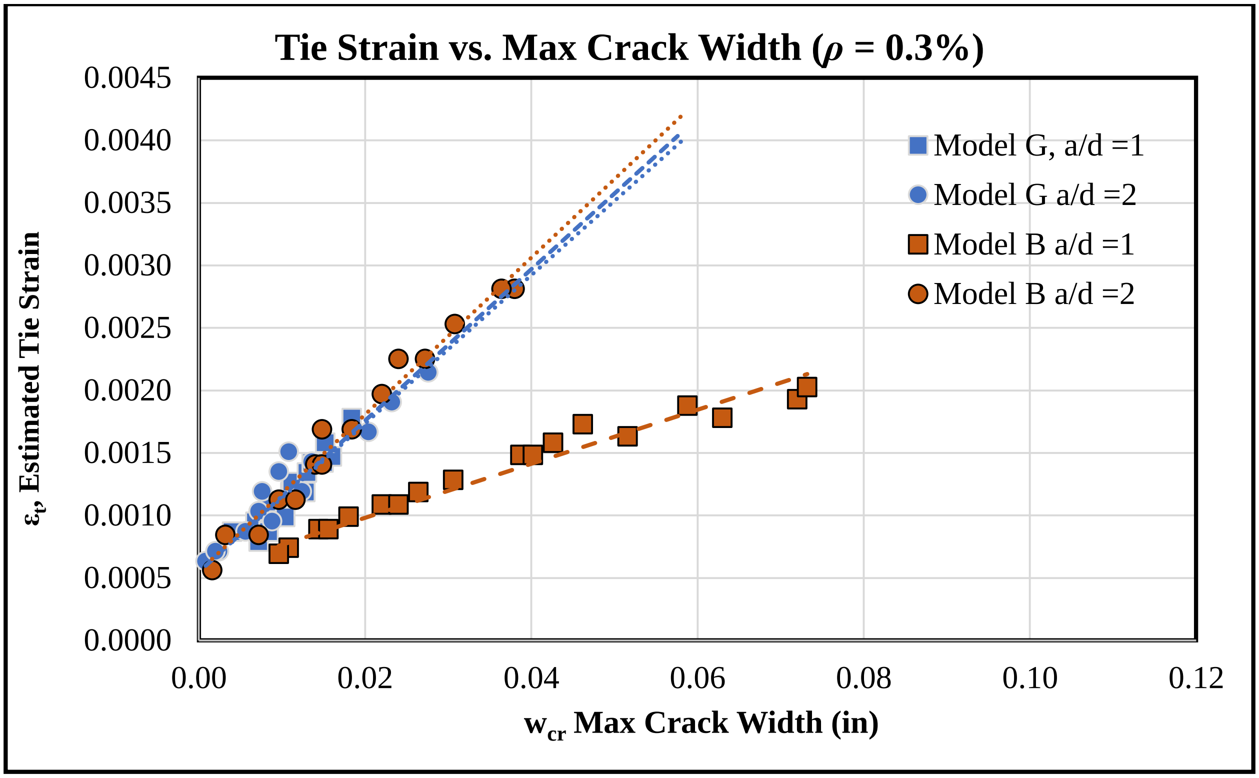

Figure 5-13: Relationship of Tie Strain and Maximum Crack Width (ρ = 0.3%)

Figure 5-13 includes all beams containing web reinforcement of 0.3%, regardless of spacing.

5.4.2 Predicting Area of Cracked Surface, A_{cr}

The second objective of this study aims to correlate strain energy in a representative STM to total crack area. It was found for *a/d* equal to 1, there is a fairly constant correlation. For *a/d* equal to 2, the correlation is more influenced by alternative load paths and orientation of tie with respect to principal stresses. Figure 5-14 illustrates this correlation.

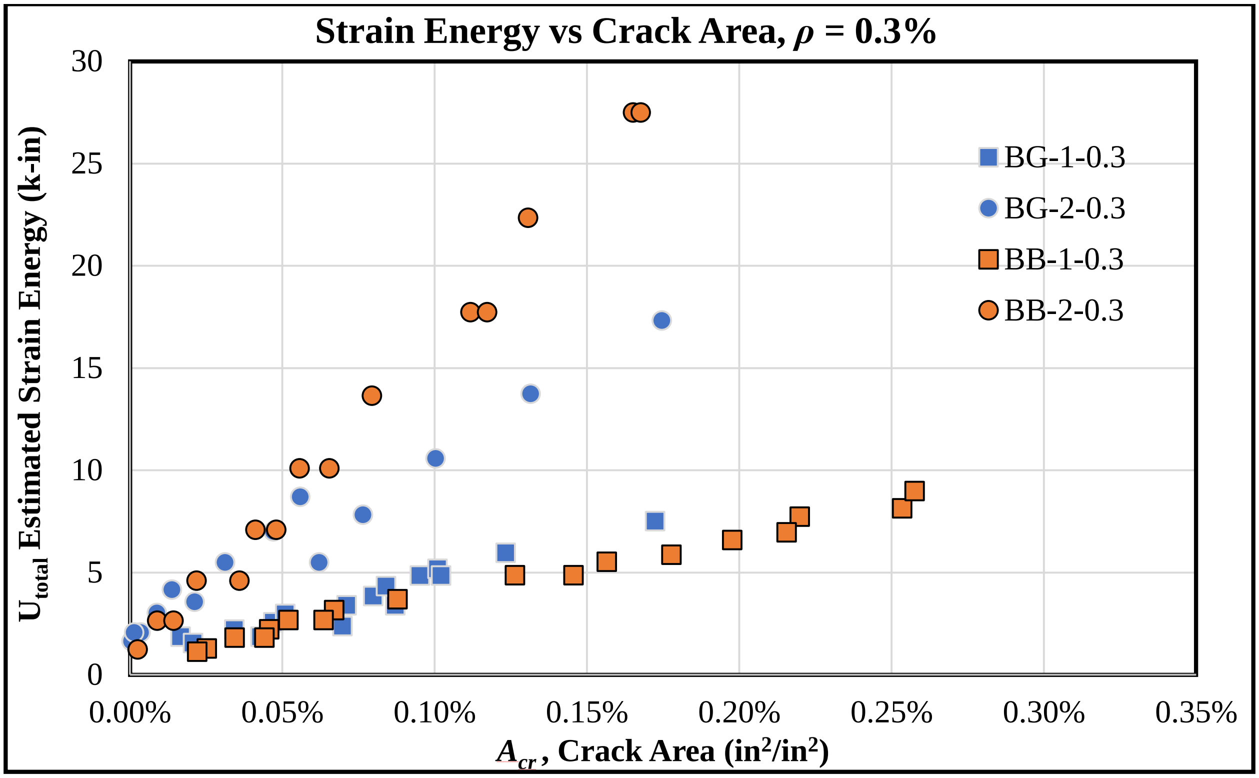

Figure 5-14: Relationship between Strain Energy and Crack Area

All data shown in Figure 5-14 contains web reinforcement of 0.3%, regardless of spacing. For *a/d* equal to 2, model configurations have more of an influence on U_{total} calculations. It is important the assumed model correlates with actual load path, especially for *a/d* approaching 2. If minimum reinforcement is provided, an improved correlation is attained.

5.4.3 Distinguishing a "Good" from a "Bad" model

The final objective of this study is to provide a procedure a designer may use to determine an optimized model and use to predict crack widths. The results indicate the ratio of strain energy in a tie (U_{tie}) to total strain energy (U_{total}) can help determine the anticipated serviceability performance of an STM based on its configuration. Figure 5-15 shows the propagation of maximum crack width for all twelve specimens up to 70% of their ultimate capacity (assumed service-level loading).

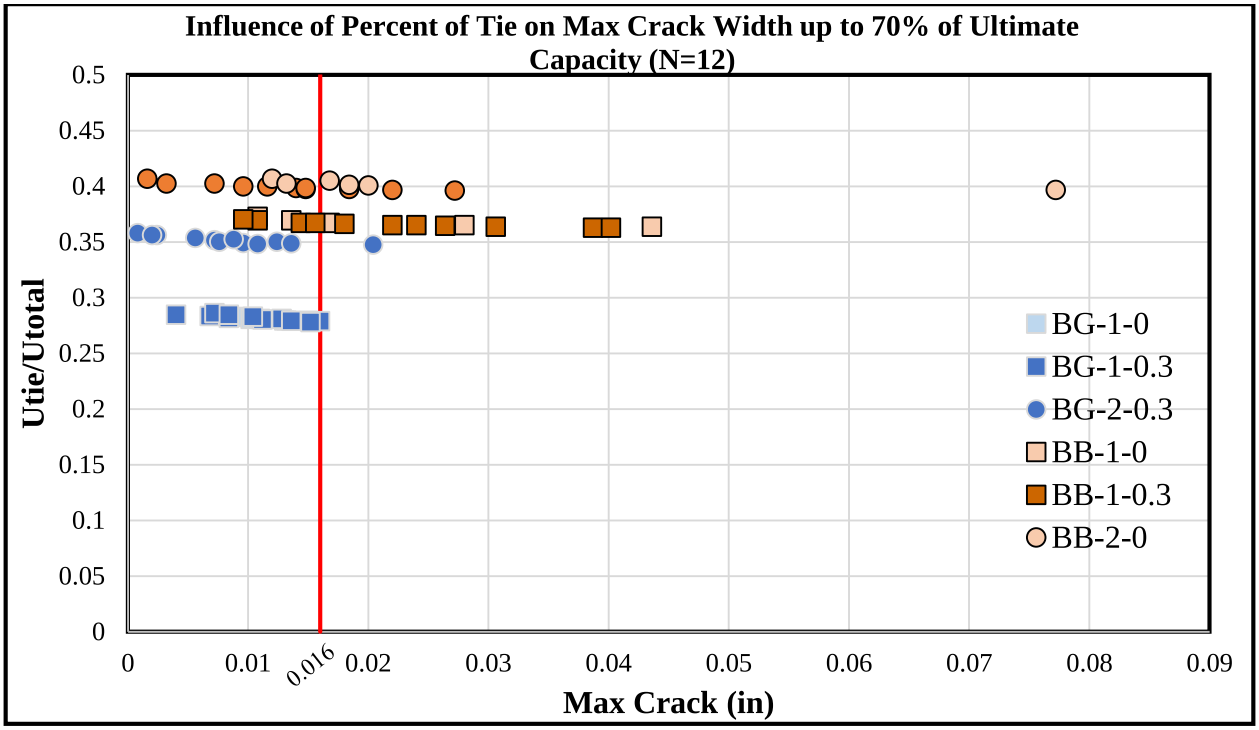

Figure 5-15: U_{tie}/U_{total} versus Maximum Crack Width up to 70% of ultimate capacity

As seen in Figure 5-15, most specimens with a U_{tie}/U_{total} less than or equal to 35% stay below an "accepted" maximum allowable crack width of 0.016 (Oesterle, 1997). These results agree with the recommendations of Schlaich et al. (1987). Based on the results, to optimize an STM, it is recommended to limit the percentage of U_{tie}/U_{total} to less than or equal to 35%.

Strain energy for each STM was calculated using Equation 2-9. To illustrate, the total strain energy in each STM series, is shown in Table 5-1. All strain energy calculations are given in Appendix F.

Table 5-1: Strain Energy Normalized by Load

	Load (kip)	% Ultimate	Tie Model	U_{total} (kip-in)	U_{tie} (kip-in)	U_{tie}/U_{total}
Series 1	110	54%	B	2.67	0.98	36%
		57%	G	1.86	0.53	28%
Series 2	75	46%	B	7.08	2.82	40%
		48%	G	5.49	1.92	35%

If web reinforcement equal to 0.3% of the cross-section is provided and U_{tie}/U_{total} is less than or equal to 35%, a reasonable estimator of maximum crack width is given in Figure 5-16.

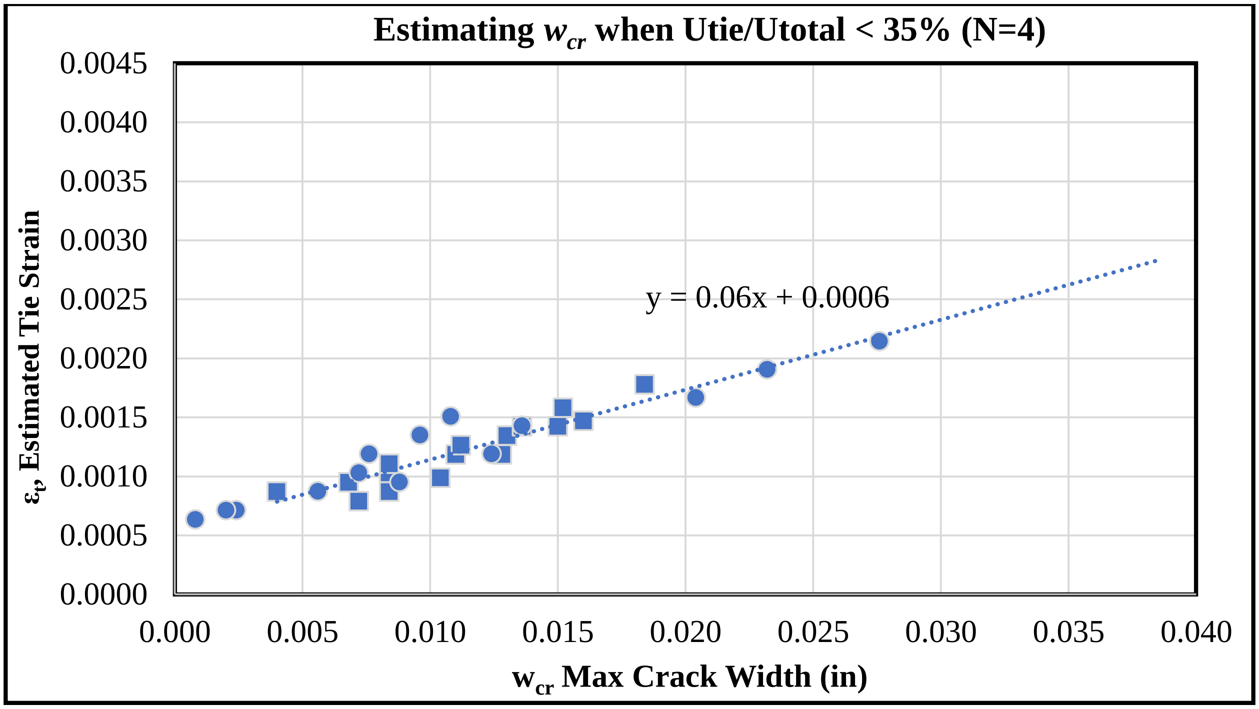

Figure 5-16: Design Tool for Estimating Crack Widths (ρ = 0.3%)

The four specimens used to derive the above figure include model G beams with *a/d* of 1 and 2 containing 0.3% web reinforcement. The above design tool is for *a/d* ratios ranging from 1 to 2. The relationship between strain in tie and crack width are given in Equation 5-1.

Equation 5-1

$$\varepsilon_t = 0.060w_{cr} + 0.0006$$

Where,

ε_t = Estimated strain energy in tie

w_{cr} = Predicted crack maximum crack width in inches

When 0.3% web reinforcement is provided, total crack area can reasonably be estimated for *a/d* between 1 and 2 using U_{total}. Figure 5-17 illustrates this correlation.

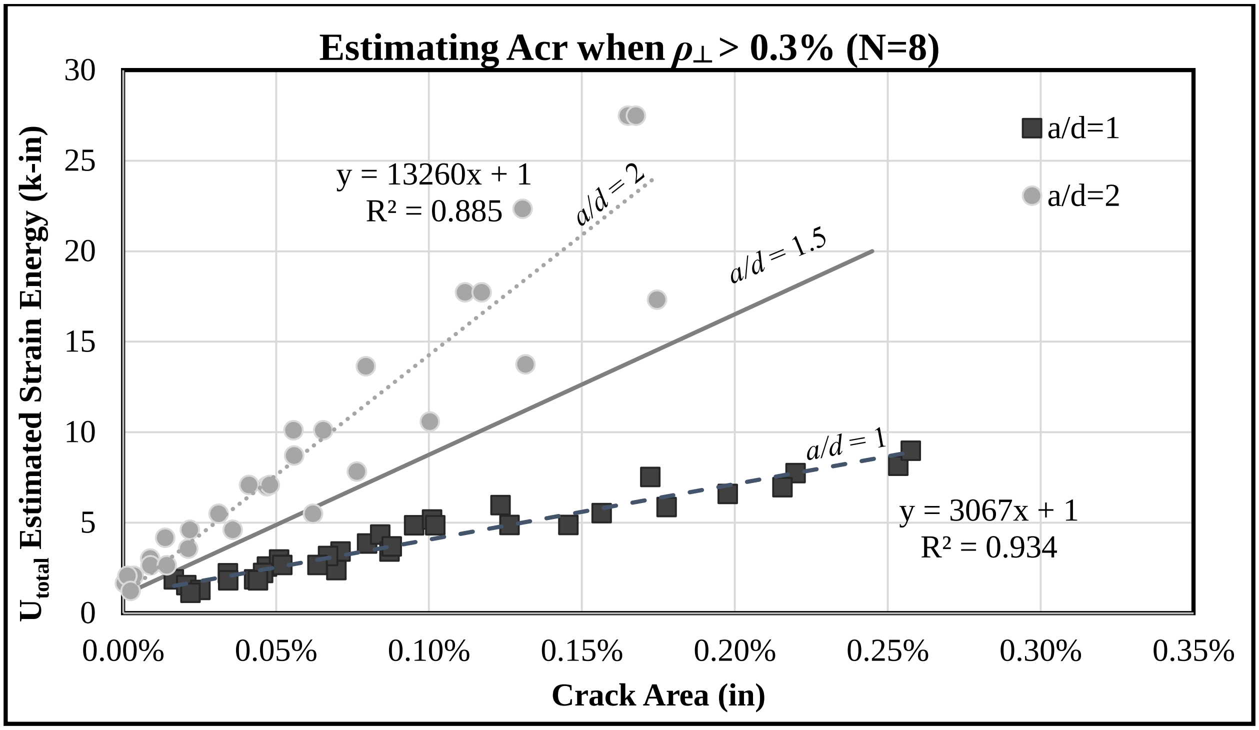

Figure 5-17: Design Tool for Predicting Crack Area

The above graph was derived from all eight specimens containing web reinforcement of 0.3%. Figure 5-17 gives an intermediate proposed line for *a/d* equal to 1.5. This line is assumed and does not have any experimental data to support.

5.5 IMPLICATIONS AND LIMITATIONS OF RESULTS

Findings are reported in the context of the limitations of the testing program. For models with U_{tie}/U_{total} less than or equal to 35%, maximum crack widths can be predicted to a reasonable degree, provided 0.3% web reinforcement, as shown in Figure 5-16 regardless of *a/d*. The ratio of U_{tie}/U_{total} gives designers a way of measuring serviceability. For example, a model with U_{tie}/U_{total} equal to 37% will perform more poorly than a model with U_{tie}/U_{total} equal to 30%. The ability to predict maximum crack width at U_{tie}/U_{total} greater than 35% is not as certain as there are more variables to consider such as alternate load paths in the presence of web reinforcement and for larger *a/d* with relationship between principal tension and tie orientation.

For STM, total cracked area can be predicted to a reasonable degree (within 20%), however, predications are more reliable at smaller *a/d* and when 0.3% web reinforcement is provided. Though prediction of crack area is possible for larger *a/d*, a simple model with one load path likely will not correlate to the actual path taken. Also, it is observed that crack area follows similar trends as the maximum crack width for diagonal cracks. This means the use of maximum diagonal crack width as a measurement of serviceability is not unreasonable. However, this is based on a very small amount of data. Further data need to be collected to compile a database in which these trends can be verified.

With regards to serviceability, it is possible to predict the performance of a D-region based on percent of estimated strain energy in the ties to the STM. In short, minimizing this percentage (U_{tie}/U_{total}) will lead to better service level performance.

A secondary finding of this study is the use of digital images for the purposed of crack measurement is practical form of data collection as shown. The reliability of the results for this study are consistent with Ballard et al (2016) and Rivera et al. (2015).Though the collection of crack area used for this study was labor intensive, an automation of this process similar to Rivera et al. (2015) but for smaller cracks (0.002 to 0.016 in.) is likely obtainable in the foreseeable future.

5.6 SUGGESTIONS FOR FUTURE WORK

The scope of this study includes the investigation of influence of web reinforcement, spacing of web reinforcement, tie model and shear span-to-depth ratio. The findings were inconclusive for *a/d* equal to 2 due to lack of collected crack data during testing of BG-2-0-0. The following tasks relate to the suggested future work to progress this study:

1) Examine the alternate load paths used for models with web reinforcement at *a/d* larger than 1,
2) Verify the trends of max crack to strain energy given in this study using the database of maximum crack widths in D-regions (Chapter 2),
3) Validate the proposed design tool in Figure 5-16 against the database,
4) Calibrate experimental results to a nonlinear finite analysis for additional parametric studies,
5) Conduct a multivariable analysis considering interdependent influence of variables on each other, and
6) Calibrate strain energy estimates against external work done on specimen.

CHAPTER 6

Conclusion

6.1 SUMMARY

Methods available to engineers for the design of discontinuity regions include nonlinear analysis and strut and tie modeling. Due the complexity of nonlinear analysis and exhaustive computational efforts required, strut and tie modeling is the more common method. Strut and tie modeling is a lower bound estimate of a structure's ultimate capacity, in which serviceability is not measured, but assumed. Given this fact, there is a need for a design procedure which can be used to determine the cracking behavior expected under service-level loading. This study addresses this need by investigating the influence of web reinforcement, spacing of web reinforcement, tie model, and *a/d* on crack behavior through the collection of load, displacement, strain and crack data for twelve deep beams.

6.2 CONCLUSIONS AND RECOMMENDATIONS

6.2.1 Project Goal

The goal of this project is to investigate the serviceability behavior of discontinuity regions using the strut and tie modeling method. To accomplish this objective, the following aims are targeted:

1. To investigate the serviceability behavior of concrete in terms of maximum crack width and tie strain estimated in representative STM;
2. To investigate the serviceability behavior of concrete in terms of total crack area and strain energy estimated in representative STM;

3. To recommend a procedure for distinguishing a ‘good’ strut and tie model from a ‘bad’ model.

The secondary goal of this project was to refine existing methods for processing digital images in the collection of crack width, crack area and displacement data. The reliability of the results for this study are consistent with past studies using similar methods in the collection of crack width, crack area and displacement data.

6.2.2 Maximum crack width, w_{cr}, versus estimated strain in tie, ε_t

- Addition of web reinforcement decreases maximum crack
- Spacing of web reinforcement does not have significant influence on maximum crack width
- Tie model has significant influence on maximum crack widths especially when orientation of tie is nearly parallel with principal tension.
- *a/d* does not have influence maximum crack width

6.2.3 Area of crack surface, A_{cr}, versus estimated stain energy in STM, U_{total}

- The presence of 0.3% web reinforcement show minimal influence in decreasing total cracked area when *a/d* equals 1.
- The influence of web reinforcement on specimens with *a/d* equal to 2 is inconclusive. Likely, the transfer of shear across the cross-section is more influential.
- Spacing of web reinforcement indicates a possible influence however, the interaction between tie strain and sectional shear transfer contribute to this effect.
- A minimal difference between tie models was observed for specimens with *a/d* equal to 1 and *a/d* equal to 2 was inconclusive due to insufficient data.

- The relationship between A_{cr} and U_{total} is highly dependent on and requires careful consideration of assumed STM for beams with an *a/d* of 2.

6.2.4 Distinguishing a "good" STM from a "bad" STM

- Minimizing U_{tie}/U_{total} will result in better serviceability performance
- U_{tie}/U_{total} less than or equal to 0.35 results in crack widths less than 0.016 inches for loads up to 70% of ultimate.
- When 0.3% web reinforcement in both directions is provided and ratio of estimated U_{tie}/U_{total} is less than or equal to 0.35, max crack widths can be reasonably estimated (Equation 5-1).
- Crack area can reasonably be estimated when web reinforcement of 0.3% is provided in both directions for *a/d* of 1 and 2. (Figure 5-17).

6.2.5 Design Recommendations

- Provide web reinforcement greater than or equal to 0.3% in both directions.
- Minimize U_{tie}/U_{total} to less than or equal to 0.35 for satisfactory serviceability performance
- For satisfactory serviceability behavior of beams with *a/d* of 2, careful consideration of STM load paths is required.

References

AASHTO. 2007. AASHTO LRFD Bridge Design Specifications. 4th ed. American Association of State Highway and Transportation Officials.

ACI Committee 224. 2008. Control of cracking in concrete structures (ACI 224R-01). American Concrete Institute. Vol. 2008.

ACI Committee 318. 2008. Building Code Requirements for Structural Concrete (ACI 318-08). American Concrete Institute. Vol. 2007. doi:10.1016/0262-5075(85)90032-6.

ASTM A615 / A615M-16. 2016. Standard Specification for Deformed and Plain Carbon-Steel Bars for Concrete Reinforcement. ASTM International, West Conshohocken, PA.

ASTM C31 / C31M-15ae1. 2015. Standard Practice for Making and Curing Concrete Test Specimens in the Field. ASTM International, West Conshohocken, PA

Bathe, K., Walczak, A. Welsh, and N. Mistry. 1989. "Nonlinear Analysis of Concrete Structures." Computers & Structures 563-590.

Ballard, Sabrina, and Robin Tuchscherer. 2016. "Use of Photogrammetry to Measure the Condition of Existing Structures." Conference on Undergraduate Research. Ashville: NCUR.

Birrcher, David, Robin Tuchscherer, Matt Huizinga, Sharon Wood, and James Jirsa. 2009. “FHWA/TX-09/0-5253-1: Strength and Serviceability Design of Reinforcement Concrete Deep Beams.” Vol. 7. Austin.

Celesco. 2013. "Celesco." Feburary 26. Accessed March 31, 2016. http://www.celesco.com/_datasheets/sp2.pdf.

Cemex. 2015. MAG AA 4000 #57 Air Ash Flag. Flagstaff, June.

Collins, Michael P, and Denis Mitchell. 1980. "Shear and Torsion Design of Prestress and Non-Prestressed Concrete Beams." PCI Journal 25 (5): 32-100.

Collins, Michael P, and Denis Mitchell. 1987. Prestressed Concrete Basics. Ontario: Canadian Prestressed Concrete Institute.

Crow, J. M. 2008. "The Concrete Conundrum." Chemistry World March: 62-66.

Deschenes, Dean. 2009. ASR/DEF-DAMAGED BENT CAPS: Sheart Tests and Field Implications. Austin:University of Texas at Austin

EMI Supplies. 2016. Concrete Forming Systems and Accessories. EMI Supplies. http://www.emisupplies.com/catalog.pdf.

Enerpac. 2016 "Enerpac.com." Accessed March 2016. http://www.enerpac.com/sites/default/files/rc_e327_us.pdf.

fib. 2010. Model Code for Concrete Structures. Ernst & Sohn.

Frosch, R. 1999. Another look at cracking and crack control in reinforced concrete. ACI Structural Journal 96(3): 437-442 ISI.

Gergely, P., and Lutz, L. A., "Maximum Crack Width in Reinforced Concrete Flexural Members," Causes, Mechanism, and Control of Cracking in Concrete, SP-20, American Concrete Institute, Farmington Hills, Mich., 1968, pp. 87–117.

Guyon, Y. 1953. Prestressed Concrete. London: Contractor's Recod Ltd.

Interface. 2016. "Interface Advanced Force Measurment." Accessed March 31, 2016. http://www.interfaceforce.com/index.php?1200-High-Capacity-Precision-Low-Profile-%E2%84%A2-Load-Cell-Capacities-to-2M-lbf&mod=product&show=6.

Klein, Gary. 2008. "Curved-Bar Nodes." Concrete International 42-47.

Kong, Fung-Kew, Peter J. Robins, and Davi F. Cole. 1970. “Web Reinforcement Effects on Deep Beams.” ACI Journal, 1010–18.

Kumar, Prabhat. 1977. “Optimal Force Tansmission in Reinforced Concrete Deep Beams.” Computers & Structures 8: 223–29.

Liang, Qing Quan, Brian Uy, and Grant Steven. 2013. “Performace-Based Optimization for Strut-Tie Modeling of Structural Concrete” 53 (9): 1689–99. doi:10.1017/CBO9781107415324.004.

Mihaylov, Boyan I, Evan C Bentz, and Michael P Collins. 2014. “Two-Parameter Kinematic Theory for Shear Behavior of Deep Beams.” ACI Structural Journal, no. 110.

Morsch, Emil. 1909. Concrete-Steel Construction. New York: The Engineering News Publishing Company.

Muttoni, A., J. Schwartz and B. Thurlimann. 1997. Design of Concrete Structures with Stress Fields. Basel: Birkhauser Verlag.

National Instruments. 2000. National Instruments. August. Accessed March 31, 2016. http://www.ni.com/pdf/manuals/322859a.pdf.

—. 2003. "National Instruments." April. Accessed March 31, 2016. http://www.ni.com/pdf/manuals/320999e.pdf.

Nikon. 2013. D7100 Digital Camera User's Manual. Nikon Corporation.

—. 2016. Nikonusa.com. Accessed March 2016. http://www.nikonusa.com/en/nikon-products/product/camera-lenses/nikkor-24mm-f%252f2.8.html.

Oesterle, R G. 1997. “The Role of Concrete Cover in Crack Control Criteria and Corrosion Protection,” no. 2054.

Park, Jung-woong, and Daniel Kuchma. "Strut-and-Tie Model Analysis for Strength Prediction of Deep Beams." ACI Structural Journal 104, no. 6 (November/December 2007): 657-66.

Photomodeler. 2014. Photomodeler.com. Accessed March 31, 2016. http://www.photomodeler.com/products/modeler/default.html.

Ritter, W. “Die Bauweise Hennebique.” Schweizerische Bauzeitung. Vol. 33, No. 7, pp. 49-52, 1899

Rivera, J. P., G. Joipovic, E. Lejeune, B. N. Luna, and A. Whittaker. 2015. "Automated Detection and Measurements of Cracks in Reinforced Concrete Components." ACI Structural Journal 397-406.

Schlaich, Jorg, Kurt Schafer, and Mattias Jennewein. n.d. “Toward a Consistent Design of Structural Concrete.” PCI Journal, 74–161.

Smith, K.N, and A.S. Vantsiotis. 1982. “Shear Strength of Deam Beams.” ACI Journal. American Concrete Institution, 201–13.

Thompson, M. K. 2002. The Anchorage Behavior of Headed Reinforcement in CCT Nodes and Lap Splices. Austin:University of Texas at Austin.

Tokyo Sokki Kenkyyujo. 2015. Developing Strain Gauges and Instruments.

Vishay Precision Group, Inc. 2014. "Micro Measurements." vishaypg.com. July 15. Accessed 03 31, 2016. http://www.vishaypg.com/docs/11030/mcoatf.pdf.

Walraven, J.C. 1981. "Theory and experiments on the mechnical behavior of cracks in plain and reinforced concrete subject to shear loading." HERON.

Yun, Young Mook. 2000. " Nonlinear Strut-Tie Model Approach for Structural Concrete." ACI Structural Journal 581-590.

List of Appendices

Appendix A: Crack Width Database

Appendix B: Specimen Shop Drawing

Appendix C: STM Dimensions

Appendix D: Concrete Control Cylinders

Appendix E: Strain Gauge Locations

Appendix F: Strain Energy Calculations

Appendix G: Crack Patterns

Appendix A: Crack Width Database

Crack Width Database (1 of 6)

ID	f'_c (psi)	fy (ksi)	fyv (ksi)	b_w (in)	h (in)	θ (deg)	a (in)	d (in)	a/d	ρ_v	ρ_l	A_s (in^2)	E_s (ksi)	E_c (ksi)	V_{test} (kip)	V_{50} (kip)	w_{50} (in)
Smith & Vantsiotis (1982)																	
1A1-10	2710	62.5	63.4	4	14	37	12.0	12.8	0.94	0.0028	0.019	0.93	29000	2967	36.25	18.16	0.004
1A3-11	2615	62.5	63.4	4	14	37	12.0	12.8	0.94	0.0028	0.019	0.93	29000	2915	33.35	16.71	0.004
1A4-12	2330	62.5	63.4	4	14	37	12.0	12.8	0.94	0.0028	0.019	0.93	29000	2751	31.75	15.91	0.004
1A4-51	2980	62.5	63.4	4	14	38	12.0	12.8	0.94	0.0028	0.019	0.93	29000	3112	38.43	19.25	0.004
1A6-37	3055	62.5	63.4	4	14	38	12.0	12.8	0.94	0.0028	0.019	0.93	29000	3151	41.39	20.73	0.004
2A1-38	3145	62.5	63.4	4	14	38	12.0	12.8	0.94	0.0063	0.019	0.93	29000	3197	39.23	19.65	0.004
2A3-39	2865	62.5	63.4	4	14	37	12.0	12.8	0.94	0.0063	0.019	0.93	29000	3051	38.35	19.21	0.004
2A4-40	2950	62.5	63.4	4	14	38	12.0	12.8	0.94	0.0063	0.019	0.93	29000	3096	38.65	19.36	0.004
2A6-41	2775	62.5	63.4	4	14	37	12.0	12.8	0.94	0.0063	0.019	0.93	29000	3003	36.40	18.24	0.004
3A1-42	2670	62.5	63.4	4	14	37	12.0	12.8	0.94	0.0125	0.019	0.93	29000	2945	36.20	18.14	0.004
3A3-43	2790	62.5	63.4	4	14	37	12.0	12.8	0.94	0.0125	0.019	0.93	29000	3011	38.83	19.45	0.004
3A4-45	3020	62.5	63.4	4	14	38	12.0	12.8	0.94	0.0125	0.019	0.93	29000	3132	40.14	20.11	0.004
3A6-46	2890	62.5	63.4	4	14	37	12.0	12.8	0.94	0.0125	0.019	0.93	29000	3064	37.80	18.94	0.004
1B1-01	3200	62.5	63.4	4	14	33	14.5	12.8	1.14	0.0024	0.019	0.93	29000	3224	33.15	16.62	0.004
1B3-29	2915	62.5	63.4	4	14	32	14.5	12.8	1.14	0.0024	0.019	0.93	29000	3077	32.28	16.18	0.004
1B4-30	3020	62.5	63.4	4	14	33	14.5	12.8	1.14	0.0024	0.019	0.93	29000	3132	31.55	15.82	0.004
1B6-31	2830	62.5	63.4	4	14	32	14.5	12.8	1.14	0.0024	0.019	0.93	29000	3032	34.48	17.28	0.004
2B1-05	2780	62.5	63.4	4	14	32	14.5	12.8	1.14	0.0042	0.019	0.93	29000	3005	29.00	14.54	0.004
2B3-06	2755	62.5	63.4	4	14	32	14.5	12.8	1.14	0.0042	0.019	0.93	29000	2992	29.50	14.79	0.004
2B4-07	2535	62.5	63.4	4	14	32	14.5	12.8	1.14	0.0042	0.019	0.93	29000	2870	28.35	14.22	0.004
2B4-52	3160	62.5	63.4	4	14	33	14.5	12.8	1.14	0.0042	0.019	0.93	29000	3204	33.70	16.89	0.004
2B6-32	2865	62.5	63.4	4	14	32	14.5	12.8	1.14	0.0042	0.019	0.93	29000	3051	32.65	16.37	0.004
3B1-08	2355	62.5	63.4	4	14	32	14.5	12.8	1.14	0.0063	0.019	0.93	29000	2766	29.40	14.74	0.004
3B1-36	2960	62.5	63.4	4	14	33	14.5	12.8	1.14	0.0077	0.019	0.93	29000	3101	35.74	17.91	0.004

Crack Width Database (2 of 6)

`	f'_c (psi)	fy (ksi)	fyv (ksi)	b_w (in)	h (in)	θ (deg)	a (in)	d (in)	a/d	ρ_v	ρ_l	A_s (in^2)	E_s (ksi)	E_c (ksi)	V_{test} (kip)	V_{50} (kip)	w_{50} (in)
3B3-33	2755	62.5	63.4	4	14	32	14.5	12.8	1.14	0.0077	0.019	0.93	29000	2992	35.60	17.84	0.004
3B4-34	2790	62.5	63.4	4	14	32	14.5	12.8	1.14	0.0077	0.019	0.93	29000	3011	34.85	17.47	0.004
3B6-35	2995	62.5	63.4	4	14	33	14.5	12.8	1.14	0.0077	0.019	0.93	29000	3119	37.35	18.72	0.004
4B1-09	2480	62.5	63.4	4	14	32	14.5	12.8	1.14	0.0125	0.019	0.93	29000	2839	34.50	17.29	0.004
1C1-14	2790	62.5	63.4	4	14	27	18.0	12.8	1.41	0.0018	0.019	0.93	29000	3011	26.75	13.43	0.005
1C3-02	3175	62.5	63.4	4	14	28	18.0	12.8	1.41	0.0018	0.019	0.93	29000	3212	27.75	13.93	0.005
1C4-15	3290	62.5	63.4	4	14	34	18.0	12.8	1.41	0.0018	0.019	0.93	29000	3269	29.45	14.78	0.005
1C6-16	3160	62.5	63.4	4	14	34	18.0	12.8	1.41	0.0018	0.019	0.93	29000	3204	27.50	13.80	0.005
2C1-17	2880	62.5	63.4	4	14	34	18.0	12.8	1.41	0.0031	0.019	0.93	29000	3059	27.90	14.00	0.005
2C3-03	2790	62.5	63.4	4	14	34	18.0	12.8	1.41	0.0031	0.019	0.93	29000	3011	23.30	11.70	0.005
2C3-27	2800	62.5	63.4	4	14	34	18.0	12.8	1.41	0.0031	0.019	0.93	29000	3016	25.93	13.02	0.005
2C4-18	2965	62.5	63.4	4	14	34	18.0	12.8	1.41	0.0031	0.019	0.93	29000	3104	28.00	14.05	0.005
2C6-19	3010	62.5	63.4	4	14	34	18.0	12.8	1.41	0.0031	0.019	0.93	29000	3127	27.90	14.00	0.005
3C1-20	3050	62.5	63.4	4	14	34	18.0	12.8	1.41	0.0056	0.019	0.93	29000	3148	31.65	15.88	0.005
3C3-21	2400	62.5	63.4	4	14	34	18.0	12.8	1.41	0.0056	0.019	0.93	29000	2792	28.10	14.10	0.005
3C4-22	2650	62.5	63.4	4	14	34	18.0	12.8	1.41	0.0056	0.019	0.93	29000	2934	28.70	14.40	0.005
3C6-23	2755	62.5	63.4	4	14	34	18.0	12.8	1.41	0.0056	0.019	0.93	29000	2992	30.85	15.48	0.005
4C1-24	2840	62.5	63.4	4	14	34	18.0	12.8	1.41	0.0077	0.019	0.93	29000	3038	32.95	16.53	0.005
4C3-04	2690	62.5	63.4	4	14	34	18.0	12.8	1.41	0.0063	0.019	0.93	29000	2956	28.90	14.50	0.005
4C3-28	2790	62.5	63.4	4	14	34	18.0	12.8	1.41	0.0077	0.019	0.93	29000	3011	34.25	17.18	0.005
4C4-25	2685	62.5	63.4	4	14	34	18.0	12.8	1.41	0.0077	0.019	0.93	29000	2954	34.30	17.20	0.005
4C6-26	3080	62.5	63.4	4	14	34	18.0	12.8	1.41	0.0077	0.019	0.93	29000	3163	35.85	17.98	0.005
4D1-13	2330	62.5	63.4	4	14	26	25.0	12.8	1.96	0.0028	0.019	0.93	29000	2751	19.65	9.90	0.007
Kong, Robins, & Cole (1970)																	
1-30	3120	41.6	40.6	3	30	71	10.0	28.5	0.35	0.0025	0.005	0.44	29000	3184	53.70	14.10	0.004
1-20	3080	41.6	40.6	3	20	62	10.0	18.5	0.54	0.0025	0.008	0.44	29000	3163	42.60	14.40	0.004
1-10	3140	41.6	40.6	3	10	41	10.0	8.5	1.18	0.0025	0.017	0.44	29000	3194	20.10	15.48	0.002
2-30	2785	41.6	44.0	3	30	71	10.0	28.5	0.35	0.0086	0.005	0.44	29000	3008	56.00	16.53	0.008

Crack Width Database (3 of 6)

ID	f'_c (psi)	fy (ksi)	fyv (ksi)	b_w (in)	h (in)	θ (deg)	a (in)	d (in)	a/d	ρ_v	ρ_l	A_s (in^2)	E_s (ksi)	E_c (ksi)	V_{test} (kip)	V_{50} (kip)	w_{50} (in)
2-20	2880	41.6	44.0	3	20	62	10.0	18.5	0.54	0.0086	0.008	0.44	29000	3059	48.40	14.50	0.004
2-10	2920	41.6	44.0	3	10	41	10.0	8.5	1.18	0.0086	0.017	0.44	29000	3080	22.40	17.18	0.005
3-30	3270	41.6	40.6	3	30	71	10.0	28.5	0.35	0.0000	0.005	0.44	29000	3259	62.10	17.20	0.002
3-20	2790	41.6	40.6	3	20	62	10.0	18.5	0.54	0.0000	0.008	0.44	29000	3011	46.70	17.98	0.003
3-10	3280	41.6	40.6	3	10	41	10.0	8.5	1.18	0.0000	0.017	0.44	29000	3264	19.40	9.90	0.006
4-30	3190	41.6	44.0	3	30	71	10.0	28.5	0.35	0.0000	0.005	0.44	29000	3219	54.40	27.26	0.004
4-20	2920	41.6	44.0	3	20	62	10.0	18.5	0.54	0.0000	0.008	0.44	29000	3080	40.60	20.34	0.008
4-10	3280	41.6	44.0	3	10	41	10.0	8.5	1.18	0.0000	0.017	0.44	29000	3264	21.50	10.77	0.014
5-30	2690	41.6	40.6	3	30	71	10.0	28.5	0.35	0.0061	0.005	0.44	29000	2956	53.80	26.96	0.002
5-20	2920	41.6	40.6	3	20	62	10.0	18.5	0.54	0.0061	0.008	0.44	29000	3080	38.80	19.44	0.014
5-10	3270	41.6	40.6	3	10	41	10.0	8.5	1.18	0.0061	0.017	0.44	29000	3259	17.50	8.77	0.005
6-30	3782	41.6	44.0	3	30	71	10.0	28.5	0.35	0.0000	0.005	0.44	29000	3505	69.20	566.30	0.002
6-20	3782	41.6	44.0	3	20	62	10.0	18.5	0.54	0.0000	0.008	0.44	29000	3505	55.00	583.60	0.004
6-10	3640	41.6	44.0	3	10	41	10.0	8.5	1.18	0.0000	0.017	0.44	29000	3439	22.10	441.90	0.008
Birrcher and Tuchscherer (2008)																	
M-03-4-CCC2436	4100	67	61.0	36	48	31	74.0	40	1.85	0.0031	0.029	42.1	29000	3650	1128	566.30	0.03
M-02-4-CCC2436	2800	65	62.5	36	48	31	74.0	40	1.85	0.0022	0.029	42.1	29000	3016	1102	583.60	0.035
M-03-4-CCC0812	3000	65	62.5	36	48	30	74.0	40	1.85	0.0031	0.029	42.1	29000	3122	930	441.90	0.025
II-03-CCC2021	3290	64	65.0	21	42	33	71.0	38.6	1.84	0.0031	0.023	18.7	29000	3269	499.5	258.90	0.018
II-030CCC1007	3480	64	65.0	21	42	32	71.0	38.6	1.84	0.0031	0.023	18.7	29000	3363	477.4	251.70	0.018
III-1.85-00	3170	66	0.0	21	42	33	71.0	38.6	1.84	0.0000	0.023	18.7	29000	3209	365.3	186.70	0.063
II-03-CCT1021	4410	66	71.0	21	42	33	71.0	38.6	1.84	0.0031	0.023	18.7	29000	3785	635.4	301.50	0.035
II-03-CCT0507	4210	66	71.0	21	42	33	71.0	38.6	1.84	0.0031	0.023	18.7	29000	3698	597.4	323.80	0.033

Crack Width Database (4 of 6)

ID	f'_c (psi)	fy (ksi)	fyv (ksi)	b_w (in)	h (in)	θ (deg)	a (in)	d (in)	a/d	ρ_v	ρ_l	A_s (in^2)	E_s (ksi)	E_c (ksi)	V_{test} (kip)	V_{50} (kip)	w_{50} (in)
III-1.85-02	4100	66	64.0	21	42	32	71.0	38.6	1.84	0.0020	0.023	18.7	29000	3650	487.8	259.20	0.049
III-1.85-025	4100	66	64.0	21	42	32	71.0	38.6	1.84	0.0024	0.023	18.7	29000	3650	515.6	248.10	0.031
III-1.85-03	4990	69	64.0	21	42	32	71.0	38.6	1.84	0.0029	0.023	18.7	29000	4026	412.3	205.80	0.024
III-1.85-01	5010	69	63.0	21	42	32	71.0	38.6	1.84	0.0010	0.023	18.7	29000	4035	272.6	159.30	0.036
II-02-CCT0507	3120	69	64.0	21	42	34	71.0	38.6	1.84	0.0020	0.023	18.7	29000	3184	401.4	193.90	0.038
II-02-CCC1007	3140	69	64.0	21	42	33	71.0	38.6	1.84	0.0020	0.023	18.7	29000	3194	334.80	191.00	0.013
I-03-2	5240	73	67.0	21	44	32	71.0	38.5	1.84	0.0029	0.023	18.5	29000	4126	569.20	302.50	0.022
I-03-4	5330	73	73.0	21	44	32	71.0	38.5	1.84	0.0030	0.023	18.5	29000	4161	657.40	355.90	0.028
I-02-2	3950	73	67.0	21	44	32	71.0	38.5	1.84	0.0020	0.023	18.5	29000	3582	453.70	247.60	0.045
I-02-4	4160	73	73.0	21	44	32	71.0	38.5	1.84	0.0021	0.023	18.5	29000	3676	528.10	246.90	0.025
III-1.85-03b	3300	69	62	21	42	33	71.0	38.6	1.84	0.0031	0.023	18.7	29000	3274	471.1	244.30	0.029
III-1.85-02b	3300	69	62	21	42	33	71.0	38.6	1.84	0.0020	0.023	18.7	29000	3274	467.6	240.10	0.036
III-1.2-02	4100	66	60	21	42	44	46.3	38.6	1.20	0.0020	0.023	18.7	29000	3650	846.5	452.40	0.035
III-1.2-03	4220	66	68	21	42	44	46.3	38.6	1.20	0.0031	0.023	18.7	29000	3703	829.2	421.90	0.02
III-2.5-02	4630	66	62	21	42	25	96.3	38.6	2.49	0.0020	0.023	18.7	29000	3879	298.3	140.20	0.023
III-2.5-03	5030	66	65	21	42	24	96.3	38.6	2.49	0.0031	0.023	18.7	29000	4043	516.0	232.30	0.038
II-02-CCC1021	4620	69	67	21	42	31	71.0	38.6	1.84	0.0020	0.023	18.7	29000	3874	329.0	159.30	0.023
II-02-CCT0521	4740	69	67	21	42	32	71.0	38.6	1.84	0.0020	0.023	18.7	29000	3924	567.4	305.10	0.05
IV-2175-1.85-02	4930	68	66	21	74.5	32	127.6	68.9	1.85	0.0020	0.024	34.3	29000	4002	762.7	396.70	0.033
IV-2175-1.85-03	4930	68	66	21	74.5	32	127.6	68.9	1.85	0.0031	0.024	34.3	29000	4002	842.4	476.70	0.033
IV-2175-2.5-02	5010	68	64	21	74.5	25	172.5	68.9	2.50	0.0021	0.024	34.3	29000	4035	509.9	269.80	0.023

Crack Width Database (5 of 6)

Specimen ID	f'c (psi)	fy (ksi)	fyv (ksi)	b_w (in)	h (in)	θ (deg)	a (in)	d (in)	a/d	ρ_v	ρ_l	A_s (in^2)	E_s (ksi)	E_c (ksi)	V_{test} (kip)	V_{50} (kip)	w_{50} (in)
IV-2175-1.2-02	5010	68	64	21	74.5	44	82.8	68.9	1.20	0.0021	0.024	34.3	29000	4035	1222.8	630.90	0.038
IV-2123-1.85-03	4160	66	66	21	22.5	32	36.0	19.5	1.85	0.0030	0.023	9.5	29000	3676	328.5	166.60	0.021
IV-2123-1.85-02	4220	66	81	21	22.5	32	36.0	19.5	1.85	0.0020	0.023	9.5	29000	3703	347.0	164.90	0.022
IV-2123-2.5-02	4570	65	58	21	22.5	24	48.8	19.5	2.50	0.0020	0.023	9.5	29000	3853	160.7	76.10	0.015
Deschenes (2009)																	
Validation Beam	5061	66	65	21	42	31	66.9	36.1	1.85	0.0030	0.031	23.5	29000	4055	571.1	321.20	0.02
NR1	7250	66	65	21	42	31	66.9	36.1	1.85	0.0030	0.031	23.5	29000	4853	560.8	319.30	0.017
Kettelkamp and Tuchscherer (2016)																	
BG-1-0.3-6	5220	60		10	20	31	18	18.1	0.99	0.003	0.012	2.4	29000	4115	274	136.81	0.008
BG-1-0.3-2	5220	60		10	20	31	18	18.1	0.99	0.003	0.012	2.4	29000	4115	277	138.50	0.012
BB-1-0.3-6	5220	60		10	20	31	18	18.1	0.99	0.003	0.012	2.4	29000	4115	223	111.50	0.02
BB-1-0.3-2	5220	60		10	20	31	18	18.1	0.99	0.003	0.012	2.4	29000	4115	210	104.78	0.01
BG-1-0-0	5220	60		10	20	31	18	18.1	0.99	0	0.012	2.4	29000	4115	240	120.00	0.009
BB-1-0-0	5220	60		10	20	31	18	18.1	0.99	0	0.012	2.4	29000	4115	183	91.50	0.017
BG-2-0.3-6	5220	60		10	20	31	36	18.1	1.99	0.003	0.012	2.4	29000	4115	160.4	80.19	0.010
BG-2-0.3-2	5220	60		10	20	31	36	18.1	1.99	0.003	0.012	2.4	29000	4115	147.4	73.69	0.012
BB-2-0.3-6	5220	60		10	20	31	36	18.1	1.99	0.003	0.012	2.4	29000	4115	159.4	79.69	0.014
BB-2-0.3-2	5220	60		10	20	31	36	18.1	1.99	0.003	0.012	2.4	29000	4115	165.4	82.69	0.017
BG-2-0-0	5220	60		10	20	31	36	18.1	1.99	0	0.012	2.4	29000	4115	58.4	29.19	
BB-2-0-0	5220	60		10	20	31	36	18.1	1.99	0	0.012	2.4	29000	4115	168.9	84.44	0.06

Appendix B: Specimen Shop Drawings

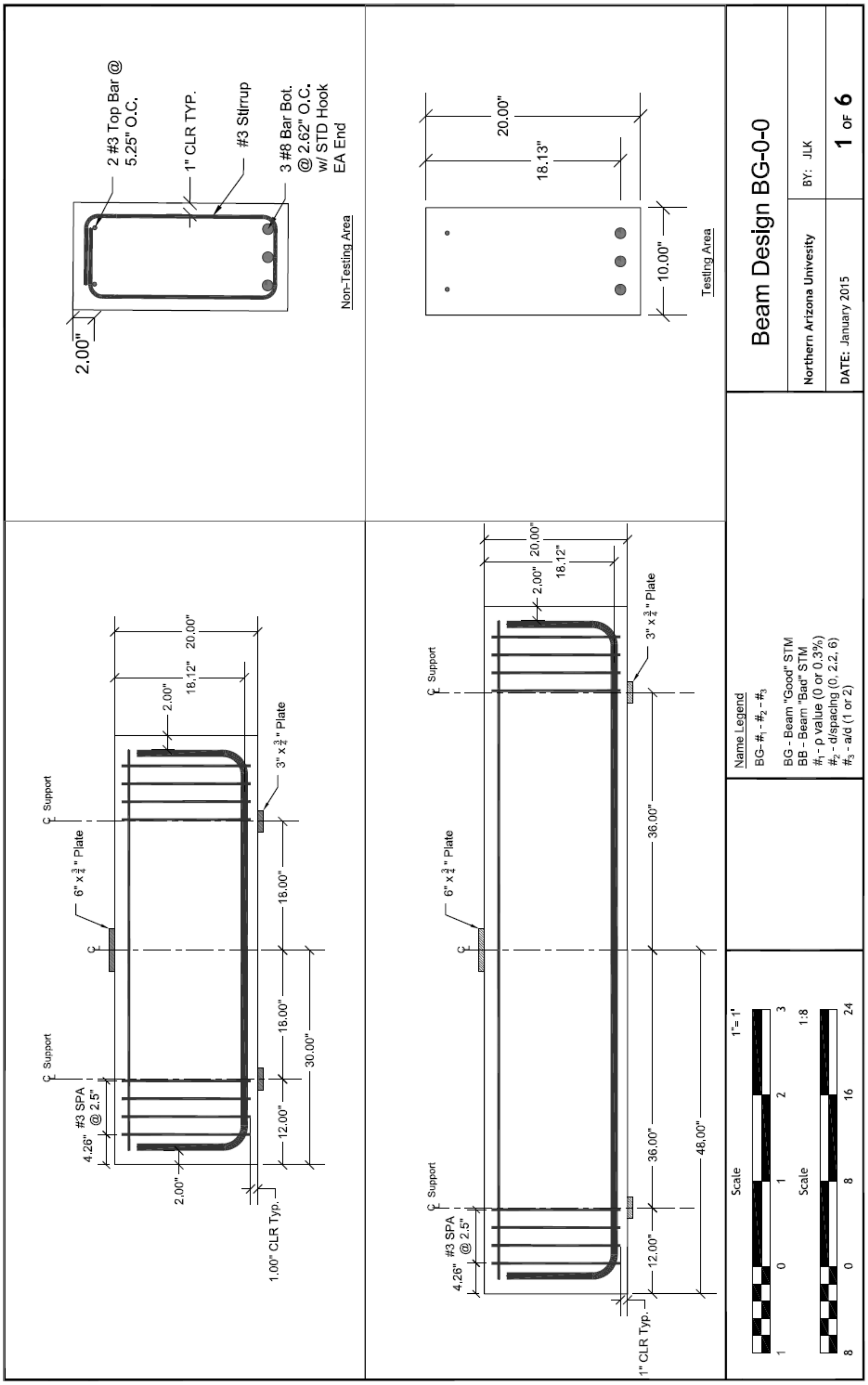

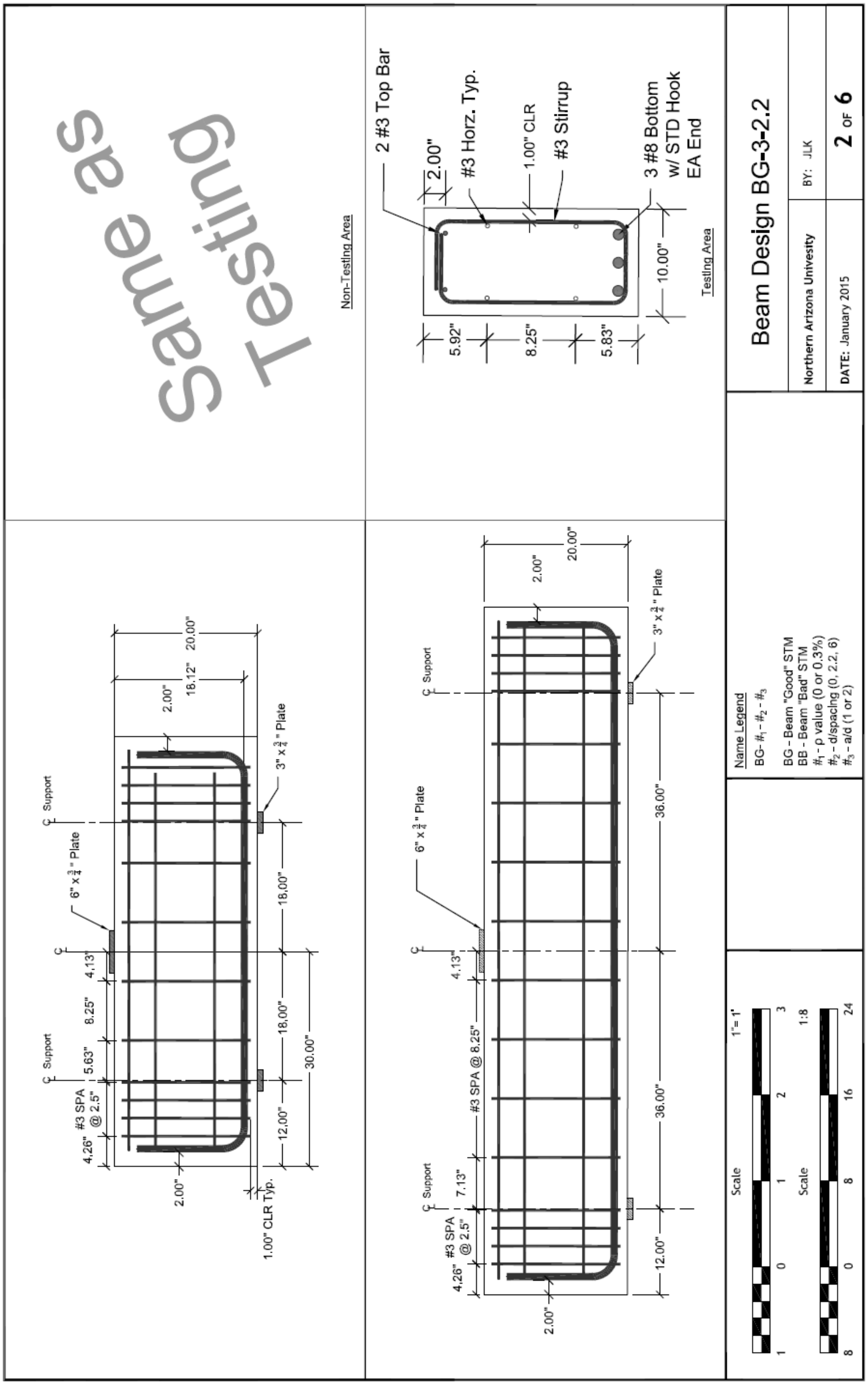
Same as Testing
Non-Testing Area
2 #3 Top Bar
2.00"
#3 Horz. Typ.
1.00" CLR
#3 Stirrup
3 #8 Bottom
w/ STD Hook
EA End
5.92"
8.25"
5.83"
10.00"
Testing Area
Beam Design BG-3-2.2
Northern Arizona Univesity
BY: JLK
DATE: January 2015
2 OF 6
Name Legend
BG - Beam "Good" STM
BB - Beam "Bad" STM
#1 - ρ value (0 or 0.3%)
#2 - d/spacing (0, 2.2, 6)
#3 - a/d (1 or 2)
Scale 1"= 1'
Scale 1:8
Support
6" x 3/4" Plate
3" x 3/4" Plate
#3 SPA @ 2.5"
#3 SPA @ 8.25"
1.00" CLR Typ.
4.26"
5.63"
8.25"
4.13"
7.13"
12.00"
18.00"
30.00"
36.00"
18.12"
20.00"

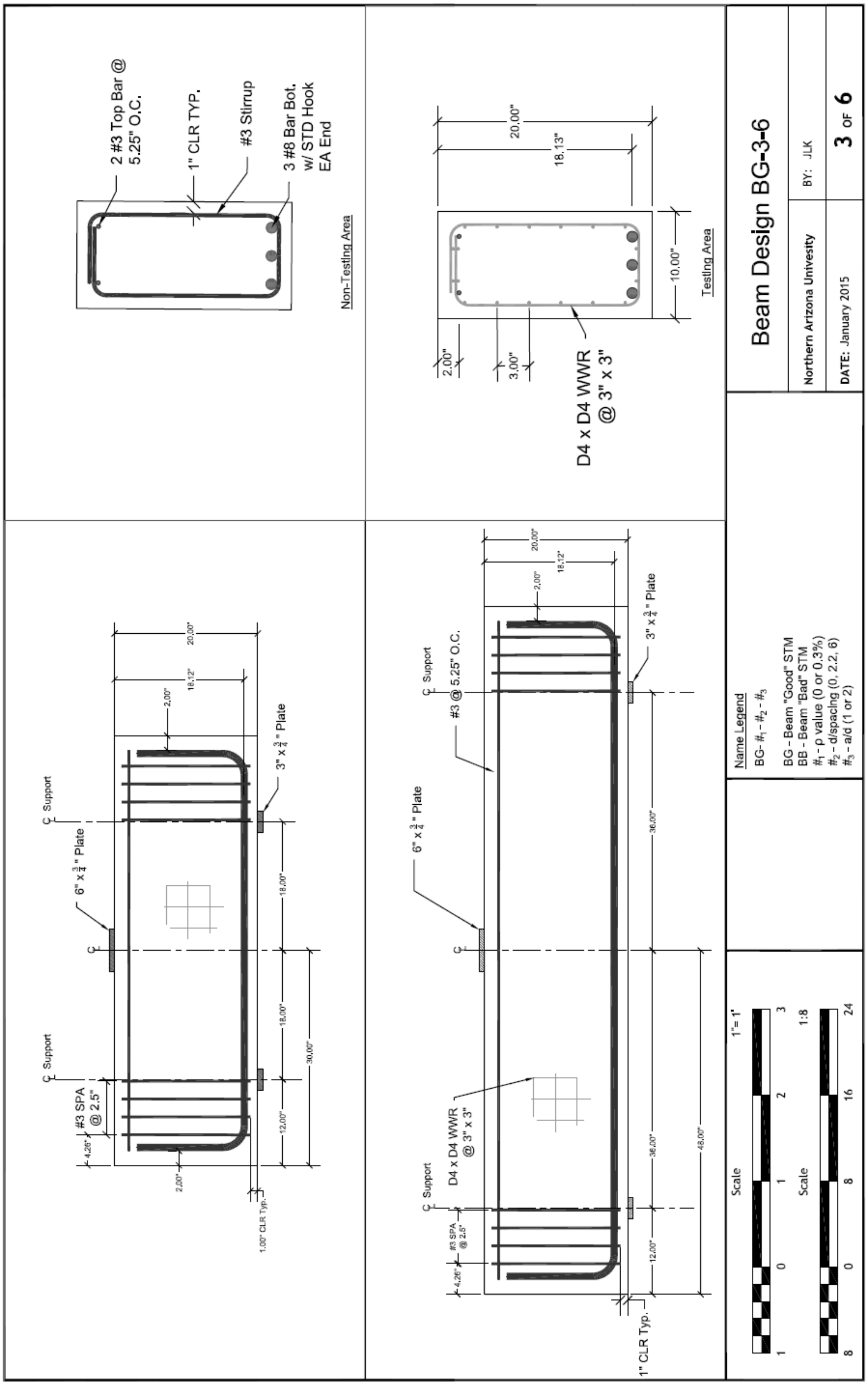
2 #3 Top Bar @ 5.25" O.C.
1" CLR TYP.
#3 Stirrup
3 #8 Bar Bot. w/ STD Hook EA End
Non-Testing Area
D4 x D4 WWR @ 3" x 3"
Testing Area
#3 SPA @ 2.5"
#3 @ 5.25" O.C.
1" CLR Typ.
Name Legend
BG - Beam "Good" STM
BB - Beam "Bad" STM
Scale
Beam Design BG-3-6
Northern Arizona University
BY: JLK
DATE: January 2015
3 OF 6

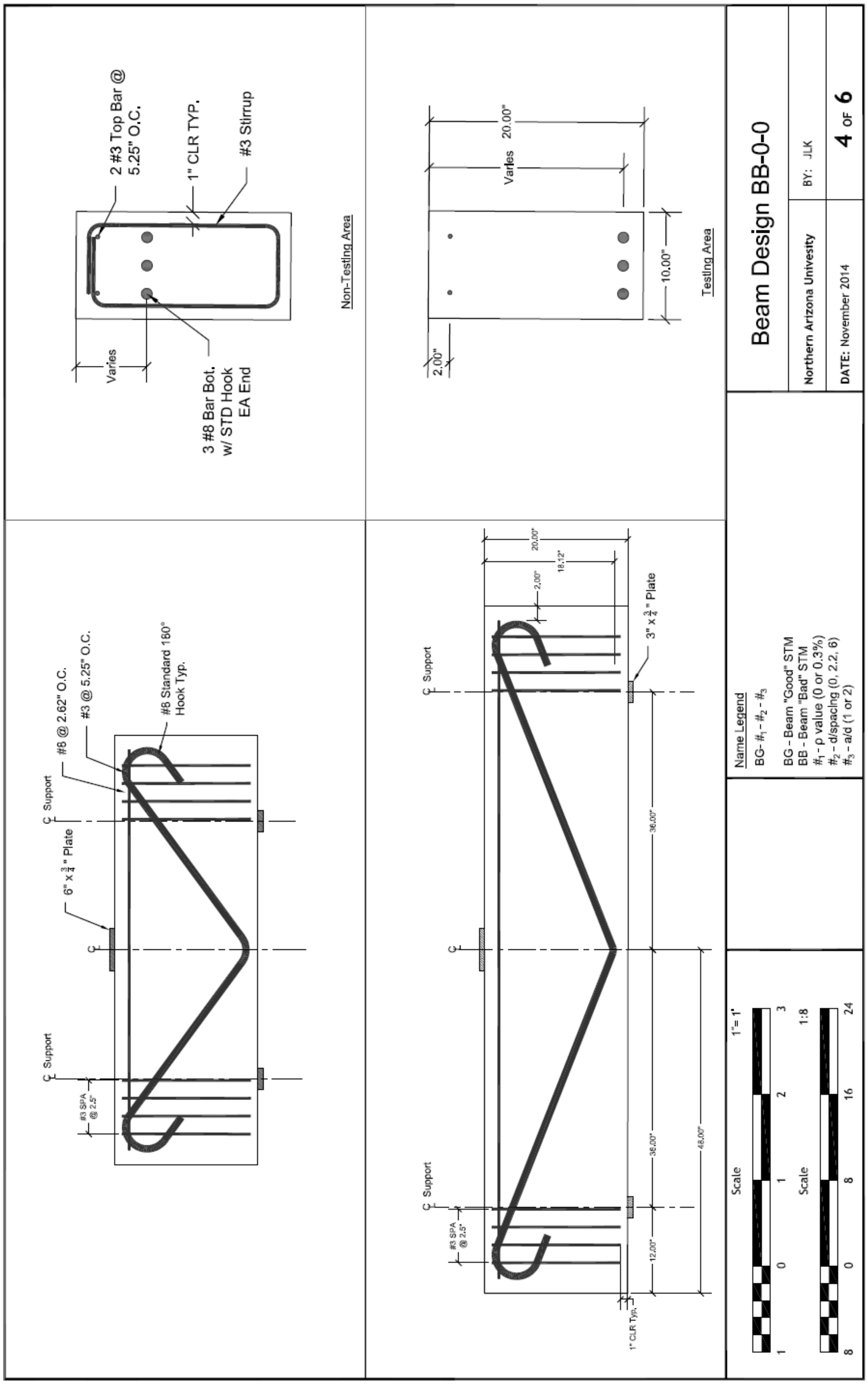

Beam Design BB-0-0
Northern Arizona University
BY: JLK
DATE: November 2014
4 OF 6
Name Legend
BG- $\#_1$ - $\#_2$ - $\#_3$
BG - Beam "Good" STM
BB - Beam "Bad" STM
$\#_1$ - ρ value (0 or 0.3%)
$\#_2$ - d/spacing (0, 2.2, 6)
$\#_3$ - a/d (1 or 2)
Scale
1"= 1'
Scale
1:8
2 #3 Top Bar @ 5.25" O.C.
1" CLR TYP.
#3 Stirrup
3 #8 Bar Bot. w/ STD Hook EA End
Varies
Non-Testing Area
20.00"
Varies
10.00"
2.00"
Testing Area
#8 @ 2.62" O.C.
#3 @ 5.25" O.C.
#8 Standard 160° Hook Typ.
6" x $\frac{3}{4}$" Plate
3" x $\frac{3}{4}$" Plate
℄ Support
#3 SPA @ 2.5"
1" CLR Typ.
12.00"
36.00"
48.00"
18.12"

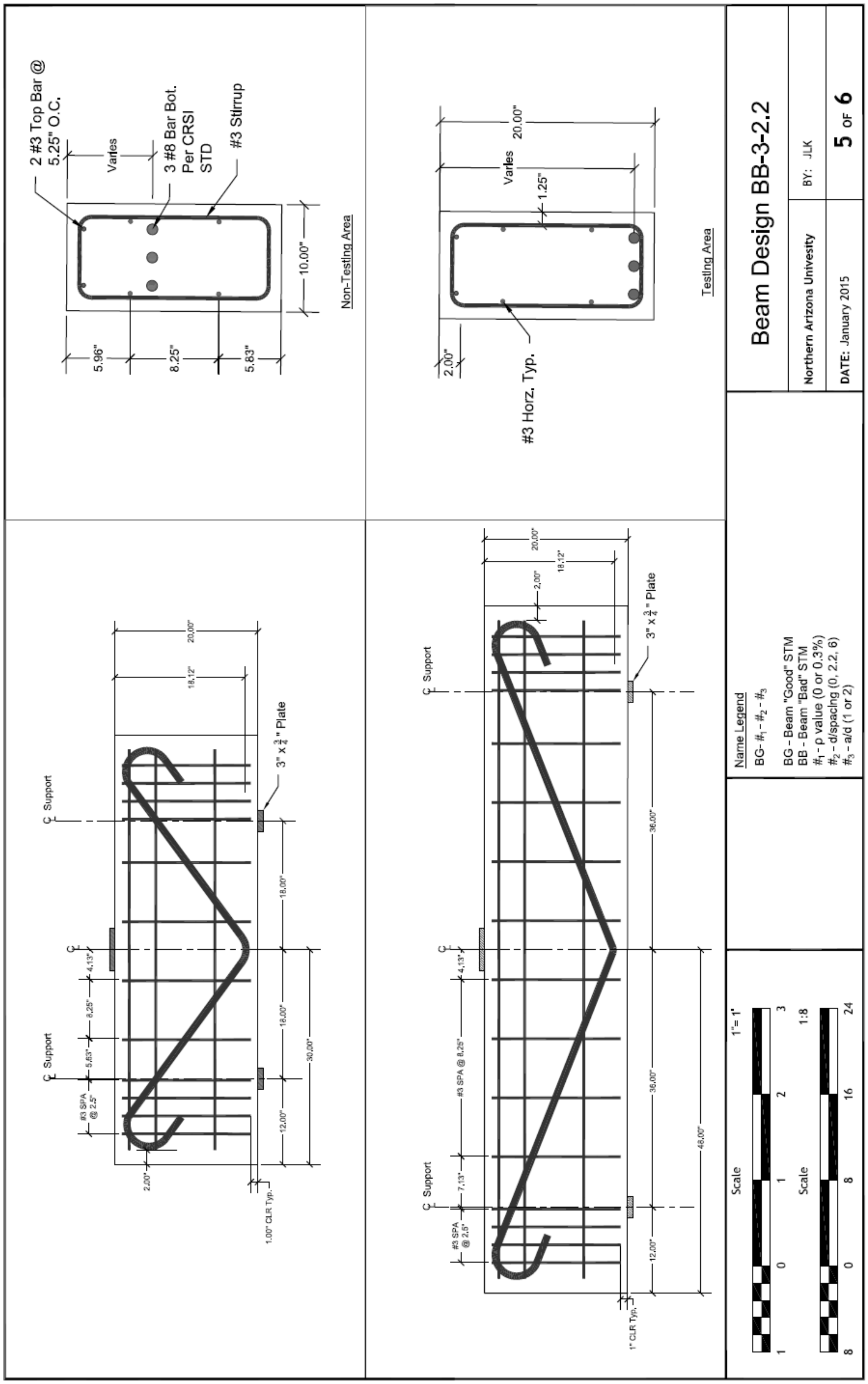

2 #3 Top Bar @ 5.25" O.C.
3 #8 Bar Bot. Per CRSI STD
#3 Stirrup
Varies
10.00"
5.96"
8.25"
5.83"
Non-Testing Area
20.00"
Varies
1.25"
2.00"
#3 Horz. Typ.
Testing Area
C Support
3" x 3/4" Plate
#3 SPA @ 2.5"
#3 SPA @ 8.25"
1.00" CLR Typ.
1" CLR Typ.
Name Legend
BG- #1 - #2 - #3
BG - Beam "Good" STM
BB - Beam "Bad" STM
#1 - ρ value (0 or 0.3%)
#2 - d/spacing (0, 2.2, 6)
#3 - a/d (1 or 2)
Scale 1"= 1'
Scale 1:8
Beam Design BB-3-2.2
Northern Arizona University
BY: JLK
DATE: January 2015
5 OF 6

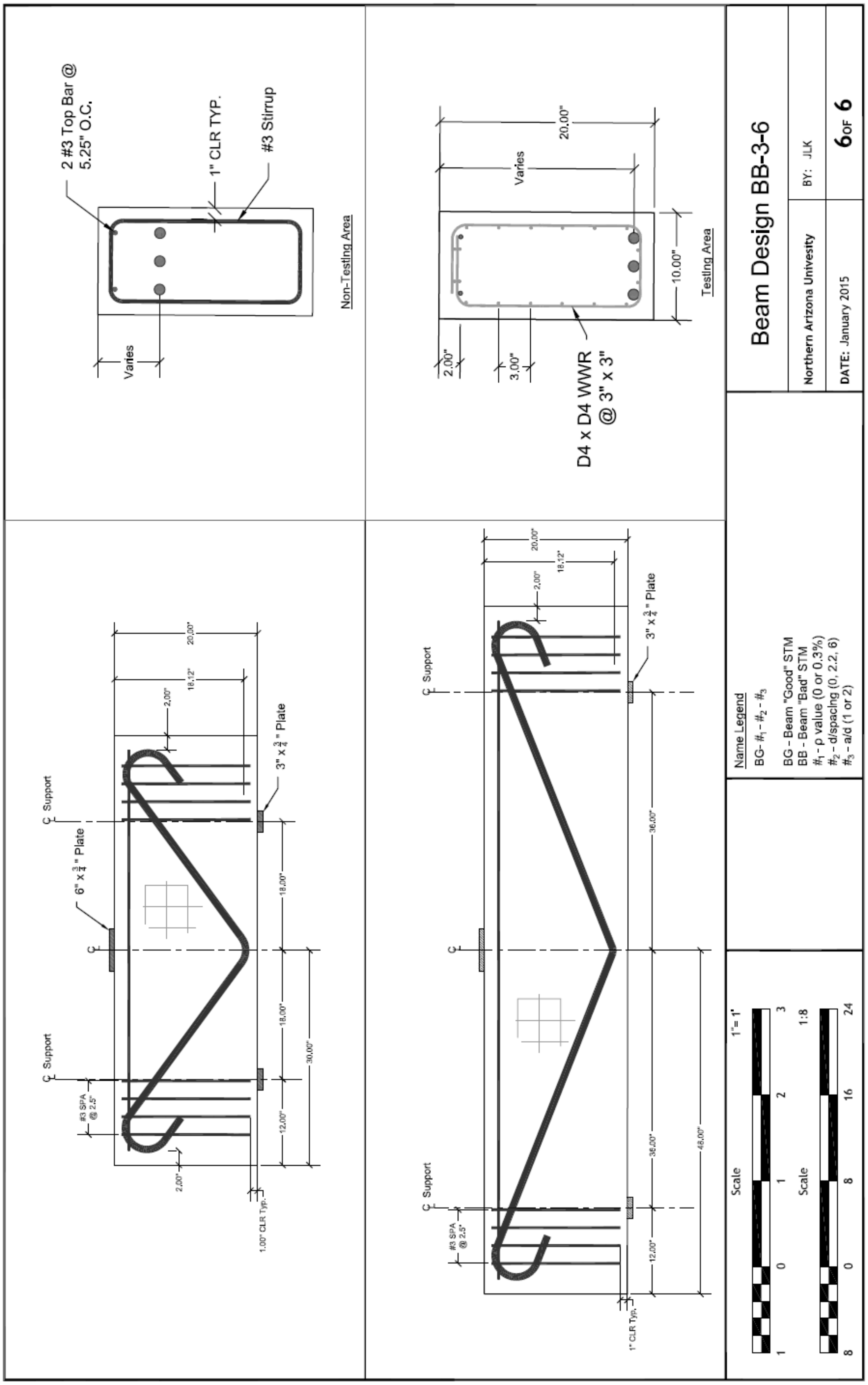
2 #3 Top Bar @ 5.25" O.C.
1" CLR TYP.
#3 Stirrup
Varies
Non-Testing Area
20.00"
Varies
10.00"
2.00"
3.00"
D4 x D4 WWR @ 3" x 3"
Testing Area
Beam Design BB-3-6
BY: JLK
Northern Arizona Univesity
DATE: January 2015
6 OF 6
Name Legend
BG- #1 - #2 - #3
BG - Beam "Good" STM
BB - Beam "Bad" STM
#1 - ρ value (0 or 0.3%)
#2 - d/spacing (0, 2.2, 6)
#3 - a/d (1 or 2)
Scale
1"= 1'
Scale
1:8
C Support
6" x 3/4 " Plate
3" x 3/4 " Plate
#3 SPA @ 2.5"
1.00" CLR Typ.
1" CLR Typ.
18.00"
30.00"
12.00"
36.00"
48.00"
18.12"

Appendix C: STM Dimensions

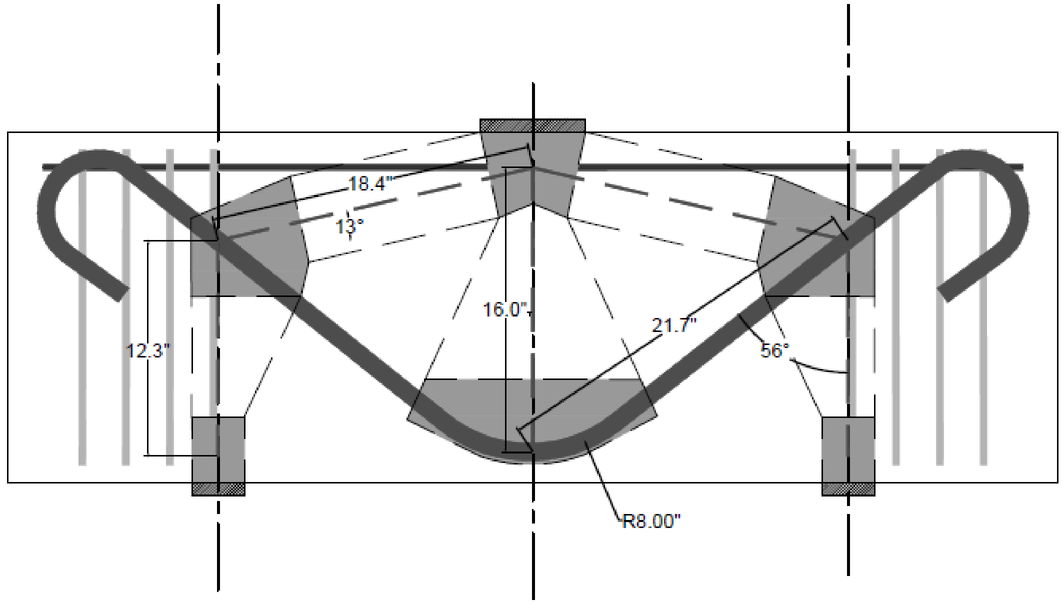

Series 1 Model B
Scale 1:10

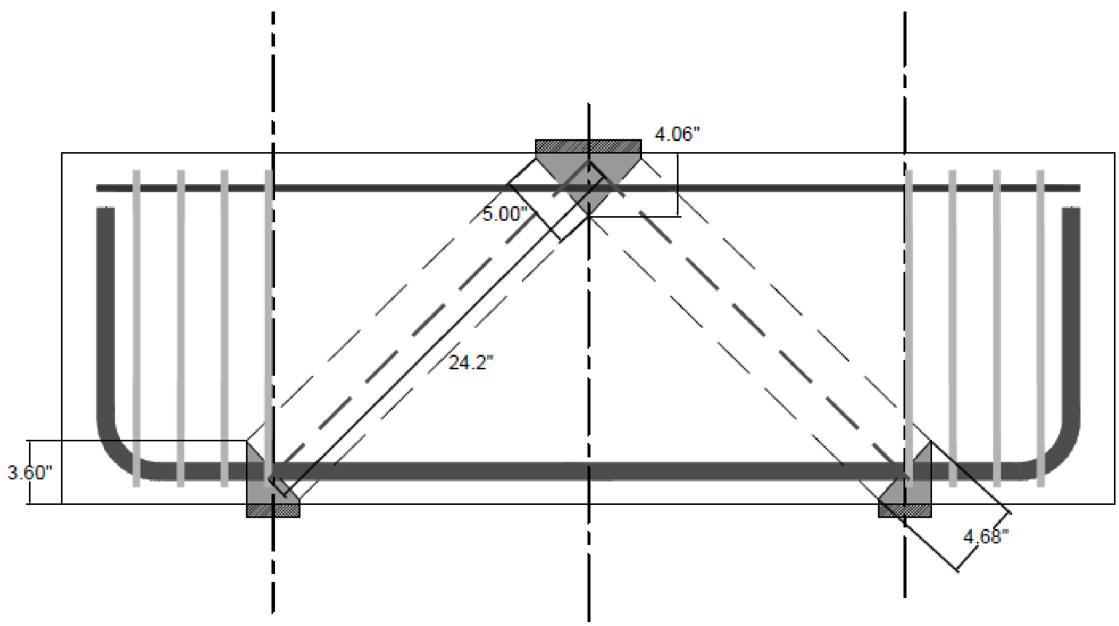

Series 1 Model G
Scale 1:10

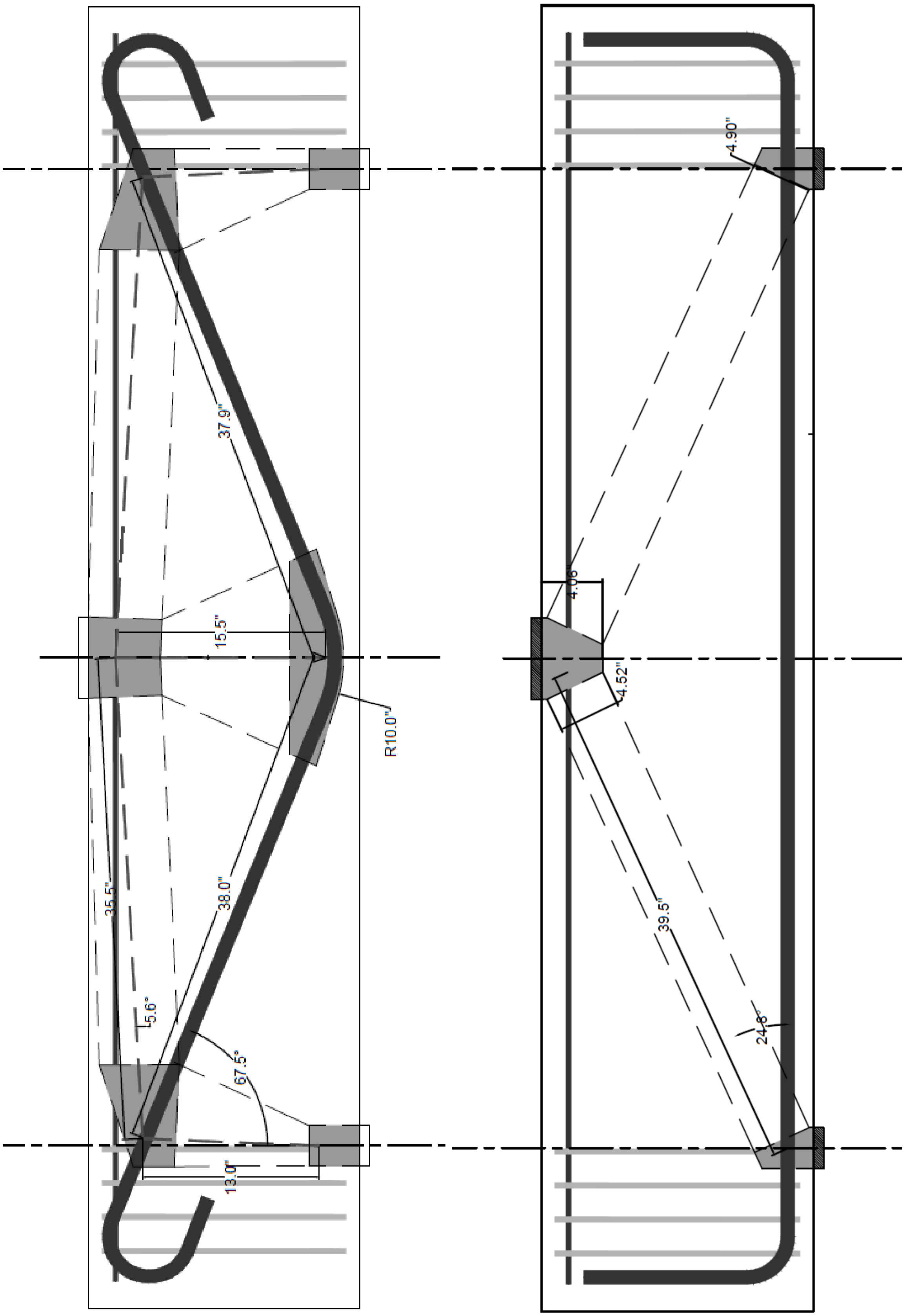
37.9"
15.5"
R10.0"
35.5"
38.0"
5.6°
67.5°
13.0"
4.90"
4.08"
4.52"
39.5"
24.8°

Appendix D: Concrete Control Cylinders

Control Cylinder Tests

Pour Date 6/16/2015

Test Date	Number of Days Old	f'c (ksi)	E (ksi) (57sqrt f'c)	E (ksi) (measured)
8/5/2015	50	4.80	3950	4465
8/22/2015	67	5.24	4125	3895
8/27/2015	72	4.94	4008	3320
8/27/2015	72	4.78	3941	3615
9/4/2015	80	4.68	3898	3968
9/10/2015	86	5.20	4109	3185
9/15/2015	91	4.62	3873	3636
9/15/2015	91	5.29	4144	3590
10/16/2015	122	5.30	4151	3606
10/16/2015	122	5.32	4156	3700
11/5/2015	142	5.75	4322	3922
11/5/2015	142	5.37	4177	3715
11/5/2015	142	5.72	4310	4651
11/18/2015	155	5.60	4267	4023
11/18/2015	155	5.69	4298	4337
Max		5.75	4322	4651
Min		4.62	3873	3185
Average		5.22	4115	3842

Appendix E: Strain Gauge Locations

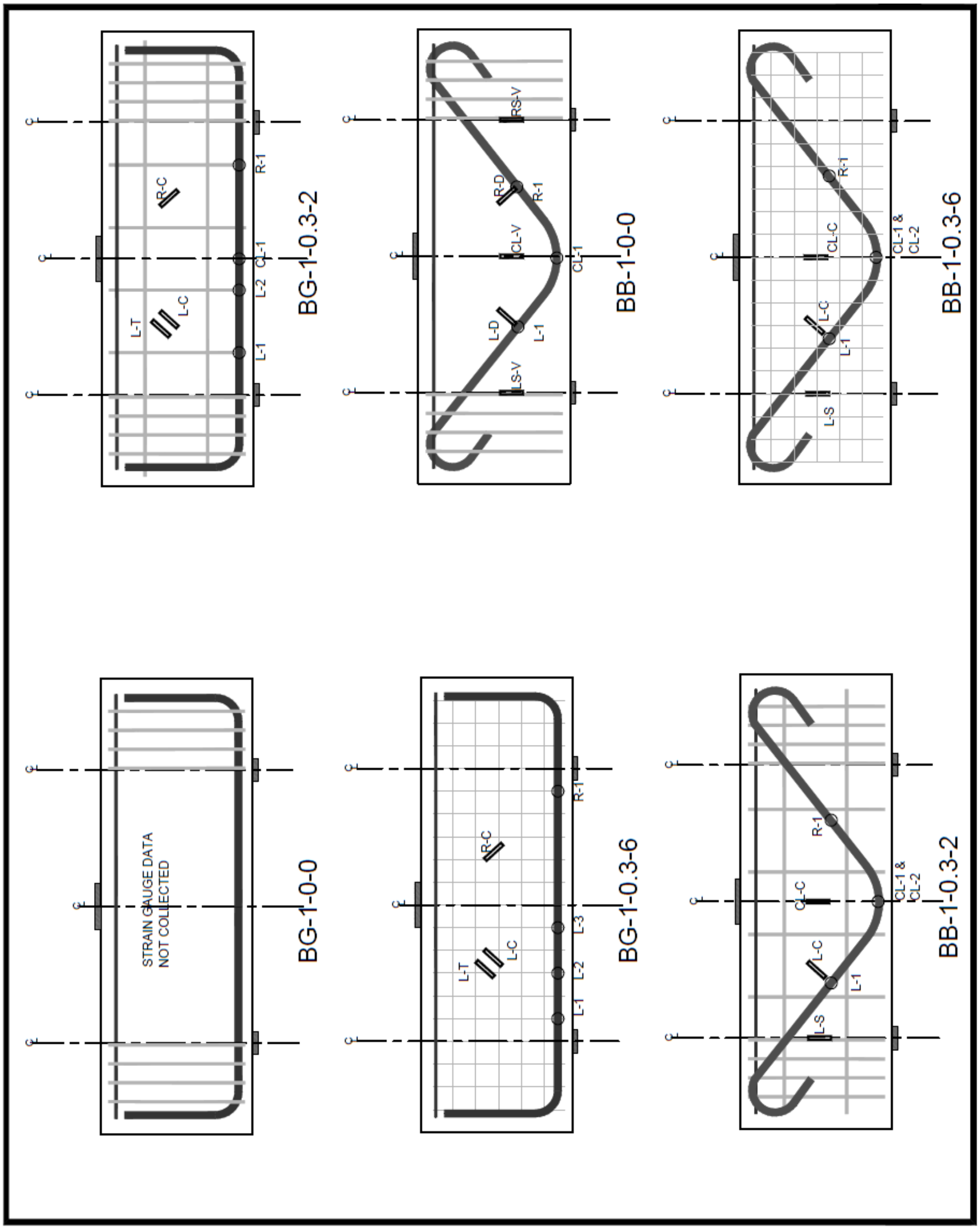

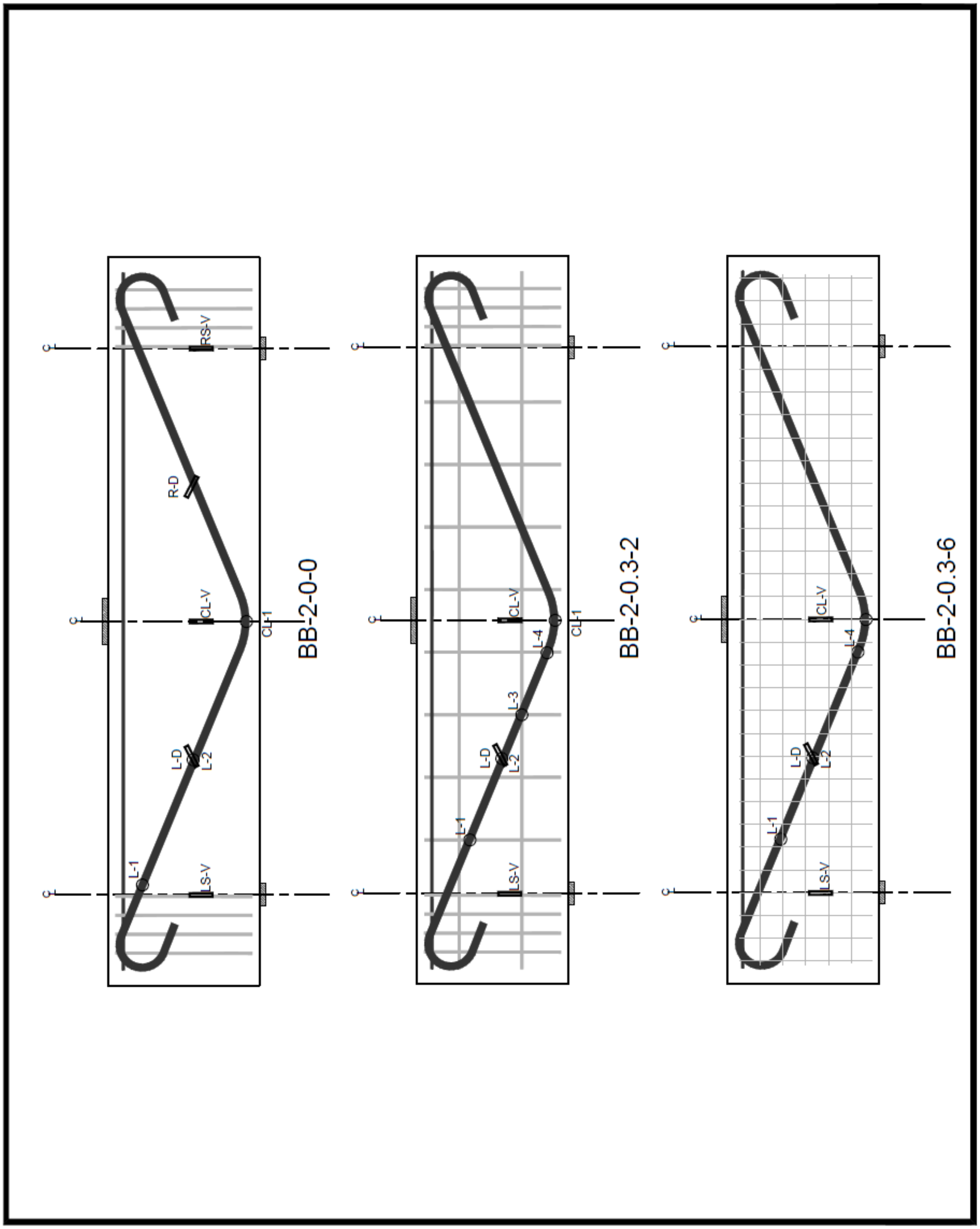
BB-2-0-0
RS-V
R-D
CL-V
CL-1
L-D
L-2
L-1
LS-V
BB-2-0.3-2
CL-V
CL-1
L-4
L-3
L-D
L-2
L-1
LS-V
BB-2-0.3-6
CL-V
L-4
L-D
L-2
L-1
LS-V

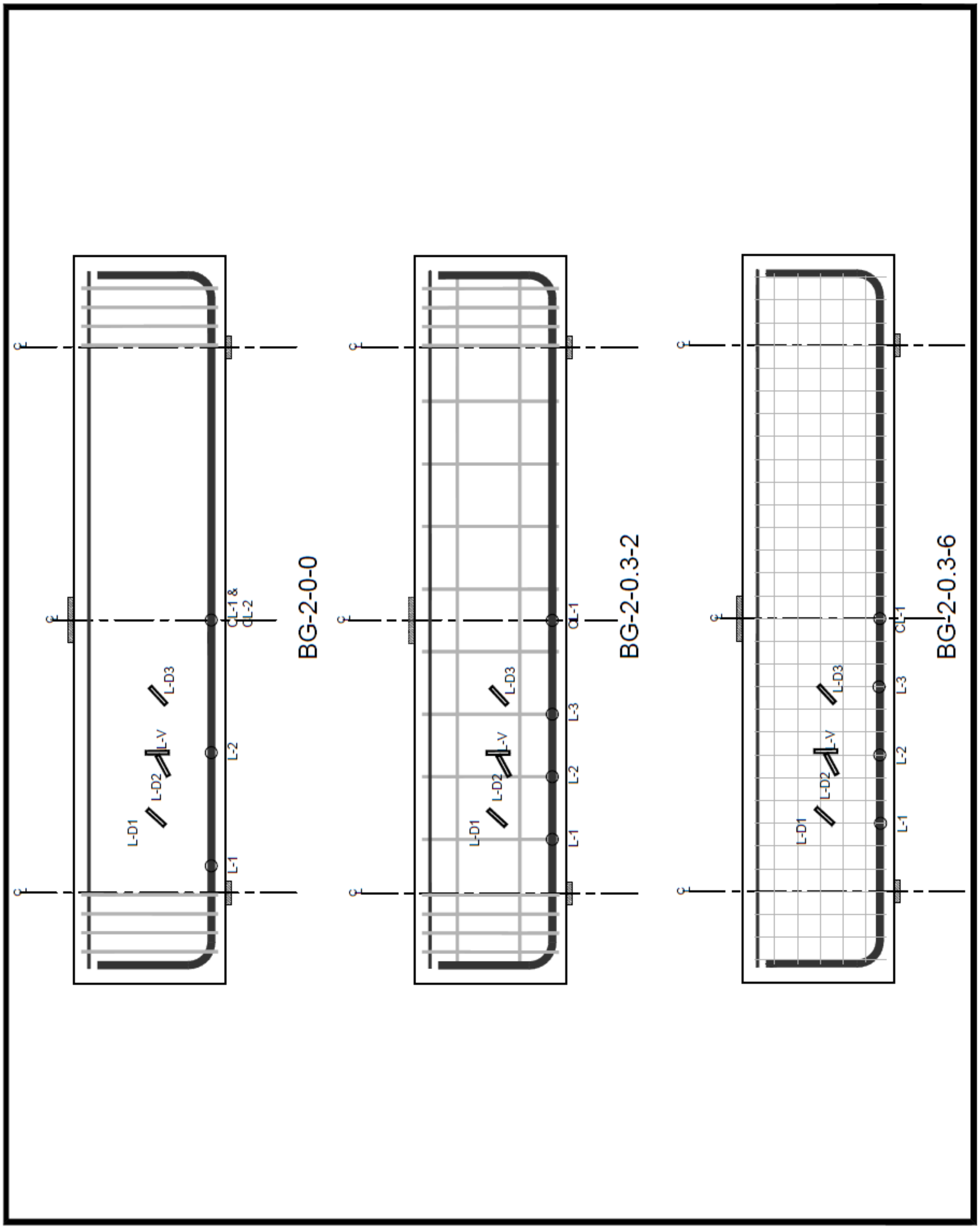
BG-2-0-0
CL-1 &
CL-2
L-1
L-2
L-D1
L-D2
L-V
L-D3
BG-2-0.3-2
CL-1
L-1
L-2
L-3
L-D1
L-D2
L-V
L-D3
BG-2-0.3-6
CL-1
L-1
L-2
L-3
L-D1
L-D2
L-V
L-D3

Appendix F: Strain Energy Calculations

Model G Strain Energy Database (1 of 2)

Beam ID	P (kip)	P_{ult} (kip)	b_w (in)	a/d	E_s (ksi)	E_c (ksi)	θ (deg)	F_{strut} (kip)	L_{strut} (in)	A_{strut} (in^2)	F_{tie} (kip)	L_{tie} (in)	A_{tie} (in^2)	U_{tie} (k-in)	ε_{tie}	U_{total} (k/in)	A_{Cr} (in^2/ in^2)	w_{cr} (in)
BG-1-0.3-6	110	274	10	0.99	29000	4115	42.6	81.3	24.2	48.5	59.8	18	2.37	0.53	0.00087	1.86	0.00017	0.004
	120	274	10	0.99	29000	4115	42.6	88.6	24.2	48.5	65.2	18	2.37	0.62	0.00095	2.20	0.00034	0.0068
	130	274	10	0.99	29000	4115	42.6	96.0	24.2	48.5	70.7	18	2.37	0.73	0.00103	2.57	0.00047	0.0084
	140	274	10	0.99	29000	4115	42.6	103.4	24.2	48.5	76.1	18	2.37	0.84	0.00111	2.97	0.00051	0.0084
	150	274	10	0.99	29000	4115	42.6	110.8	24.2	48.5	81.6	18	2.37	0.95	0.00119	3.40	0.00071	0.011
	160	274	10	0.99	29000	4115	42.6	118.2	24.2	48.5	87.0	18	2.37	1.08	0.00127	3.85	0.00080	0.0112
	170	274	10	0.99	29000	4115	42.6	125.6	24.2	48.5	92.4	18	2.37	1.21	0.00134	4.34	0.00084	0.013
	180	274	10	0.99	29000	4115	42.6	133.0	24.2	48.5	97.9	18	2.37	1.35	0.00142	4.85	0.00095	0.015
	186	274	10	0.99	29000	4115	42.6	137.4	24.2	48.5	101.1	18	2.37	1.44	0.00147	5.17	0.00101	0.016
BG-1-0.3-2	100	278	10	0.99	29000	4115	42.6	73.9	24.2	48.5	54.4	18	2.37	0.44	0.00079	1.55	0.00021	0.0072
	110	278	10	0.99	29000	4115	42.6	81.3	24.2	48.5	59.8	18	2.37	0.53	0.00087	1.86	0.00043	0.0084
	125	278	10	0.99	29000	4115	42.6	92.3	24.2	48.5	68.0	18	2.37	0.67	0.00099	2.38	0.00070	0.0104
	150	278	10	0.99	29000	4115	42.6	110.8	24.2	48.5	81.6	18	2.37	0.95	0.00119	3.40	0.00087	0.0128
	180	278	10	0.99	29000	4115	42.6	133.0	24.2	48.5	97.9	18	2.37	1.35	0.00142	4.85	0.00102	0.0136
	200	278	10	0.99	29000	4115	42.6	147.7	24.2	48.5	108.7	18	2.37	1.66	0.00158	5.97	0.00123	0.0152
	225	278	10	0.99	29000	4115	42.6	166.2	24.2	48.5	122.3	18	2.37	2.09	0.00178	7.52	0.00172	0.0184
BG-1-0-0	110	240	10	0.99	29000	4115	42.6	81.3	24.2	48.5	59.8	18	2.37	0.53	0.00087	1.86	0.00026	0.0078
	130	240	10	0.99	29000	4115	42.6	96.0	24.2	48.5	70.7	18	2.37	0.73	0.00103	2.57	0.00038	0.0096
	150	240	10	0.99	29000	4115	42.6	110.8	24.2	48.5	81.6	18	2.37	0.95	0.00119	3.40	0.00052	0.0102
	170	240	10	0.99	29000	4115	42.6	125.6	24.2	48.5	92.4	18	2.37	1.21	0.00134	4.34	0.00062	0.0132
	190	240	10	0.99	29000	4115	42.6	140.4	24.2	48.5	103.3	18	2.37	1.50	0.00150	5.39	0.00099	0.0222
	210	240	10	0.99	29000	4115	42.6	155.1	24.2	48.5	114.2	18	2.37	1.82	0.00166	6.57	0.00114	0.0228
	220	240	10	0.99	29000	4115	42.6	162.5	24.2	48.5	119.6	18	2.37	2.00	0.00174	7.19	0.00136	0.0288

Model G Strain Energy Database (2 of 2)

Beam ID	P (kip)	P_{ult} (kip)	b_w (in)	a/d	E_s (ksi)	E_c (ksi)	θ (deg)	F_{strut} (kip)	L_{strut} (in)	A_{strut} (in^2)	F_{tie} (kip)	L_{tie} (in)	A_{tie} (in^2)	U_{tie} (k-in)	ε_{tie}	U_{total} (k/in)	A_{Cr} (in^2/ in^2)	w_{cr} (in)
BG-2-0.3-6	40	162	10	1.98	29000	4115	24.6	48.0	39.5	47.3	43.7	36	2.37	0.59	0.00064	1.65	0.00001	0.0008
	45	162	10	1.98	29000	4115	24.6	54.1	39.5	47.3	49.1	36	2.37	0.73	0.00072	2.06	0.00003	0.0024
	55	162	10	1.98	29000	4115	24.6	66.1	39.5	47.3	60.1	36	2.37	1.07	0.00087	3.02	0.00009	0.0056
	65	162	10	1.98	29000	4115	24.6	78.1	39.5	47.3	71.0	36	2.37	1.47	0.00103	4.17	0.00014	0.0072
	75	162	10	1.98	29000	4115	24.6	90.1	39.5	47.3	81.9	36	2.37	1.92	0.00119	5.49	0.00031	0.0076
	85	162	10	1.98	29000	4115	24.6	102.1	39.5	47.3	92.8	36	2.37	2.45	0.00135	7.01	0.00047	0.0096
	95	162	10	1.98	29000	4115	24.6	114.1	39.5	47.3	103.7	36	2.37	3.03	0.00151	8.70	0.00056	0.0108
BG-2-0.3-2	45	149	10	1.98	29000	4115	24.6	54.1	39.5	47.3	49.1	36	2.37	0.73	0.00072	2.06	0.00001	0.002
	60	149	10	1.98	29000	4115	24.6	72.1	39.5	47.3	65.5	36	2.37	1.26	0.00095	3.57	0.00021	0.0088
	75	149	10	1.98	29000	4115	24.6	90.1	39.5	47.3	81.9	36	2.37	1.92	0.00119	5.49	0.00062	0.0124
	90	149	10	1.98	29000	4115	24.6	108.1	39.5	47.3	98.3	36	2.37	2.73	0.00143	7.83	0.00076	0.0136
	105	149	10	1.98	29000	4115	24.6	126.1	39.5	47.3	114.7	36	2.37	3.68	0.00167	10.58	0.00100	0.0204
	120	149	10	1.98	29000	4115	24.6	144.1	39.5	47.3	131.1	36	2.37	4.77	0.00191	13.74	0.00132	0.0232
	135	149	10	1.98	29000	4115	24.6	162.2	39.5	47.3	147.4	36	2.37	5.99	0.00215	17.32	0.00175	0.0276
BG-2-0-0	50	60	10	1.98	29000	4115	24.6	60.1	39.5	47.3	54.6	36	2.37	0.89	0.00079	2.52	0.00007	0.004
	55	60	10	1.98	29000	4115	24.6	66.1	39.5	47.3	60.1	36	2.37	1.07	0.00087	3.02	0.00015	0.0068

Model B Strain Energy Database (1 of 2)

ID	P (kip)	P_{ult} (kip)	a/d	θ (°)	α (°)	Strut Force F_1 (kip)	Strut Force F_2 (kip)	Strut Force F_5 (kip)	Strut Length L_1 (in)	Strut Length L_2 (in)	Strut Length L_5 (in)	Strut Area A_1 (in^2)	Strut Area A_2 (in^2)	Strut Area A_5 (in^2)	F_{tie} (kip)	L_{tie} (in)	A_{tie} (in^2)	U_{tie} (k-in)	ε_{tie}	U_{total} (k/in)	A_{Cr} (in^2/in^2)	w_{cr} (in)
BB-1-0.3-6	75	210	1.0	56	13	37.5	43.2	57.0	12.3	18.4	16.0	46.3	50.0	82.7	51.0	21.7	2.4	0.47	0.0007	1.28	0.00025	0.011
	90	210	1.0	56	13	45.0	51.9	68.4	12.3	18.4	16.0	46.3	50.0	82.7	61.2	21.7	2.4	0.67	0.0009	1.81	0.00034	0.014
	100	210	1.0	56	13	50.0	57.6	76.0	12.3	18.4	16.0	46.3	50.0	82.7	68.0	21.7	2.4	0.81	0.0010	2.22	0.00046	0.018
	110	210	1.0	56	13	55.0	63.4	83.6	12.3	18.4	16.0	46.3	50.0	82.7	74.8	21.7	2.4	0.98	0.0011	2.67	0.00052	0.022
	120	210	1.0	56	13	60.0	69.1	91.2	12.3	18.4	16.0	46.3	50.0	82.7	81.6	21.7	2.4	1.15	0.0012	3.16	0.00067	0.026
	150	210	1.0	56	13	75.0	86.4	114.1	12.3	18.4	16.0	46.3	50.0	82.7	102.0	21.7	2.4	1.77	0.0015	4.87	0.00126	0.039
	160	210	1.0	56	13	80.0	92.2	121.7	12.3	18.4	16.0	46.3	50.0	82.7	108.8	21.7	2.4	2.00	0.0016	5.53	0.00156	0.043
	175	210	1.0	56	13	87.5	100.8	133.1	12.3	18.4	16.0	46.3	50.0	82.7	119.0	21.7	2.4	2.38	0.0017	6.58	0.00198	0.046
	190	210	1.0	56	13	95.0	109.5	144.5	12.3	18.4	16.0	46.3	50.0	82.7	129.2	21.7	2.4	2.79	0.0019	7.73	0.00220	0.059
BB-1-0.3-2	70	225	1.0	56	13	35.0	40.3	53.2	12.3	18.4	16.0	46.3	50.0	82.7	47.6	21.7	2.4	0.42	0.0007	1.12	0.00022	0.010
	90	225	1.0	56	13	45.0	51.9	68.4	12.3	18.4	16.0	46.3	50.0	82.7	61.2	21.7	2.4	0.67	0.0009	1.81	0.00044	0.016
	110	225	1.0	56	13	55.0	63.4	83.6	12.3	18.4	16.0	46.3	50.0	82.7	74.8	21.7	2.4	0.98	0.0011	2.67	0.00064	0.024
	130	225	1.0	56	13	65.0	74.9	98.8	12.3	18.4	16.0	46.3	50.0	82.7	88.4	21.7	2.4	1.34	0.0013	3.69	0.00088	0.031
	150	225	1.0	56	13	75.0	86.4	114.1	12.3	18.4	16.0	46.3	50.0	82.7	102.0	21.7	2.4	1.77	0.0015	4.87	0.00146	0.040
	165	225	1.0	56	13	82.5	95.1	125.5	12.3	18.4	16.0	46.3	50.0	82.7	112.2	21.7	2.4	2.13	0.0016	5.87	0.00178	0.052
	180	225	1.0	56	13	90.0	103.7	136.9	12.3	18.4	16.0	46.3	50.0	82.7	122.4	21.7	2.4	2.52	0.0018	6.96	0.00216	0.063
	195	225	1.0	56	13	97.5	112.4	148.3	12.3	18.4	16.0	46.3	50.0	82.7	132.6	21.7	2.4	2.94	0.0019	8.14	0.00253	0.072
	205	225	1.0	56	13	102.5	118.1	155.9	12.3	18.4	16.0	46.3	50.0	82.7	139.4	21.7	2.4	3.24	0.0020	8.98	0.00258	0.073
BB-1-0-0	60	184	1.0	56	13	30.0	34.6	45.6	12.3	18.4	16.0	46.3	50.0	82.7	40.8	21.7	2.4	0.31	0.0006	0.84	0.00021	0.011
	75	184	1.0	56	13	37.5	43.2	57.0	12.3	18.4	16.0	46.3	50.0	82.7	51.0	21.7	2.4	0.47	0.0007	1.28	0.00033	0.014
	90	184	1.0	56	13	45.0	51.9	68.4	12.3	18.4	16.0	46.3	50.0	82.7	61.2	21.7	2.4	0.67	0.0009	1.81	0.00043	0.017
	110	184	1.0	56	13	55.0	63.4	83.6	12.3	18.4	16.0	46.3	50.0	82.7	74.8	21.7	2.4	0.98	0.0011	2.67	0.00087	0.028
	130	184	1.0	56	13	65.0	74.9	98.8	12.3	18.4	16.0	46.3	50.0	82.7	88.4	21.7	2.4	1.34	0.0013	3.69	0.00154	0.044
	150	184	1.0	56	13	75.0	86.4	114.1	12.3	18.4	16.0	46.3	50.0	82.7	102.0	21.7	2.4	1.77	0.0015	4.87	0.00207	0.051
	170	184	1.0	56	13	85.0	98.0	129.3	12.3	18.4	16.0	46.3	50.0	82.7	115.6	21.7	2.4	2.25	0.0017	6.22	0.00240	0.065

Model B Strain Energy Database (2 of 2)

						Strut Force			Strut Length			Strut Area										
ID	**P (kip)**	**P_{ult} (kip)**	**a/d**	**θ (°)**	**α (°)**	**F_1 (kip)**	**F_2 (kip)**	**F_5 (kip)**	**L_1 (in)**	**L_2 (in)**	**L_5 (in)**	**A_1 (in^2)**	**A_2 (in^2)**	**A_5 (in^2)**	**F_{tie} (kip)**	**L_{tie} (in)**	**A_{tie} (in^2)**	**U_{tie} (k-in)**	**ε_{tie}**	**U_{total} (k/in)**	**A_{Cr} (in^2/in^2)**	**w_{cr} (in)**
BB-2-0.3-6	45	161	2.0	67.5	5.6	22.5	54.3	40.8	13.0	36.0	15.0	52.6	56.7	99	58.0	38.4	2.4	1.07	0.0008	2.65	0.00009	0.003
	60	161	2.0	67.5	5.6	30.0	72.5	54.4	13.0	36.0	15.0	52.6	56.7	99	77.4	38.4	2.4	1.84	0.0011	4.60	0.00022	0.010
	75	161	2.0	67.5	5.6	37.5	90.6	68.0	13.0	36.0	15.0	52.6	56.7	99	96.7	38.4	2.4	2.82	0.0014	7.08	0.00041	0.014
	90	161	2.0	67.5	5.6	45.0	108.7	81.7	13.0	36.0	15.0	52.6	56.7	99	116.0	38.4	2.4	4.02	0.0017	10.10	0.00056	0.015
	105	161	2.0	67.5	5.6	52.5	126.8	95.3	13.0	36.0	15.0	52.6	56.7	99	135.4	38.4	2.4	5.42	0.0020	13.65	0.00079	0.022
	120	161	2.0	67.5	5.6	60.0	144.9	108.9	13.0	36.0	15.0	52.6	56.7	99	154.7	38.4	2.4	7.03	0.0023	17.73	0.00112	0.024
	135	161	2.0	67.5	5.6	67.5	163.0	122.5	13.0	36.0	15.0	52.6	56.7	99	174.1	38.4	2.4	8.84	0.0025	22.34	0.00131	0.031
	150	161	2.0	67.5	5.6	75.0	181.2	136.1	13.0	36.0	15.0	52.6	56.7	99	193.4	38.4	2.4	10.87	0.0028	27.49	0.00165	0.038
BB-2-0.3-2	30	167	2.0	67.5	5.6	15.0	36.2	27.2	13.0	36.0	15.0	52.6	56.7	99	38.7	38.4	2.4	0.50	0.0006	1.23	0.00002	0.002
	45	167	2.0	67.5	5.6	22.5	54.3	40.8	13.0	36.0	15.0	52.6	56.7	99	58.0	38.4	2.4	1.07	0.0008	2.65	0.00014	0.007
	60	167	2.0	67.5	5.6	30.0	72.5	54.4	13.0	36.0	15.0	52.6	56.7	99	77.4	38.4	2.4	1.84	0.0011	4.60	0.00036	0.012
	75	167	2.0	67.5	5.6	37.5	90.6	68.0	13.0	36.0	15.0	52.6	56.7	99	96.7	38.4	2.4	2.82	0.0014	7.08	0.00048	0.015
	90	167	2.0	67.5	5.6	45.0	108.7	81.7	13.0	36.0	15.0	52.6	56.7	99	116.0	38.4	2.4	4.02	0.0017	10.10	0.00065	0.018
	120	167	2.0	67.5	5.6	60.0	144.9	108.9	13.0	36.0	15.0	52.6	56.7	99	154.7	38.4	2.4	7.03	0.0023	17.73	0.00117	0.027
	150	167	2.0	67.5	5.6	75.0	181.2	136.1	13.0	36.0	15.0	52.6	56.7	99	193.4	38.4	2.4	10.87	0.0028	27.49	0.00168	0.036
BB-2-0-0	30	170.5	2.0	67.5	5.6	15.0	36.2	27.2	13.0	36.0	15.0	52.6	56.7	99	38.7	38.4	2.4	0.50	0.0006	1.23	0.00008	0.012
	35	170.5	2.0	67.5	5.6	17.5	42.3	31.8	13.0	36.0	15.0	52.6	56.7	99	45.1	38.4	2.4	0.67	0.0007	1.65	0.00017	0.017
	45	170.5	2.0	67.5	5.6	22.5	54.3	40.8	13.0	36.0	15.0	52.6	56.7	99	58.0	38.4	2.4	1.07	0.0008	2.65	0.00033	0.013
	50	170.5	2.0	67.5	5.6	25.0	60.4	45.4	13.0	36.0	15.0	52.6	56.7	99	64.5	38.4	2.4	1.30	0.0009	3.24	0.00048	0.018
	55	170.5	2.0	67.5	5.6	27.5	66.4	49.9	13.0	36.0	15.0	52.6	56.7	99	70.9	38.4	2.4	1.56	0.0010	3.89	0.00050	0.020
	105	170.5	2.0	67.5	5.6	52.5	126.8	95.3	13.0	36.0	15.0	52.6	56.7	99	135.4	38.4	2.4	5.42	0.0020	13.65	0.00186	0.077
	135	170.5	2.0	67.5	5.6	67.5	163.0	122.5	13.0	36.0	15.0	52.6	56.7	99	174.1	38.4	2.4	8.84	0.0025	22.34	0.00297	0.112

Appendix G: Crack Patterns

BB-1-0.3-2.2

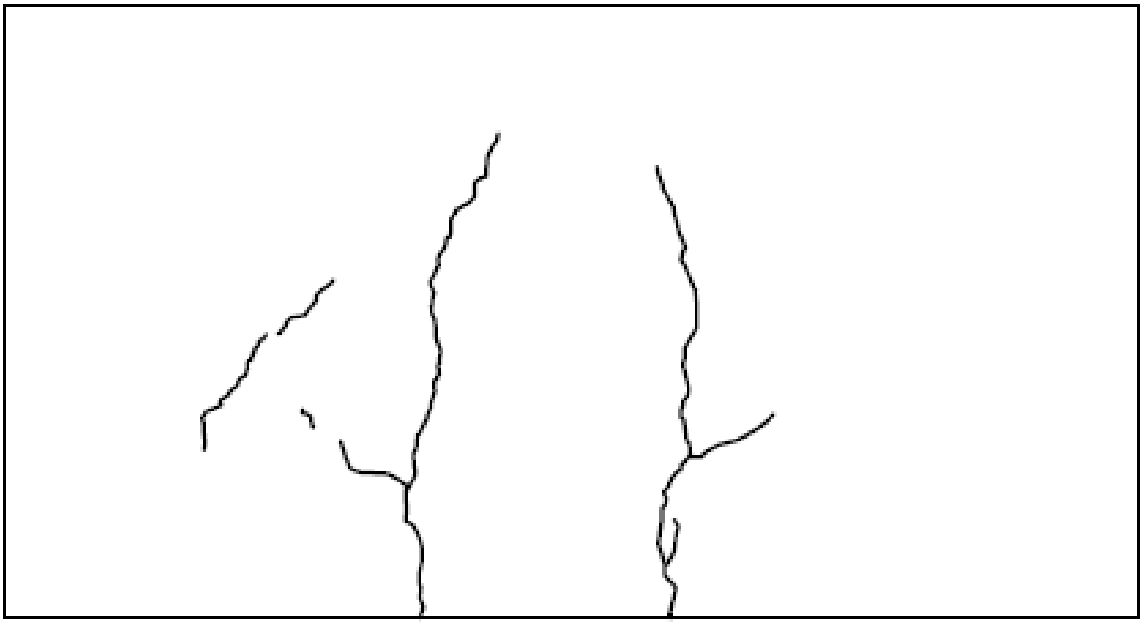

110 lb ~50% P_{ult}

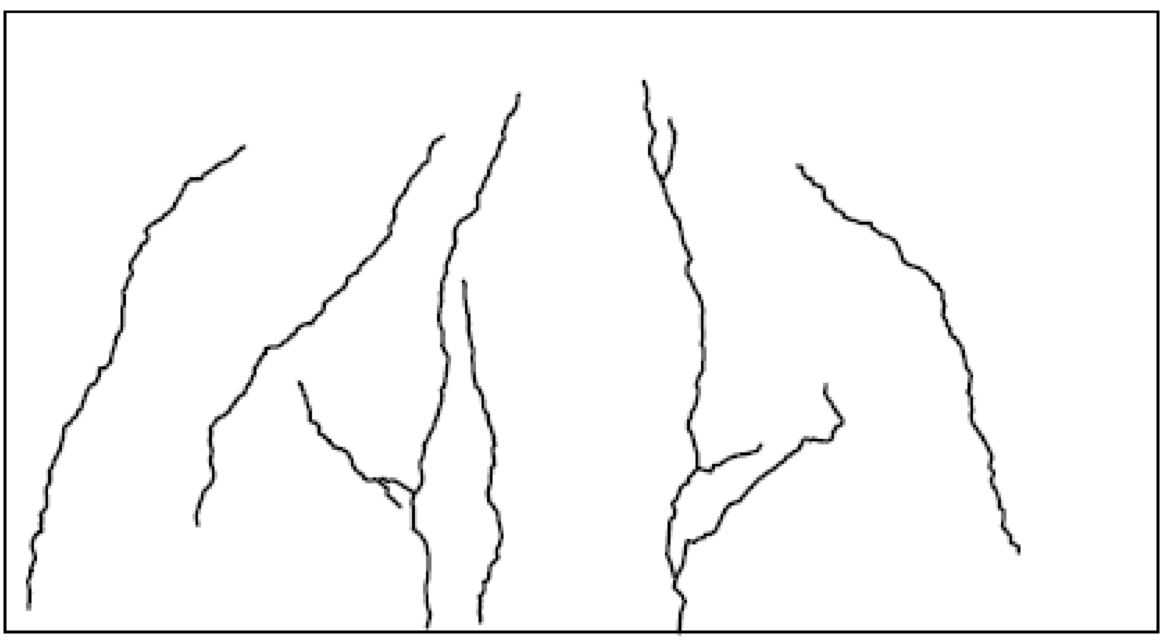

205 lb~ 91% P_{ult}

BB-1-0.3-6

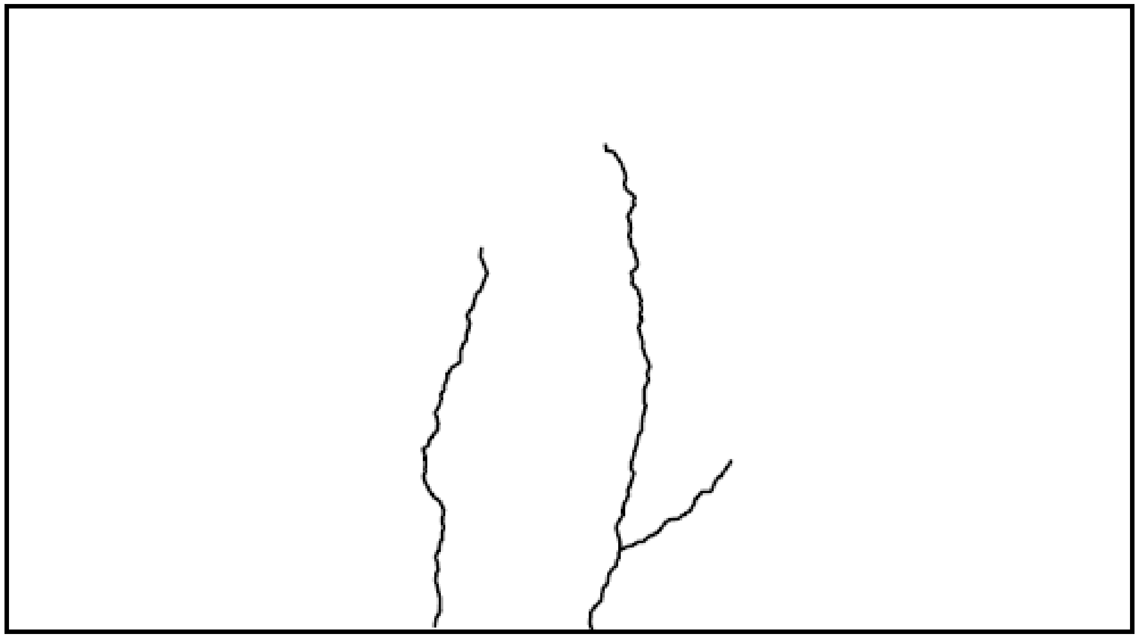

110 lb ~52% P_{ult}

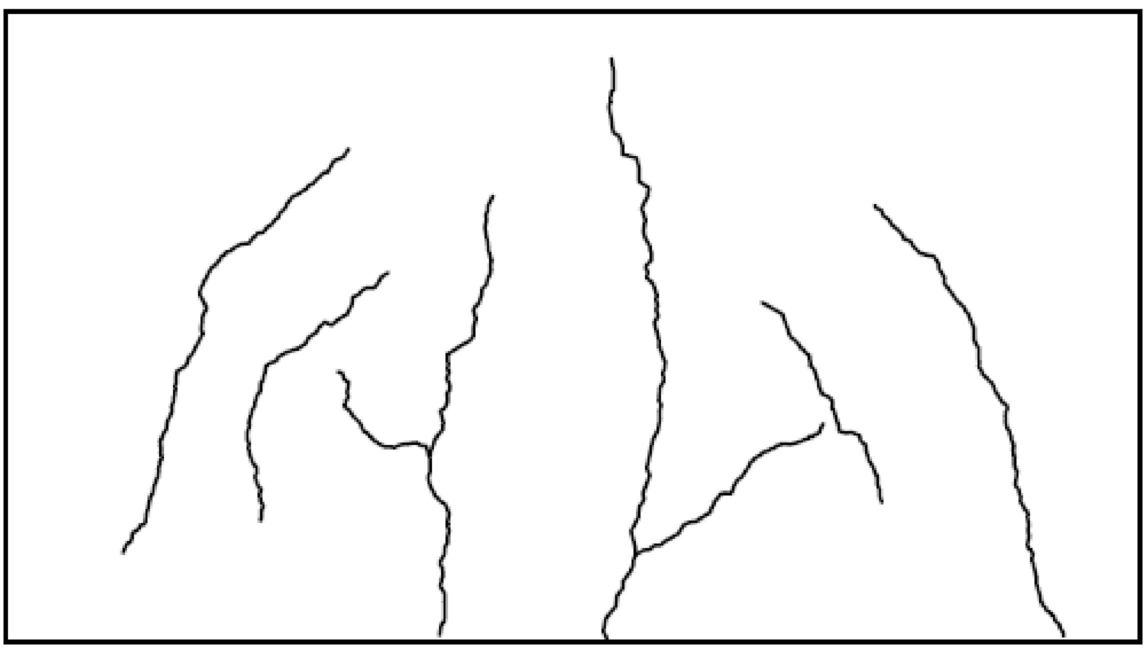

190 lb ~90% P_{ult}

BB-1-0-0

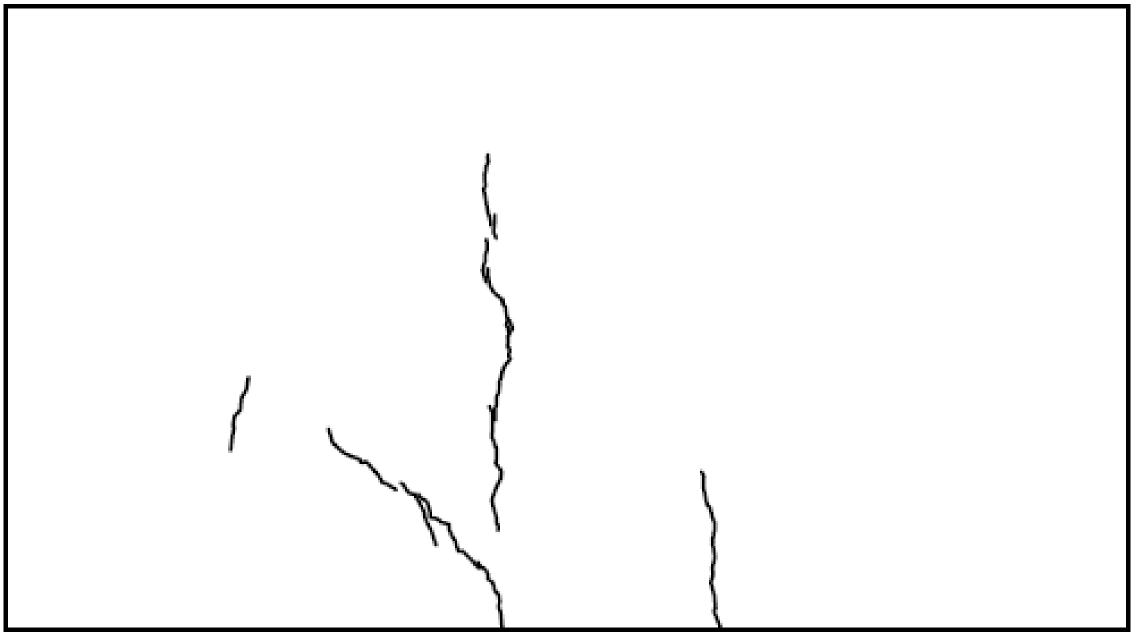

90 lb ~50% P_{ult}

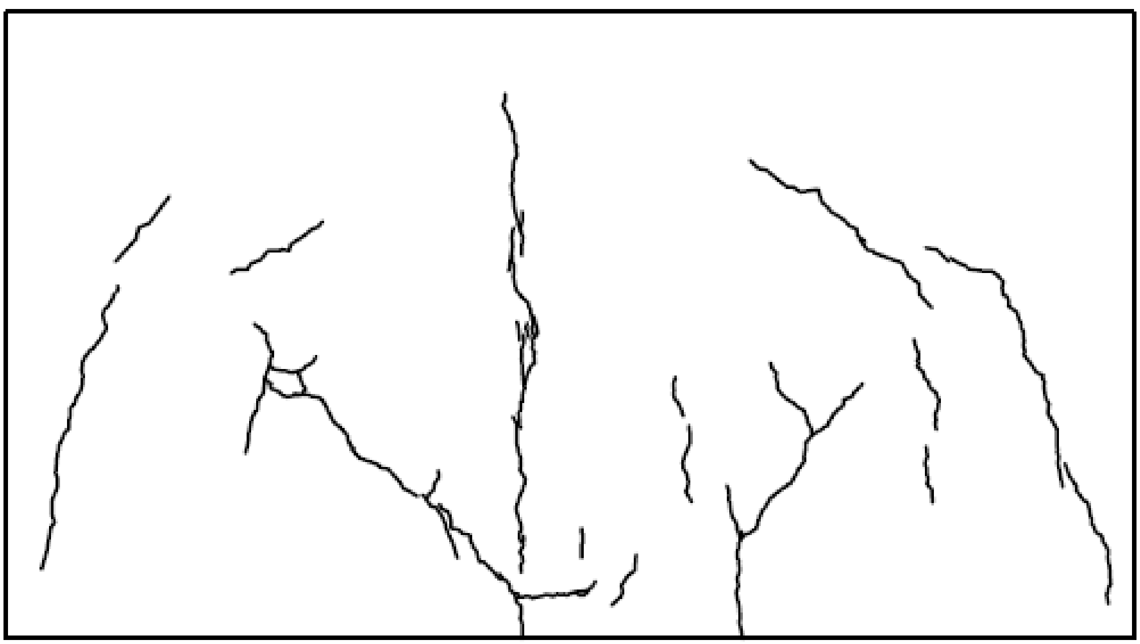

170 lb ~92% P_{ult}

BG-1-0.3-2

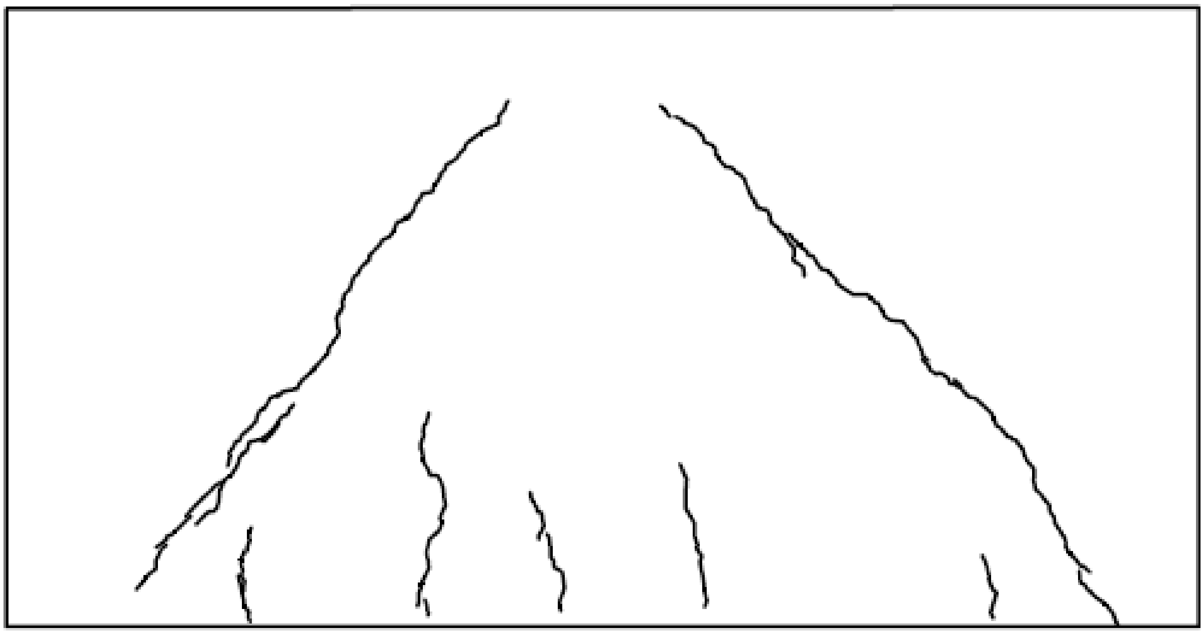

150 lb ~54% P_{ult}

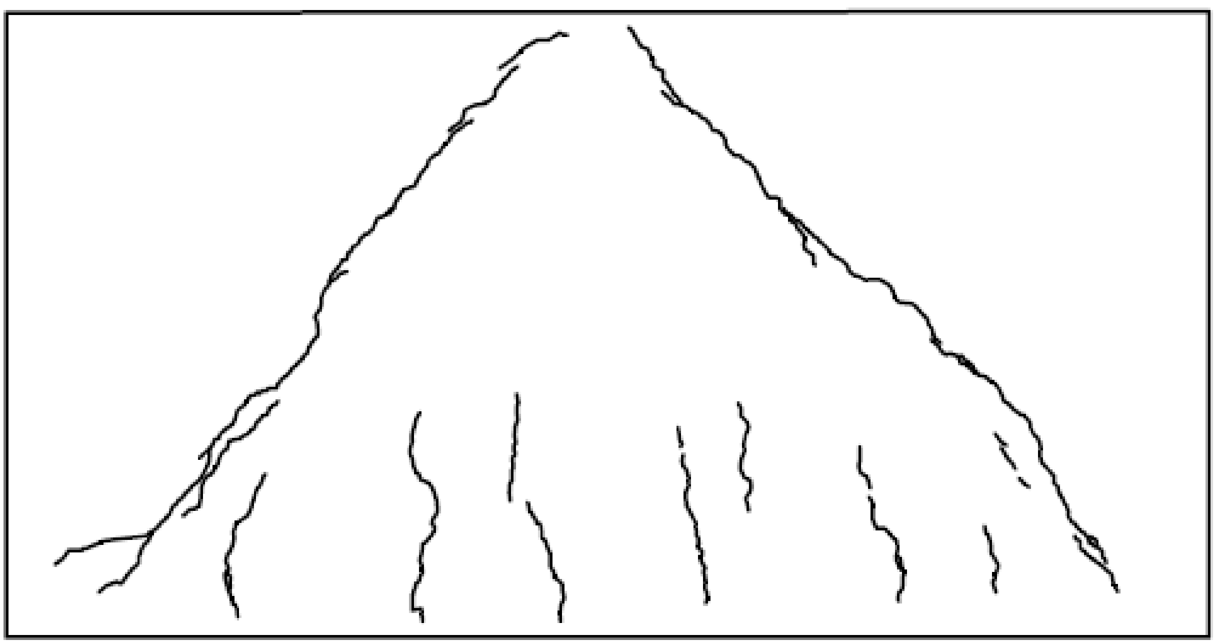

225 lb~81% P_{ult}

BG-1-0.3-6

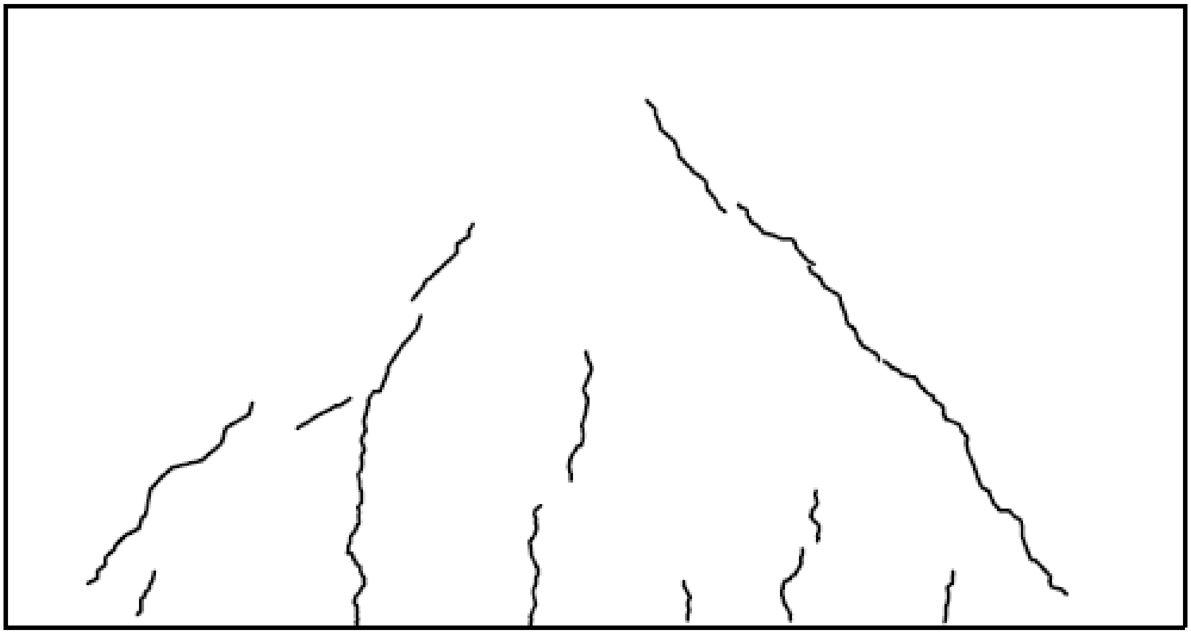

140 lb~51% P_{ult}

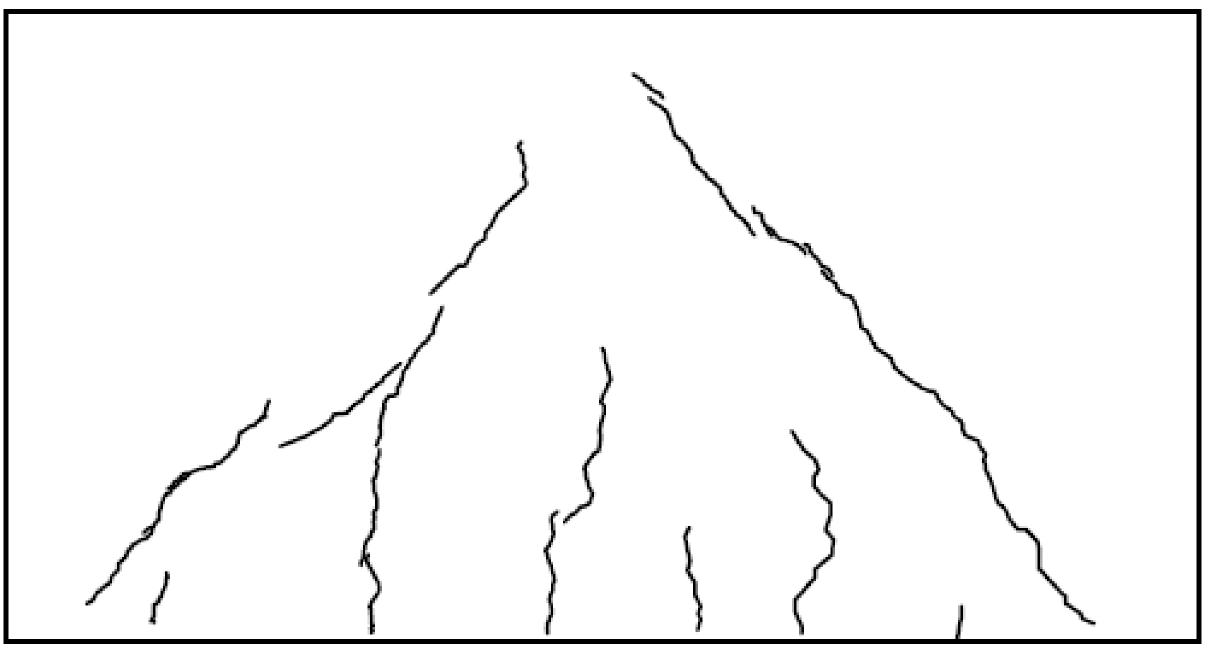

186ln ~ 68% P_{ult}

BG-1-0-0

130 lb~54% P_{ult}

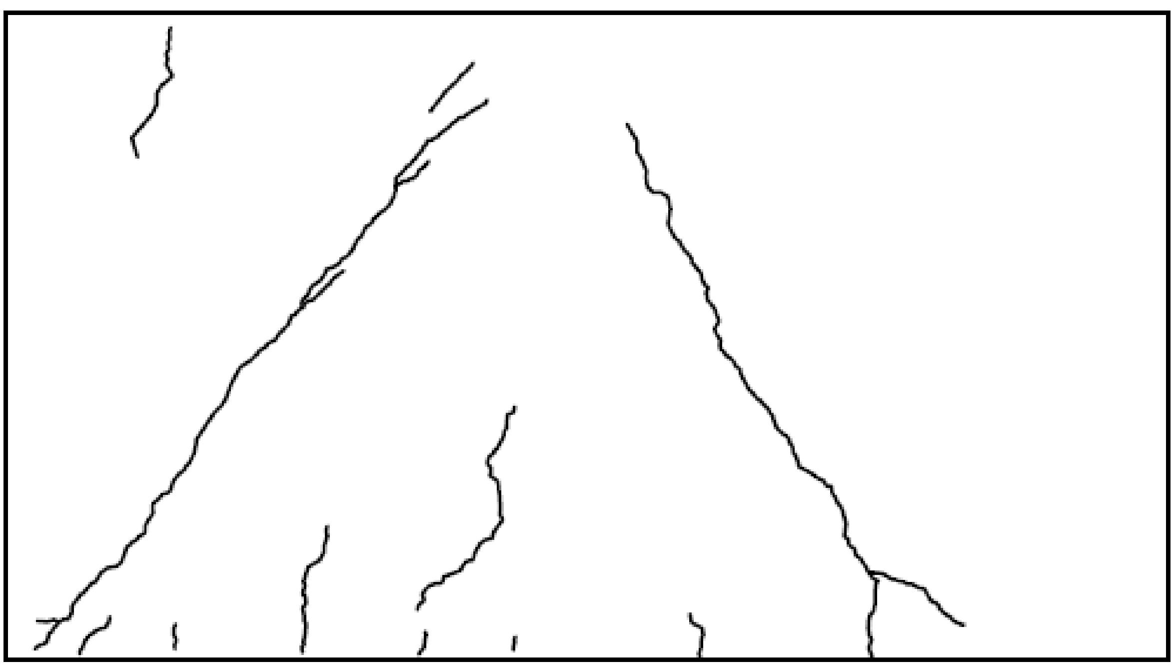

220 ~ 92% P_{ult}

BB-2-0.3-2

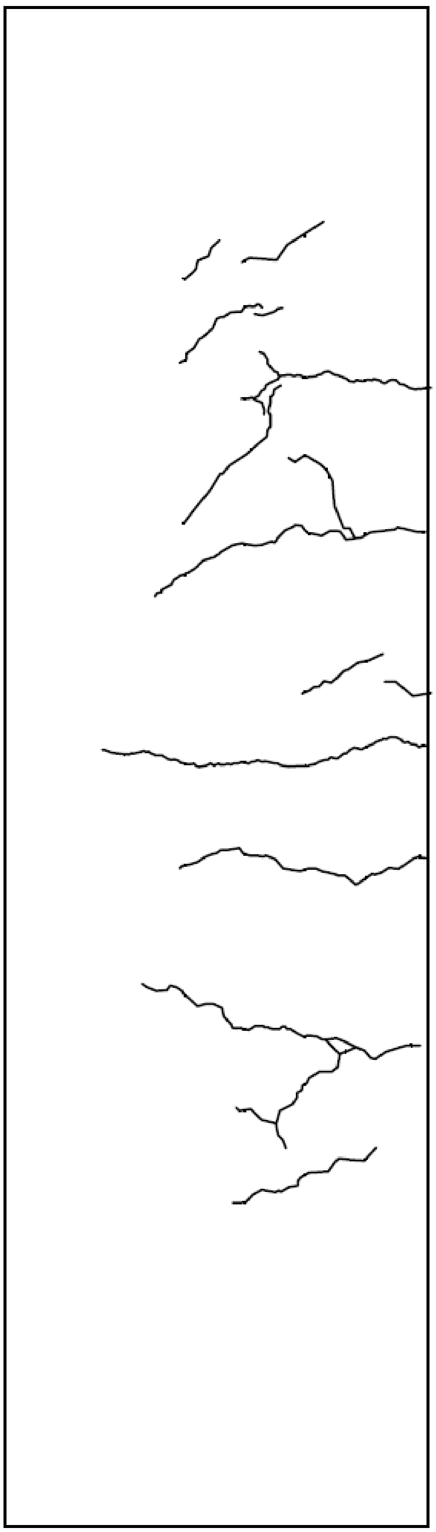

90lb ~54%

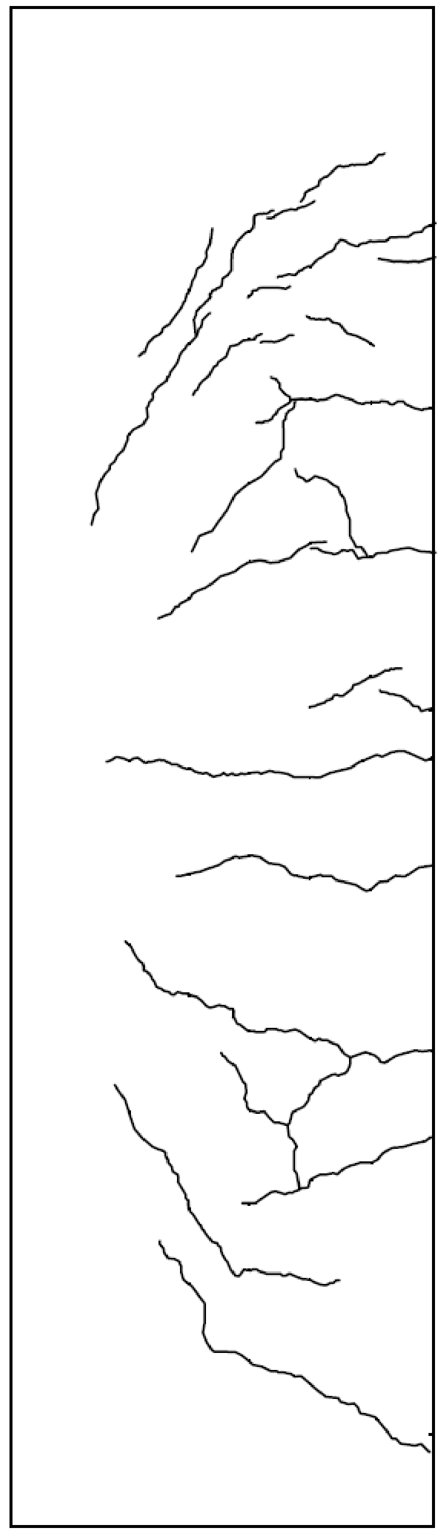

150 lb~90%

BB-2-0.3-6

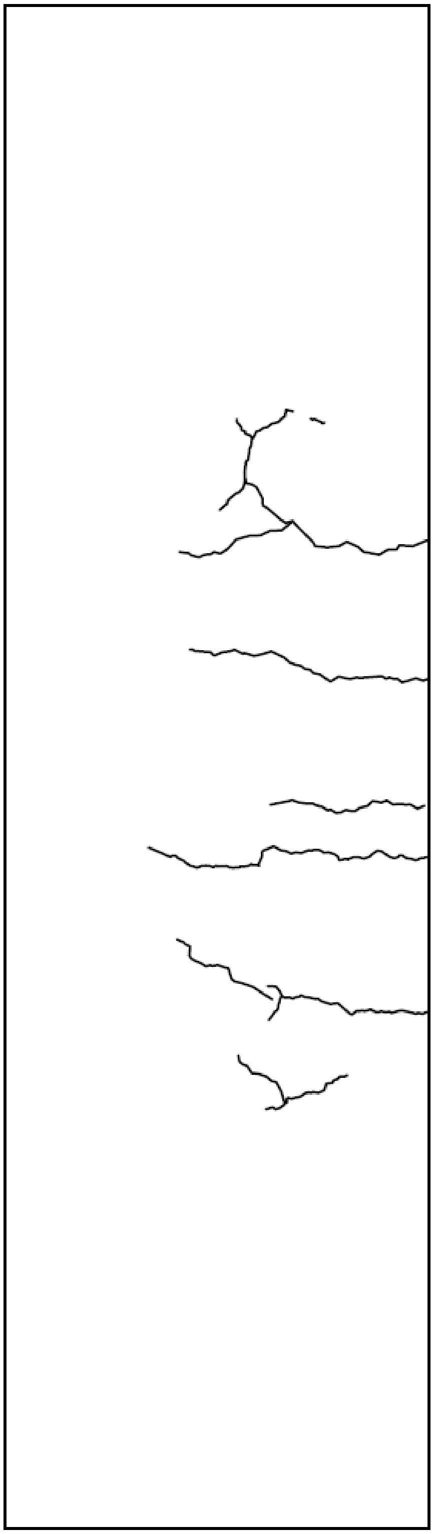

75 lb~47% P_{ult}

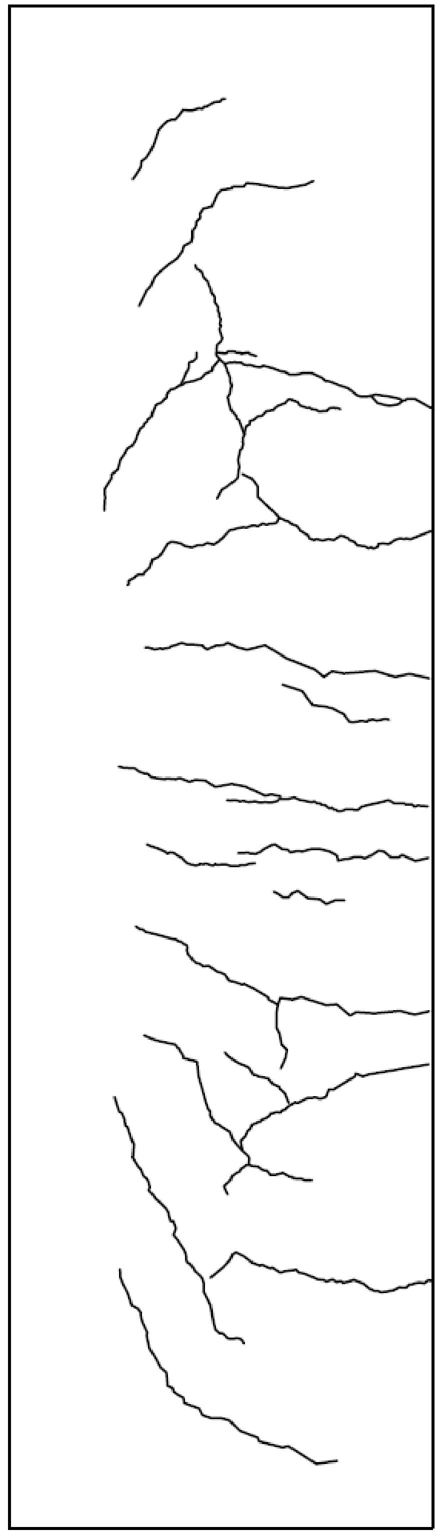

150lb ~93% P_{ult}

BB-2-0-0

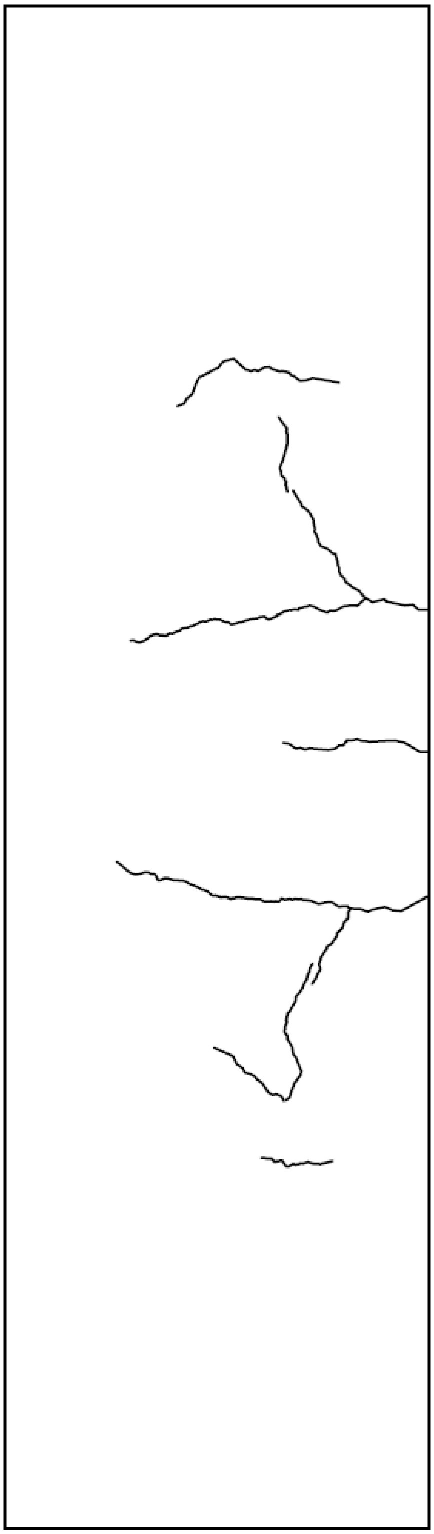

55lb ~ 32% P_{ult}

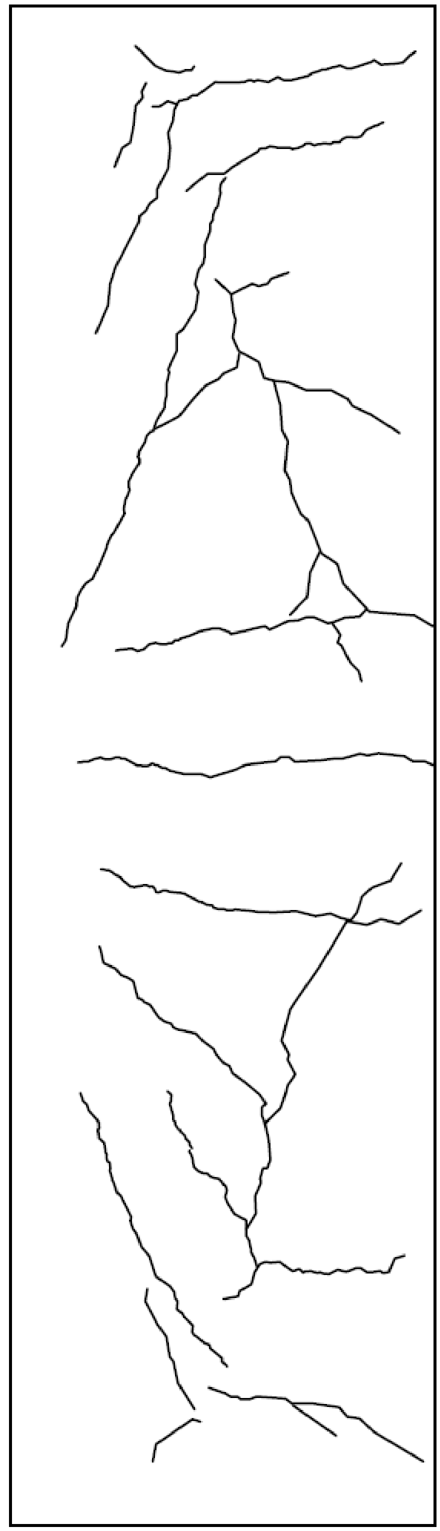

135lb ~ 85% P_{ult}

BG-2-0.3-2

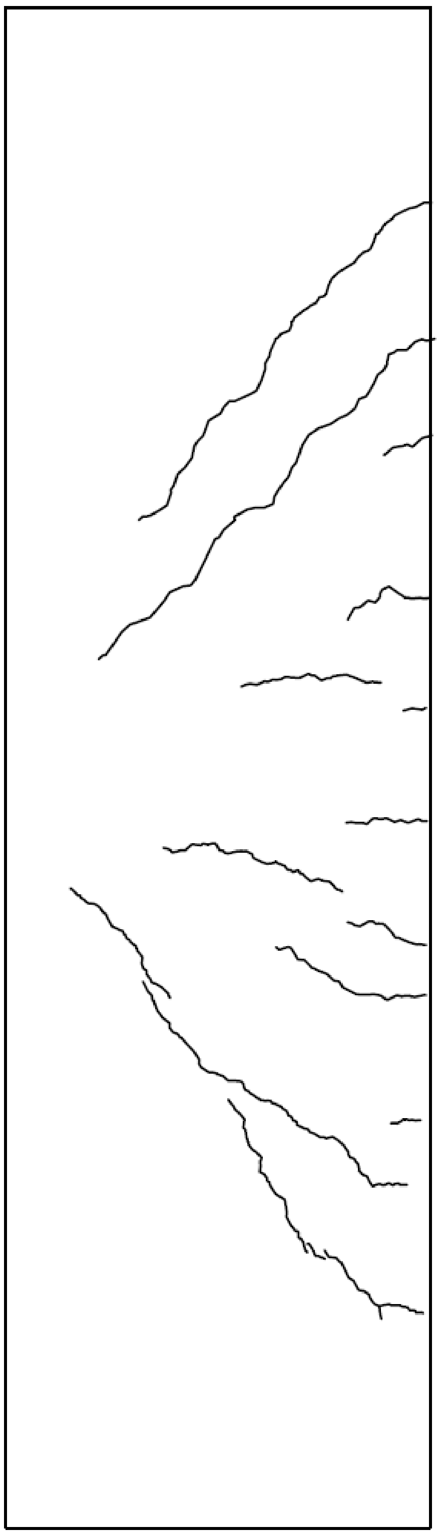

75 lb ~50% P_{ult}

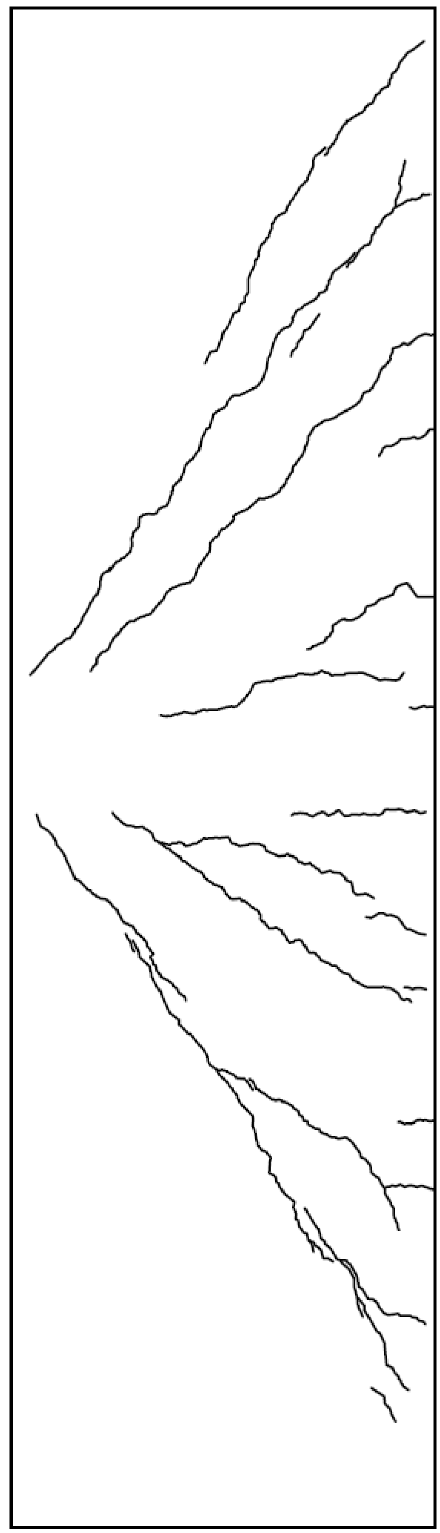

135lb ~ 91% P_{ult}

BG-2-0.3-6

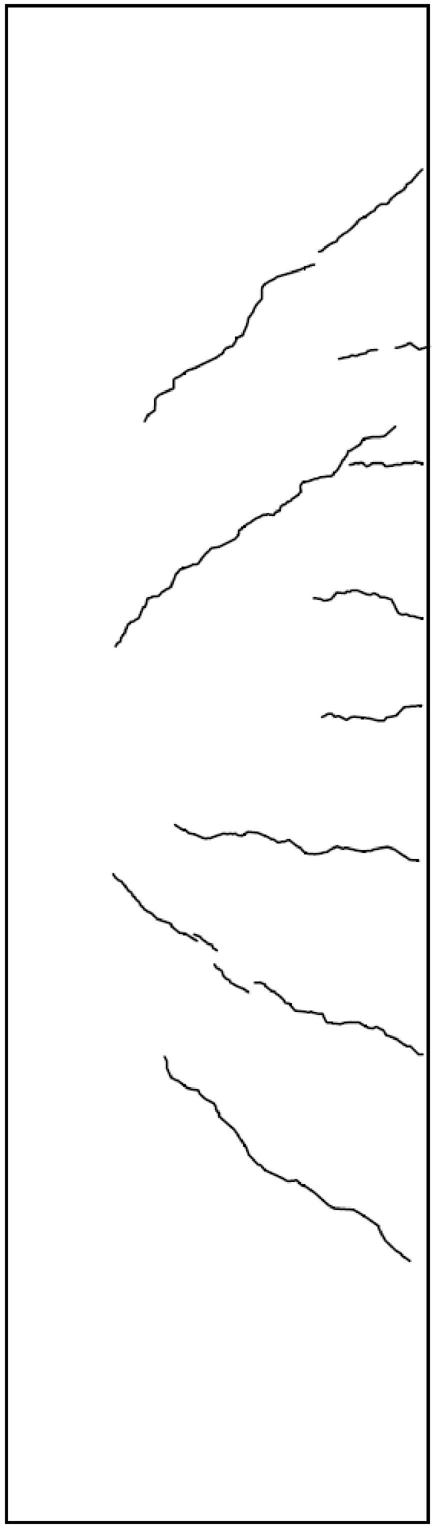

85 lb ~ 52% P_{ult}

No Measurements collected near 90% P_{ult}

BG-2-0-0

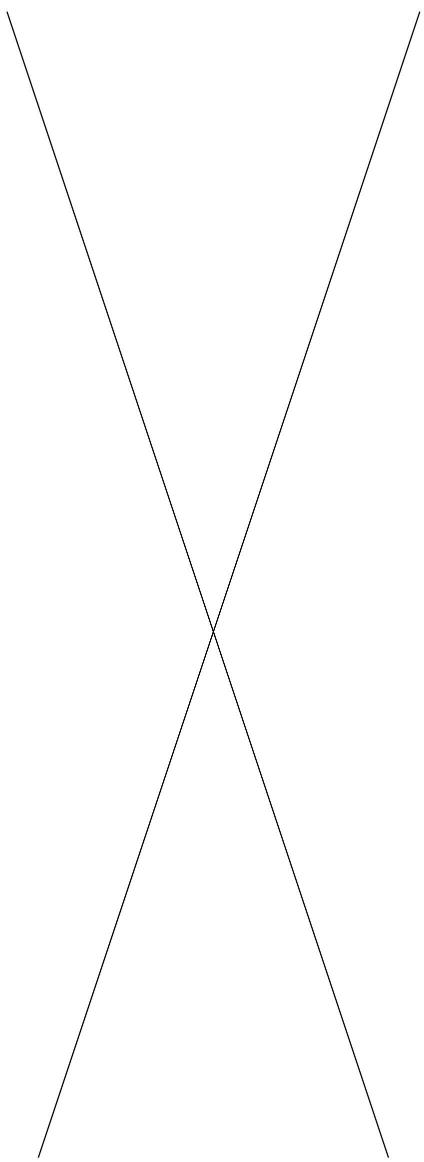

No cracks measured near 50% P_{ult}

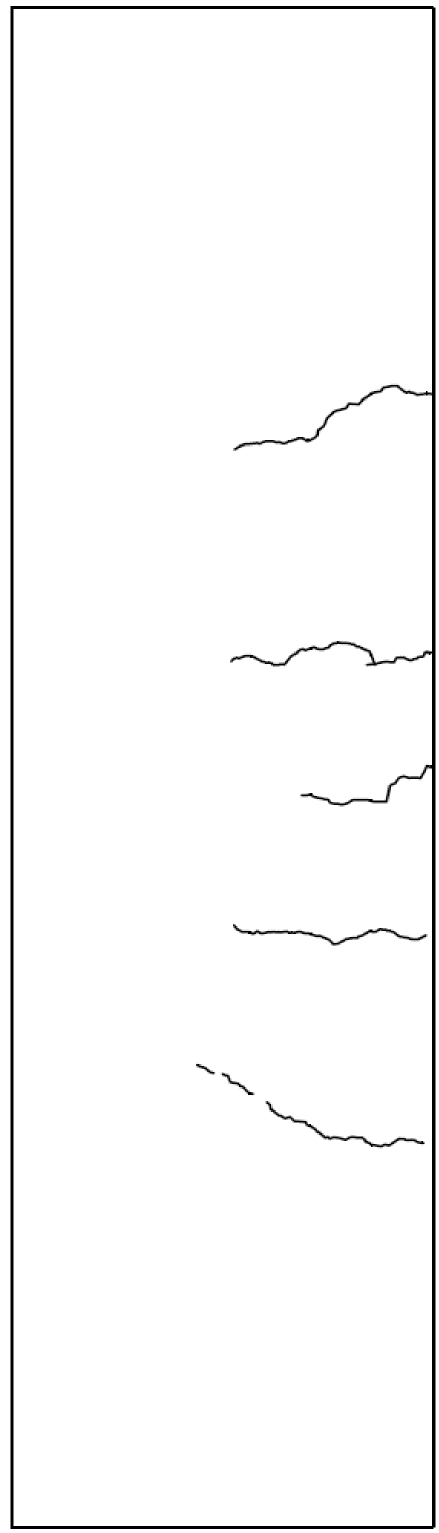

55 lb ~ 92% P_{ult}